Mechanisms of Arsenite-induced carcinogenesis

By

Bor-Jang Hwang

A dissertation submitted to the Graduate Faculty in Biochemistry in partial fulfillment of the requirements for the degree of Doctor of Philosophy, The City University of New York

2007

ProQuest Information and Learning Company
300 North Zeeb Road
P.O. Box 1346
Ann Arbor, MI 48106-1346

This manuscript has been read and accepted for the Graduate Faculty in Biochemistry in satisfaction of the dissertation requirement for the degree of Doctor of Philosophy.

Prof. Mark L. Steinberg, City College

Date

Chair of Examining Committee

Executive Officer

Prof. Lesley Davenport

Prof. Karen Hubbard, City College

Prof. Manfred Philipp, Lehman College

Prof. Tadmiri Venkatesh, City College

Prof. Toby G. Rossman, Nelson Institute of Environmental Medicine New York University School of Medicine

Supervisory Committee

THE CITY UNIVERSITY OF NEW YORK

Abstract

Mechanisms of Arsenite-induced carcinogenesis

by

Bor-Jang Hwang

Adviser: Professor Mark L. Steinberg

Inorganic arsenic is an environmental contaminant found in the American Southwest, Mexico, Chile, India and Taiwan and is associated with skin cancer, bladder cancer, Blackfoot disease, and Reynaud's syndrome. We used sodium arsenite to treat Normal Human Epidermal Keratinocyte (NHEK) as an ***in vitro*** system to study the effects of arsenic. Gene expression alteration was studied using cDNA microarray. We created expression profiles for arsenite-treated NHEKs and further studied the most affected gene: cyclin D. Next, in NHEK treated with submicromolar sodium arsenite (200, 400 and 800 nM), we observed increases of cell growth within 3 days. We also employed neutral red for viable staining on cell growth studies. The results showed similar growth stimulation on arsenite-treated cells. Flow cytometry was used for arsenite-treated NHEKs stained with propidium iodide. Analysis of cell

subpopulations in the G_1 and G_2 phases of the cell cycle showed that in arsenite-treated cultures, more cells were entering G_2/S compartments than in untreated controls.

We then performed Quantitative Polymerase Chain Reaction (Real time PCR) to examine cyclin D1 transcription in arsenite-treated NHEK cells. Our results showed that arsenite-treated NHEK exhibits a 3-fold increase in cyclin D1 transcription on day 3. Protein expression of cyclin D1 was examined in western blot analysis. Our results showed that 400 nM arsenite caused a time dependent induction of cyclin D1 protein expression. Results of electrophoretic mobility shift assays (EMSA) showed that arsenite also stimulated binding of the transcription factors, AP1 and CREBP to their respective binding motifs within 3 days. This supports a mechanism of oncogenesis based on persistent upregulation of D-type cyclins leading to a concomitant loss of G1/S checkpoint control.

The second part of my research focuses on the mitochondrial DNA (mtDNA) deletions and ROS (reactive oxygen species) caused by sub-micromolar arsenite in NHEK cells. Ultraviolet B (UVB) radiation was employed to observe the synergistic effect on NHEKs treated with arsenite. Our results showed that arsenite markedly enhanced mtDNA deletions and deletions were formed in a UVB

dose-dependent manner in arsenite treated NHEKs. Reactive oxygen species (ROS) formation, as measured by oxidation of 5', 6'-carboxy-2', 7'-dichlorodihydrofluorescein diacetate (DC-FDA) indicated that UVB may enhance ROS within 2 hours but, surprisingly, arsenite was found to bring about a reduction in UVB-irradiated NHEKs after 24 hours.

Acknowledgments

I would like to take this chance to express my great gratitude to my mentor Dr. Mark L. Steinberg who helped me through all these research works. I have learned lots of research skills and ideas from him. I also appreciate the way he trains students to think, to observe, and not just rely on machines.

I wish to thank my committee, Dr. Karen Hubbard, Dr. Manfred Philipp, Dr. Tadmiri Venkatesh,and Dr. Toby G. Rossman for their patience and advice. I also thank my former colleagues, Charles Utti, Xiaoyan Yang for helping on FACS analysis, my sister, Kai-Lin Hwang for helping me on statistical analyses, and many students,Ji Fang, Zdenka Pierre, Suqing Liu, Gerard Nkeunen Jingyu Pan, Francis J. Kuttamperoor, and Julia Wu, who worked on the mitochondrial DNA study.

I would like to also thank my wife, Hsiang-Mei for her support and patience on my whole research during these years, our parents who helped taking care of my kids while I was busy doing research, and my lovely daughter and son, Pin-Yu and Brian who brought me lots of happiness to overcome the studying stress.

Table of Contents (Part I)

Results (part I)

Discussion (part I)

Table of Contents (Part II)

List of Tables (part I)

List of Figures (part I)

List of Tables (part II)

List of Figures (part II)

I. Introduction

Arsenic compounds and related research:

Arsenicals are environmental pollutants which have attracted scientists' attention for many years. They can be classified into three main groups: inorganic arsenic, organic arsenic, and arsine gas (Copenhagen, WHO Regional office for Europe, 2000). Inorganic arsenic compounds include trivalent arsenics (such as arsenic trioxide, sodium arsenite and arsenic trichloride), and pentavalent arsenics (arsenic pentaoxide, arsenic acid, and arsenates). Organic arsenic compounds were observed as arsanilic acid, methylarsonic acid, dimethylarsinic acid and arsenobetaine. In general, in aerobic environment, pentavalent arsenics are predominant and under reducing conditions like deep well-waters, more trivalent arsenics are favored. In living organisms, the inorganic arsenic compounds are methylated to methyl- or dimethyl- arsenic compounds. Some marine lifes have abilities to transform inorganic arsenic into more complex organic forms such as arsenobetaine, arsenocholine and arsoniumphospholipids.

Arsenics exist primarily in nature in the sulfide form (arsenic sulfide, As_2S_3) with the ores of silver, lead,

copper, and other metals. Other natural arsenics are found in well waters and soils. At mid-1940s, inorganic arsenics were wildly spread through the use of arsenic pesticides and insecticides. Although the agricultural use of arsenics has been banned in most countries, contaminations have been absorbed in soil and underground water widely. Today, inorganic arsenics are still used for wood and leather preservation, poisonous baits, and various industrial applications.

Dietary arsenic is easily absorbed in the gastrointestinal tract. Acute symptoms of arsenic ingestion include severe vomiting, diarrhea, shock, muscle cramps and cardiac abnormalities. Inorganic arsenicals can be transported into mammalian cells through aquaglycoporins for the trivalent form (Liu, Z. *et. al.* 2002.) and phosphate transporter for the pentavalent form (Huang, R.N. *et. al.* 1996.) Arsenate can be quickly reduced to arsenite after entering cells. Arsenite is then metabolized by enzymatic methylation in humans via SAM and thioredoxin in the liver (Thomas, D.J. *et. al.* 2001. Rossman, T.G. 2003; Pott, W.A. *et. al.* 2001). A possible methylation reaction sequence is:

Arsenite → methyl arsonoic acid (MMA^{V}) → methyl arsonous acid (MMA^{III}) → dimethyl arsenic acid (DMA^{V}) →

dimethyl arsinous acid (DMA^{III}). (Structures are shown below).

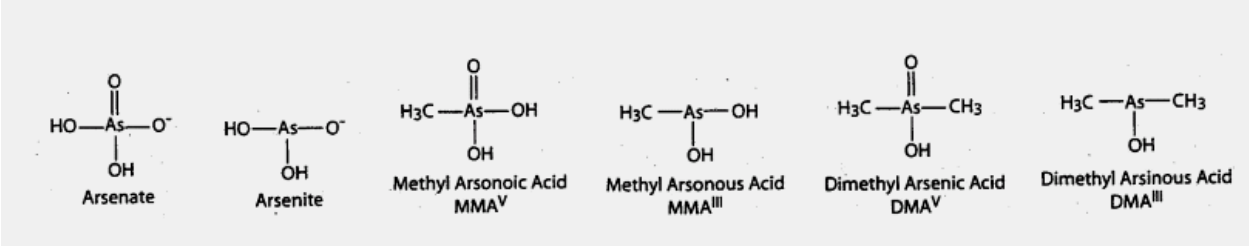

In normal human urinary excretion, DMA^{V} is the major metabolite (about 60-80 %, Vahter, M. 1999.) while the MMA^{V} and inorganic arsenic only constitute about 10-20 % of the total metabolites. In general, trivalent arsenics are more toxic than pentavalent species. The most toxic arsenic is arsenic trioxide, which has a lethal dose of ~1.5 mg/kg of body weight in human (Fawell, J.K., and Mascarenhas, R. 2003). The 50 % lethal dose of arsenite, arsenate, MMA^{V}, and DMA^{V} in rat is about 41, 100, 961, and 644 mg/kg body weight (review in Rossman, T.G. 2003). Acute arsenic intoxication from contaminated ground water has been reported at levels between 1.2 and 21 mg/L (Feinglass, E.J. 1973; Welch, A.H. *et. al.* 1988). MMA^{III} and DMA^{III} were found to inhibit GSH reductase and thioredoxin reductase (Styblo, M. *et. al.* 1997; Lin, S. *et. al.* 1999). Studies also showed that these trivalent and pentavalent arsenic metabolites generated DNA strand

breaks and induced more DNA lesions that can be recognized by the bacterial formamidopyrimidine-DNA glucosylase (Fpg) in Hela S3 cells at different concentration ranges (Schwerdtle, T. *et. al.* 2003).

The arsenic species are normally found in higher concentrations in human urine, hair, nails, and blood (Guha Mazumder, D. N. 2000). For people with no known arsenic exposure, the concentrations of arsenic are about ~0.04 mg/g in urine, 0.02-0.2 mg/kg in hair, 0.02-0.5 mg/kg in nails, and 0.3-2 μg/L in blood. The concentrations of arsenic in people in the areas that have high arsenic concentrations in drinking water were reported as 1.156 mg/g, 3-10 mg/kg, several tens of mg/kg, and about 10 μg/L in urine, hair, nails, and blood. Arsenic concentrations examined in other tissues and organs in normal peoples were between 0.01-0.08 mg/kg in dry weight.

Inorganic arsenics are widely found in the American Southwest, Mexico, Chile, Australia, Viet Nam, India, Bangladesh, and Taiwan. Based on the toxicity and the carcinogenic effects in humans, the maximum allowable concentration was set as 0.01 mg/liter (~1.3 μM) in the World Health Organization's (WHO's) Guidelines for

drinking-water quality (The allowable concentration was 0.2 mg/L at 1958; 0.05mg/L at 1963, WHO, 2006.). Epidemiological data have shown that several diseases including cancers are correlated with exposure to this worldwide contaminant. For example, people exposed to inorganic arsenic are likely to develop cancers of the lung, skin, and bladder (IARC, 1980; National Research Council, 2000). In addition to cancers, drinking ground water containing arsenic is thought to be the cause of vascular degeneration and neuropathy of the extremities (Blackfoot disease and Reynaud's syndrome, (Chen, C.-J. *et. al.* 1990., Chen, C. *et. al.* 1995., Engel, R. *et. al.* 1994). Although epidemiological evidence implicated arsenic as a causative factor in disorders, the disease mechanisms are not clearly understood.

Arsenic containing compounds act differently on many biological systems. They have been used for treatment of cancer for hundreds of years in both Western and traditional Eastern herbal medicine. The toxicity to cells makes it a chemotherapeutic agent in the treatment of acute promyelocytic leukemia. However, the non-toxic concentrations (below 5~10 μM, varies by animals and tissues) of arsenite act as a carcinogen. Here, sub-micromolar instead of supra-micromolar concentrations of

arsenite was used for these studies to more closely replicate conditions of exposure seen *in vivo*.

Part I. Studies on gene expression in human epithelial cells treated with submicromolar levels of arsenic

Introduction:

Arsenic is a weak mutagen; however, some recent studies showed that it might be an effector which may effect the action of growth factors, gene transcription, or DNA repair. (Corsini, E. *et. al.* 1999; Germolec, DR. *et. al.* 1999; Simeonova, P. P. *et. al.* 1997; Tully, D. B. *et. al.* 2000; Asmuss, M. *et. al.* 1998; Lynn, S. *et. al.* 1997; Samet, J. M. *et. al.* 1999; Chen, N. Y. *et. al.* 2000; Porter, A. C. *et. al.* 1999). To understand the mechanism of skin cancer caused by exposure to arsenic, efforts have been made to study both animal models and *in vitro* cell culture (Rossman, T.G. *et. al.* 2001; Steinberg, M. *et. al.* 1999; Germolec, DR. *et. al.* 1998.).

Arsenics (both arsenite and arsenate) have been implicated in various signaling pathways that effect cell growth, stress response and cell death. Several important arsenic involved pathway are discussed below:

Wnt signaling pathway

In cell cycles, the transition of G1 to S was mainly controlled by D type cyclins and their related CDKs. Expression of D-type cyclins in some conditions can be turned on by β-catenin, which is involved in the Wnt signaling pathway (Figure 1). In the absence of Wnt signaling, β-catenin is bound by axin, adenomatous polyposis coli protein (APC), and glycogen synthase kinase 3β (GSK-3β) as a phosphorylated form. In the presence of Wnt signaling, the GSK-3β is inhibited and the β-catenin can form a complex with Tcf-4 in an active form (dephosphorylated β-catenin). The β-catenin/Tcf-4 complexes then upregulate the expression of down stream genes such as cyclin D and Myc.

Rossman's laboratory has tested the sensitivity of mammalian cells to arsenite with regard to transformation. Human cells have been found to be more sensitive to arsenic than other mammalian cells. In preliminary studies in our laboratory, SV-40 immortalized human keratinocytes (line327) were employed for studying this environmental carcinogen (Steinberg, M. *et. al.* 1999). The results showed that arsenic (either arsenite or arsenate) has stimulatory effects on cell growth at submicromolar concentrations. When these cells were

labeled with ^{32}P phosphate followed by immunoprecipitation with phosphotyrosine antibodies, the cells treated with arsenic exhibited quite different patterns of phosphorylated proteins compared with untreated cells displayed on the gel. In that study, line 327 cells were also stained with propidium iodide and analyzed by FACS (fluorescent activated cell sorter), to examine cell cycle parameters in the treated cells. The results showed that the G1 phase of the cell cycle was significantly shortened relative to S and G2 by low concentrations of arsenic.

Recently, Rossman's laboratory showed that low concentrations of sodium arsenite can disrupt p53 function and upregulate cyclin D1 in WI38 cells (Vogt, B.L. *et. al.* 2001). P53 is a G1/S gatekeeper in the cell cycle. The D-type cyclins are known to form complexes with two cyclin-dependent kinases, CDK4 and CDK6. CDK4 and CDK6 can then phosphorylate various proteins such as the retinoblastoma (Rb) tumor suppressor which allows escape from G1 phase.

MAP Kinase pathway

At the outset my project focused mainly on alterations in signaling pathways that might effect cell cycle regulation in epithelial cells exposed to arsenite. In particular

the mitogen-activated protein kinases (MAPK) pathway is a candidate that may be responsible for the toxicity and tumorgenesis of arsenic.

MAPKs are important mechanisms for cells to respond to extracellar stimuli through protein kinase cascades. Three major groups of MAPKs were classified as ERK1/2, JNKs, and p38 kinase signals (Figure 2). In general, ERK1 and 2 are activated in response to growth factors and phorbol esters. JNKs and p38 kinase are more related to stress stimuli. Each family of MAPKs is composed of a set of three evolutionarily conserved kinases: MAPK, MAPK kinase (MAPKK), and MAPKK kinase (MAPKKK).

Tanaka-Kagawa, T.'s group showed that arsenite (100~800 μM) can induce mitogenic effects through the EGFR-Shc-Grb2-MEK1/2-ERK1/2 pathway within very short incubation time. (Tanaka-Kagawa, T. *et. al.* 2003). A similar result was obtained by Lau's laboratory (Lau, A.T.Y. *et. al.* 2004). In this study 2 μM arsenite was found to stimulate the phosphorylation of ERK1/2, while 40 μM arsenite activated the JNK1/2 phosphorylation after a 24-hour treatment.

NFκB signaling pathway:

NFκB belongs to the Rel family of transcription factors. These transcription factors regulate gene expression involved in immune and inflammatory responses. The NFκB signaling can be activated by diverse stimuli such as inflammatory cytokines, phorbol esters, bacterial toxins, viruses, UV light, and mitogens. NFκB members are normally sequestered by their natural inhibitor IκBs in cytoplasm Figure 3). The environmental stimuli can then activate IκB kinase complex and cause the phosphorylation on IκBs and release the NFκBs. The free NFκBs will then translocate into nucleus and form homo- or hetero- dimmers to activate different gene expression.

Felix's research in mesencephalic cells treated with 0.1-10 μM arsenite showed both NFκB and activator protein 1(AP-1) were induced within 2 hours (Felix, K. *et. al.* 2005). In the same study, arsenite also induced reactive oxygen species (ROS) and the addition of antioxidants such as N-acetyl cysteine (NAC) inhibited the induction of NFκB and AP-1. A similar study in murine keratinocyte line HEL30 from Corsini's research also suggests that NFκB and AP-1 played important roles in arsenic-induced skin hyperkeratoses (Corsini, E. *et. al.* 1999). Other evidence shows that sodium arsenite (1.25-5 μM) induced cyclin D1

expression through NFκB activation in human keratinocytic HaCat cells (Ouyang, W. *et. al.* 2005).

Apoptosis:

Apoptosis is an important pathway for organisms to remove unnecessary, aged, or damaged cells. The proper control of apoptosis is very important for maintenance and development of the body. The lost of apoptotic function may cause tumorigenic cells to survive. The typical morphologic change of apoptosis includes shrinkage of cells, condensation of chromatin, and disintegration of the cell into small fragments. Apoptosis can be triggered by many stimuli such as the withdrawal of essential growth factors, irradiation, and activation of certain surface receptors such as TNF-R, FAS and FASL. The apoptotic pathway can be regulated by the interplay of proapoptotic and antiapoptotic proteins of the Bcl-2 family (Figure 4). The α-helical BH3 death domain on proapoptotic proteins such as Bax, Bad, Bid, Bik, and Bim allows them to interact with the antiapoptotic proteins Bcl-2 and Bcl-XL. The heterodimer will block the antiapoptotic activity of Bcl-2 and Bcl-XL. The proapoptotic proteins then act at the mitochondrial membrane and promote leakage of cytochrome c. The released cytochrome c then interacts with Apaf-1,

causing self-cleavage and activation of caspase-9. The caspases comprise a cysteine protease family. Many members of the caspase family are involved in apoptosis for activating downstream events such as cell shrinkage, membrane blebbing, DNA fragmentation, and chromatin condensation. The downstream caspases -3, -6, and -7 can be activated by the activation of caspase-9 from Apaf-1 or caspase-8 from activation of FASL/TNF-R. If the signals are transferred from TNF-R and FASL, they then activate FADD to turn on the caspase 8 which has a death domain. In JNK mediated apoptosis, stress signals are transmitted through Daxx to JNK-MAPK pathway and induce JNK-dependent transcriptional regulated cell death. Some other signals are also transferred through TGF-β and Daxx to MAPK p38 pathway in a similar manner of cell death.

A study from Huang's laboratory indicated that high concentrations of arsenic (200 μM arsenite and arsenate) induced apoptosis through a c-Jun NH_2-terminal kinase-dependent p53-independent pathway in JB6 mouse epidermal cell line (Huang, C. *et. al*. 2004). Lau's study in rat lung epithelial cell (LEC) also showed that 40 μM arsenite induced JNK-dependent cell death while 2 μM of arsenite

induced the MAPK pathway via ERK and AP-1 (Lau, A.T.Y. *et. al*. 2004).

The idea from the findings in these, and other studies, that arsenite might modulate signaling pathways involved in cell cycle regulation formed the basis for the experiments described in the first part of the dissertation.

The carcinogenic properties of inorganic arsenicals may be through the alteration of gene expression on cell cycle regulation, mitogenic effects, and programmed cell death, or from the genotoxicity that causes DNA mutations on those genes. First, I describe studies on gene expression and cell cycle alteration by sub-micromolar arsenite. Normal human epithelial keratinocyte (NHEK) were employed as an *in vitro* system to test the effects of trivalent arsenic ($NaAsO_2$, or As_2O_3). The stimulatory effects of arsenite on cell growth, cell cycle alteration, gene expressions, and nuclear trans-activation of the cyclin D1 promoter was examined in the NHEK model system.

In additon to the alteration of gene expression by arsenite, we also studied the mutagenic effect of sub-micromolar arsenite using mitochondrial DNA deletion as a model. There is evidence that arsenic induces chromosome aberrations and inhibits DNA repair in mammalian cells (Moore, M.M. *et. al*.1997). Reactive oxygen species (ROS)

and other organic free radicals may be the cause of gene mutations resulting in carcinogenesis. Arsenite, a weak mutagen, may be a factor that potentiates UV mutagenesis and subsequent carcinogenic processes. Since the mitochondrion genome consists of DNA of about 16 kbp and has few DNA repair mechanisms, it can serve as a good model for studying mutagenesis for weak carcinogens like arsenite. The second part of my report will focus on mitochondrial DNA deletions caused by UV irradiation in arsenite-treated human epithelial cells.

Materials and methods

A. Cell culture and the treatment with arsenite.

Cryopreserved, normal human epidermal keratinocytes (NHEK) obtained commercially (Cambrex Bioscience, Walkersville, MD) were grown in keratinocyte basal medium (Boyce, S.T. and Ham, R.G. 1985) at 0.15 mM calcium and supplemented with 5 mg/ml insulin, 0.1 ng/l recombinant epidermal growth factor, 0.4% bovine pituitary extract, 0.5 mg/ml hydrocortisone, 50 mg/ml gentamicin and 50 ng/ml amphotericin-B (keratinocyte growth medium; KGM).

B. cDNA Microarray analyses:

i) The isolation of mRNA from NHEK cells. (The Promega RNA isolation system is used)

Total cellular RNAs were extracted from NHEKs using the RNAgents RNA isolation kit (Promega, cat. no. Z51211, Maidson, WI) according to the manufacturer's instructions. Briefly, cultured cells were washed with PBS three times before the RNA isolation. Cells were then lysed by adding denaturing solution (26 mM sodium citrate, pH 4.0, 0.5 % N-lauryl sarcosine, 0.125 M β-mercaptoethanol, 4 M guanidine thiocyanate.) The solution was then extracted by Phenol:Chloroform:Isoamyl Alcohol. The aqueous phase was

transferred to a new tube and precipitated by adding one-tenth volume of 2M sodium acetate and an equal volume of isopropanol (-20 $^{\circ}$C for 30 minutes). After centrifugation, the pellet was washed by 75 % ethanol. The RNA pellet was then air-dried and dissolved in nuclease-free water. The RNA samples were examined in agarose gel and stored at -70 $^{\circ}$C.

ii) The cDNA probe for the microarray

The mRNAs (~2 μg) were then reverse transcribed by MMLV reverse transcriptase together with a CDS specific primer mix to make RNA-cDNA hybrids using reagents supplied by Clontech Company. In our laboratory, [α-^{32}P]dATP (3000 Ci/mmol) is used to label on the probes. The RNA-cDNA hybrid was then denatured by 0.1 M NaOH/1 mM EDTA solution for 20 minutes and neutralized with a neutralizing solution (0.5 M NaH_2PO_4 , pH7).

iii) Probe hybridization

The microarray membranes were purchased from Clontech (Figure 5, human cancer array #7742-1; 576 genes and Figure 8, human 1.2 array #7745; 1,203 genes, BD Biosciences-Clontech, Inc. Pala Alto, CA). Before using, the membranes

were rinsed in deionized water. The membranes were then prehybridized at 68°C with ExpressHyb (hybridization solution supplied by Clontech) containing 0.5 mg salmon testes DNA for at least 30 minutes. The hybridization was then performed overnight at 68°C. The next day, the membranes were washed with different concentrations of washing solution containing SSC and SDS (2X SSC, 1% SDS at 68°C for the first three washes, 0.1X SSC, 0.5 % SDS at 68°C for the fourth wash, the last wash was performed with 2X SSC at room temperature). The array membranes were then wrapped and exposed to a phospho-imager screen. The results were scanned and analyzed using Clontech AtlasImage 2.0.

iv) Analysis of array images

In brief, we first aligned all scanned image in the AtlasImage program and saved as GMD file. Then we select "compare two arrays" and import the two GMD files into the program; an example of the compared result is shown in the screen (Figure 6). We then normalized the signals with a "Sum method" (Signals above background from each array were summed. The individual gene signals were then normalized with the ratio of the sums of two arrays). The results were further exported to a spreadsheet for analysis.

C. NHEK growth and viability staining:

1. Cell counts:

For experiments, the culture medium was replaced with fresh medium containing sodium arsenite ($NaAsO_2$) at the indicated concentrations. Medium with or without sodium arsenite was changed for treated or untreated cells every other day. Cell proliferation was determined '*in situ*' using averaged cell counts from 20 to 30 randomly chosen microscope fields per cell culture carried out on the days indicated as described previously (Steinberg, M.L. and Defendi, V. 1982).

2. Neutral red viability assay:

NHEK cells were seeded into 24 well cell culture plates. Cells were allowed to attach overnight, after which culture medium was replaced with fresh medium containing arsenite at the indicated concentrations (0.5 ml medium/well). At the indicated times, the medium in the wells to be tested for neutral red uptake was replaced with 0.5 ml of fresh arsenic-containing medium with neutral red (50 μg/ml) and cells were incubated for 3 hours and then assayed for neutral red uptake. Cells were quickly washed with a solution containing 1% formaldehyde and 1% calcium chloride and the internalized neutral red was then extracted with

500 μl of extraction solution (1% acetic acid, 50% ethanol). Plates were incubated at room temperature with gentle shaking for 15 minutes and absorbance was read at 540 nm in a Spectronic 301 spectrophotometer (Milton Roy).

D. Fluorescence Activated Cell Sorter analysis of DNA content in arsenite-treated NHEK

Cells grown to approximately 70% confluence in monolayer culture were harvested with trypsin-EDTA, washed twice with phosphate buffered saline (PBS) by centrifugation and then fixed by resuspension in 3% formaldehyde in PBS for 1 hour at 4 °C. The fixed cells were washed twice with PBS and resuspended in permeabilization buffer (5 mM HEPES, pH 7.5, 150 mM NaCl, 4% fetal bovine serum, 0.1% Triton X-100) at 4°C. After 10 minutes, the cell suspension was diluted with one volume of PBS, pelleted by centrifugation and then stained with propidium iodide in PBS containing 0.5 mg/ml RNase for 2 hours at room temperature. Cells were washed three times in PBS and used for flow cytometry on a Becton Dickinson LSRII cell sorter. In order to generate histograms, FCS files were translated into Excel spreadsheets using FCS Express software from De Novo

Software (Thornhil, Canada) to allow graphical display of frequency as a linear function of PI fluorescence. Gaussian approximations of the G1, S and G2 subpopulations from which their fractional parts were estimated were modeled using ModFit software package (Verity Software, Topsham, ME).

E. RT- PCR of cyclin D1 gene

Total cellular RNAs were extracted from experimental NHEKs as described above for the cDNA microarray section.

Reverse transcription:

1µg of oligo dT primer $p(dT)_{15}$, Boehringer Mannheim) was mixed with 1~5 µg of total RNA. The tubes were heated in 70°C for 10 minutes and then allowed to cool down to room temperature. The first strand reverse transcription was carried out with MMLV reverse transcriptase at 42 °C for 90 minutes using the PowerScript™ Reverse Transcriptase kit according the protocol provided by the manufacturer (Clontech cat. no. 639500).

PCR amplification:

Two primers mapping within the coding region of cyclin D1 (+114, 4L (Left primer: CCCTCGGTGTCCTACTTCAA) and +504, 3R (Right primer: CTGGCATTTTGGAGAGGAAG) for RT-PCR examination were used for this study. For endogenous control, primers for β-actin were used: (+2147, Left primer: ACACTGTGCCCATCTACGAGG) and (+2954, Right primer AGGGGCCGGACTCGTCATACT).

MMLV reverse transcriptase was applied with primer 3R and the isolated RNAs to make cDNAs. The products of reverse transcription were then used for PCR amplification using both primer 3R and 4L for 30 cycles. The PCR product was expected to be 390 base pairs for cyclin D1 and 621 base pairs for β-actin and their identity was confirmed by DNA sequencing.

F. Real time PCR of cyclin D1 expression in arsenite treated cells:

Real time PCR (RQ method):

cDNAs from reverse transcription were used as templates for real time PCR in a 7500 Real Time PCR System (ABI, Foster City, CA). Reactions were carried out in 0.2 ml optical tubes with TaqMan PCR master mix and protocols from ABI. Primers spanning exons 2 and 3 within the cyclin D1

coding region were used together with a FAM/MGB dye labeled cyclin D1 probe; the primers and probe were purchased as a kit from Applied Biosystems (ABI cat. no. 4331182). Primers and a probe for β-actin (ABI cat. no. 4333762F) were used for endogenous controls and detection tubes were set up in the same manner as cyclin D1 detection tubes. All samples were run in duplicate in both cyclin D1 and β-actin gene expression assay mixtures. Data were then collected and analyzed in SDS v1.3.1 software from Applied Biosystems for relative levels of gene expression (Figure 15).

G. Western blot analyses

For Western blots, cells were trypsinized and then washed ×3 in PBS and pelleted by centrifugation. The pellets were resuspended in 100 µl SDS sample buffer (without β-mercaptolethanol and bromophenol blue). Protein concentrations were determined using a protein assay kit (RC-DC protein assay kit; BIO-RAD, Hercules, CA). β-mercaptolethanol and bromophenol blue were added after protein concentrations were adjusted. Samples were boiled for 5 min and 10 µg of protein from each sample was loaded onto SDS gels for electrophoresis. The separated proteins in the SDS-gel were then transferred to a nitrocellulose (NC) membrane. Membranes were processed for reaction with

antibodies essentially as described previously (Edelman *et. al.* 1985) and cyclin D proteins were visualized using a mouse monoclonal primary antibody (Labvision, Fremont, CA) and an alkaline phosphatase (AP) or horseradish peroxidase (HRP) conjugated secondary antibodies using the appropriate substrates to develop color. Images of the Western blots were scanned to disk as TIFF files and relative levels of cyclin D were quantitated using ImageQuant software (Clontech, Palo Alto, CA).

H. Electrophoretic Gel Mobility Shift Assay (EMSA)

Probe design and synthesis.

The following oligonucleotides were used as probes in EMSA assays for nuclear factors that bind to the Tcf4, CREB (cAMP binding element) and AP1 promoter elements in the cyclin D1 promoter (from Nagata, D. *et. al.* 2001 Table 2 and Figure 20):

Tcf4: TCF4D1(sense): 5′ ccgg**gctttgatc**tttgc 3′ and
TCF4D2(antisense): 5′ gcaaa**gatcaaagc**ccgg 3′;
cyclin D1 promoter location: -72 to -82

CRE: CREB1 (sense) 5′caacag**taacgtca**cacggat 3′ and
CREB2 (antisense) 5′ atccgtg**tgacgtta**ctgttg 3′;
cyclin D1 promoter location: -48 to -58

AP1: APW1 (sense) 5′ tccga**tgagtcag**ttctagagga 3′ and
APW2 (antisense) 5′ tcctctagaa**ctgactca**tcgga 3′;
cyclin D1 promoter location: -947 to –953

Each pair of oligonucleotides was combined in equal molar amounts to a final concentration of 2 pmol/µl. Tubes were boiled for 5 min and gradually cooled down to form double stranded DNA fragments. The double stranded probes were end labeled with γ-^{32}P-ATP and T4 polynucleotide kinase according to the protocol of the supplier (Promega, M4101). Probes were purified by ethanol precipitation in the presence of ammonium acetate and dissolved in nuclease free water.

Electrophoretic Gel Mobility Shift Assays (EMSA) of cyclin D1 promoter

Nuclear extracts were isolated from both control and arsenite-treated NHEK cells followed the procedure described by Edmead (Edmead, C. *et. al.* 1999). Briefly, trypsinized cells were washed in PBS and then homogenized in 2 ml of hypotonic buffer (10 mM HEPES, pH 7.9, 1.5 mM $MgCl_2$, 10 mM KCl, 0.5 mM DTT, 0.1% NP-40). Nuclei were pelleted by centrifugation in hypotonic buffer containing

10% sucrose and then resuspended in 150 µl icecold extraction buffer (10 mM HEPES, pH 7.9, 1.5 mM $MgCl_2$, 400 mM KCl, 0.2 mM EDTA, 0.5 mM DTT and a protease inhibitor cocktail (Roche Molecular Biochemicals)). The mixtures were incubated for 20 min at 4 °C with gentle agitation and then centrifuged at 14,000×g at 4 °C for 15 min. The protein concentrations of the supernatants were determined using the DC Protein Assay kit from Bio Rad (Hercules, CA). The nuclear extracts (5 µg) were then incubated with [γ-^{32}P] ATP, 5′ end-labeled DNA fragments for 30 min in binding buffer (10 mM Tris–HCl, pH 7.5, 50 mM NaCl, 1 mM $MgCl_2$, 4% v/v, glycerol, 1 mg/ml salmon testes DNA) and run into an 8% non-denaturing PAGE in TAE buffer. Autoradiography was carried out with a STORM 840 phosphoimager (Molecular Dynamics).

I. Statistical Analysis:

For each of the experiments replicates were performed as indicated in the figure and table legends and all results are shown as the mean value ± SEM. For the real time PCR and cyclin D1 induction experiments (Figures 16 and 18) statistical significance was determined using the paired Student's t-test (Student’s t test for paired samples). For the experiments shown in Table 1 and Figures 11 12, and

22 in which more than three groups were compared, levels of significance were determined by a one-way analysis of variance (ANOVA) followed by a post hoc analysis using the Fisher's Least Significant Difference (LSD) test with a software package from SPSS software (SPSS v.12.0; SPSS Inc, Chicago, IL). Mean values found to be significant at the 0.05 level or less as compared to the relevant controls are indicated in the figure legends.

Results:

1. cDNA microarray analyses of gene expression in arsenite treated NHEK

Several previous reports have suggested that induction of D-type cyclins may be involved in the oncogenic properties of arsenic (Zhao, S. *et. al.* 2002; Vogt, B.L. and Rossman, T.G. 2001). We therefore used human cancer and human 1.2 cDNA microarray (Figure 5, human cancer array #7742-1; 576 genes and Figure 8, human 1.2 array #7745-1,203 genes, BD Biosciences-Clontech, Inc. Pala Alto, CA) to examine expression of D type cyclins as well as that of components of the Wnt signaling pathway that regulates cyclin D expression using cDNA probes created from NHEK treated for 3 days with either 200 and 400 nM sodium arsenite. At 200 nM arsenite, expression of most of the Wnt pathway genes remained relatively unmodulated although β integrin 6, Wnt 10B and β catenin were all induced about 2 fold. In contrast, expression of β integrins 4 and 5 was substantially reduced by arsenite treatment (Figure 7). Expression of the integrins and Wnt genes was not significantly changed at 400 nM arsenite as compared with 200 nM but, at the higher concentration, the disheveled (DSH/DVL-1) and integrin linked kinase (ILK) genes were

induced about 3 fold while neither of these genes were induced at 200 nM arsenite. Both concentrations of arsenite brought about marked induction of the D type cyclins, particularly cyclin D1 which showed a 3.6 fold induction at 200 nM and a 5.1 fold induction at 400 nM.

2. Expression of other genes altered by exposure to arsenite at different Time points.

In addition to changes in expression of cyclin D1 and components of the Wnt signaling pathway, we also observed changes in expression of several genes not involved in Wnt signaling in cells treated with 400 nM arsenite for 4, 24, and 72 hours (Figure 9, 10).

- Ataxia telangiectasia (ATM), heme oxygenase 2 (HO2) ,glutathione S-transferase A1 (Figure 9) and Ikappa B kinase complex-associated protein (IKAP) (Figure 10) were induced within 4 hours (2.1, 2, 3.1 and 1.8 fold compared to untreated controls) and the increase was observed for up to 3 days following treatment (2.6, 2.2, 6.9 and 6.3 fold).

- Genes whose expression wasn't clearly induced at 4 hour but was upregulated at later time points, included cyclin D1 (5.8 fold at 72 hour-treatment), MCM2 DNA replication licensing factor (3.5 fold at 72 hour), proteasome

component C5 (2.2 fold), matrix metalloproteinase 15 (2.2 fold), c-mos proto-oncogene (2.4 fold) (Figure 10).

- Another group of genes showed expression that was increased at 4 hours, but exhibited a decreasing pattern of expression at 24 or 72 hours: heat shock related 70-KDa protein 2 (5.4, 0.9, and 1.0 fold compared to untreated control at 4, 24, and 72 hour), HSP90A (2.1, 1.0, and 1.1 fold), DNA topoisomerase 1 (TOP1, 5.6, 0.5, and 0.8 fold)), replication factor C 38-KDa subunit (RFC38, 2.6, 2.2, and 1.2 fold), MAP kinase kinase 3 (MKK3, 2.7, 0.7, and 0.6 fold)) and heme oxygenase 1 (HO1, 2.0,, 0.3, and 0.7 fold) (Figure 9).

- Heat shock protein HSC71 and excision repair protein ERCC6 showed induction at 4 and 24 hour but not at 3 days (Figure 10). HSC71 showed an expression ratio of about 1.9, 2.6, and 1.0 fold at 4, 24, and 72-hour treatment and ERCC6 had 2.3, 4.5, and 1.2 fold compared to untreated control.

- Some genes exhibited increased expression at 4 and 72 hour, but not at 24 hour. Cdk4, GADD153, GADD45, DNA repair protein XRCC1, and DNA excision repair protein ERCC3 are in this group (Figure 10). The expression patterns at

4, 24 and 72 hour treatment were: 1.7, 1.0, 2.5 for cdk4; 5.9, 1.5, 9.8 for GADD153; 1.8, 1.0, 3.3 for GADD45; 4.5, 0.3, 5.0 for XRCC1; and 4.3, 1.5, 2.4 for ERCC3.

In general, this microarray profile appeared to exhibit a reciprocal pattern of expression of cell proliferation vs. stress response within 3-day periods. Sub-micromolar arsenite stimulated stress response genes mostly within 4 hours while cell growth signals were induced at about 24 hours and lasted until 72 hours.

3. Cell proliferation and neutral red staining:

We tested the effect of submicromolar concentrations of sodium arsenite on the proliferation of cultured normal human epidermal keratinocytes (NHEK). As shown in figure 11, at all 3 concentrations tested, arsenite treatment produced a marked, dose-dependent stimulation of cell proliferation as compared with untreated controls that was seen within the first 24 hour of treatment. Over this time period, cells treated with 200 nM arsenite showed a 32% increase in cell number while those treated with 400 and 800 nM arsenite showed increases of 58% and 50%, respectively.

Increases in cell number were also evident after 2 days of arsenite treatment although the dose dependent increases were somewhat smaller: 2%, 20% and 21% at 200 nM, 400 nM

and 800 nM arsenite, respectively. However, after 3 days of treatment only cultures treated with 400 nM arsenite still showed a significant stimulatory effect (27%) while cells treated with 800 nM arsenite showed a slight decrease (about 2%) in cell number compared to untreated controls. The stimulatory effect of arsenite on proliferation was accompanied by a corresponding increase in viability of NHEK over the treatment period as determined by neutral red uptake (Figure 12). Dye uptake by cells treated with 200 and 400 nM arsenite showed a parallel increase at 200 and 400 nM arsenite at all the time points. Cells treated with 800 nM arsenite showed an increase in both NR uptake and proliferation relative to controls at all time points but the stimulatory effects were much less than those seen at the lower arsenite concentrations.

4. FACS Analysis of DNA Content in NHEK

Since the stimulation of cell proliferation by arsenite is likely to involve alterations in cell cycle kinetics, we examined changes in cell cycle parameters in NHEK treated for 2 days with 400 and 800 nM sodium arsenite. The cells were harvested, stained with propidium iodide (PI) and DNA content was analyzed by flow cytometry. Separate peaks corresponding to the G1 and G2 compartments were

distinguishable in the FACS histogram and their relative fractions of the total population were estimated from the peaks (Figure 13 and Table 1). These experiments showed that arsenite treatment at both concentrations tested brought about a significant shift into the G2/S compartment in cells treated with either 400 or 800 nM arsenite, and was more pronounced at 800 nM, when compared to untreated controls. For the experiments shown in Table 1, the relative shift into G2 represented about 13% of the cell population exposed to 800 nM arsenite.

5. RT-PCR and Real Time PCR of cyclin D1 gene expression

RT-PCR

Enhanced expression of cyclin D1 transcription was demonstrated by RT-PCR using reverse transcribed RNAs from arsenite-treated NHEK as templates and amplimers located within the cyclin D1 coding region.

Figure 14 shows a strong band corresponding to the anticipated 390 bp product was visible in NHEK treated with arsenite for 3 days at either 200 or 400nM arsenite (left images).

For long-term treatment, a set of NHEK was exposed to 400nM arsenite continuously for periods of 14 and 40 days.

No visible PCR product was seen in untreated controls under the PCR conditions used while 400 nM arsenite-treated NHEK exhibited clear visible PCR products (Figure 14, right images). There was a marked time-related increase in the intensity of the PCR bands in the arsenite treated cells while no visible or very small amounts of RT-PCR products were observed using RNAs from untreated controls at these time points.

Real Time PCR

Enhanced expression of cyclin D1 transcription was also demonstrated by real-time PCR using reverse transcribed RNAs from arsenite-treated NHEK as templates and amplimers spanning exons 3 and 4 within the cyclin D1 coding region. Figure 16 shows that, after 1 day of exposure of NHEK to 400 nM arsenite, cyclin D1, transcription was slightly upregulated by about 8% relative to untreated controls. This increased to a maximal induced level of almost 3.2-fold after 3 days and about 1.5-fold after 5 days. After 7 days, cyclin D1 transcription levels were not induced but, in fact, were about 19% lower in the arsenite-treated cells than in the controls. This pattern of induction may be linked to the growth of the cells; induction of cyclin D1 transcription was highest when the cells are growing

exponentially at 3 days but was reduced as the cells became confluent.

6. Western blot analyses

While arsenite at 400 nM concentrations was found to produce significant upregulation of cyclin D transcription within 3 days (Figure 16), we observed no induction of cyclin D levels for cells exposed to 100 and 200 nM arsenite over this treatment period (Figure 17). The time course of induction of cyclin D proteins at 400 nM is also illustrated in Figure 18. Cyclin D levels in NHEK treated with 400 nM arsenite for a period of 7 days were quantitated in image scans of Western blots using ImageQuant software. Averaged signals examined at various times during this period of time showed that cyclin D levels increased continuously over the 7 days of arsenite treatment. Cyclin D levels were increased by about 30-40% within the first 4 days but then increased to 2.0-fold vs. controls on day 7.

7. Electrophoretic Mobility Shift Assays (EMSA)

The cyclin D1 promoter contains binding sites for a number of transcription factors through which gene expression can be modulated. Since we had previous

evidence from microarray analyses that arsenite might upregulate signaling pathways that effect the activities of Tcf4, the cAMP response element binding protein (CREBP) and AP1 (Figure 19), we examined the binding of these factors to their cognate elements in electrophoretic mobility shift assays (EMSAs) using nuclear extracts derived from NHEKs exposed to 400 nM arsenite for treatment periods of 1, 3, 5 and 7 days (Figure 21 and 22). These experiments showed that binding of AP1 and CREB was significantly upregulated in cells treated with arsenite for 3 days but not at the 5 and 7 day time points, consistent with the real-time PCR results shown in Figure 16. After 3 days of exposure to arsenite, enhanced binding of AP1 was most dramatic (1.9-fold) while binding of CREBP was also increased but only by about 59% over that seen in untreated controls. There was also a slight increase (34%) for AP1 binding at day 1. However, binding of nuclear factors to the Tcf4 binding sequences remained virtually unchanged throughout the treatment period.

We also performed EMSA with other trans-activation elements that may activate cyclin D1 gene expression. SP1, NFκB and STAT binding sequences were located in the promoter region of the cyclin D1 gene and EMSA probes were made in a

similar manner as other EMSA probe described before. Figure 23 shows that SP1 shows essentially the degree of shift in both untreated and arsenite-treated NHEKs while NFκB and STAT showed very weak interaction to our designed DNA sequences(data not shown).

8. Gene expression in UVB irradiated cells treated with arsenite

We also performed microarray analyses experiments to study gene expression in NHEK treated with 400 nM arsenite for 24 hours and then irradiated with 27 mJ/cm^2 UVB irradiation using Clontech's human cancer cDNA microarray (Figure 5). The results are summarized in figures 24~28.

i. Cell cycle regulatory genes: (Figure 24)

In these human cancer arrays, cyclins A, D1, D2 and D3 were upregulated by 400 nM arsenite, but only cyclin D3 was induced by UVB. CDK 4 and 6 were slightly increased by UVB irradiation or both. Expression of cyclin G2 was not induced by arsenite, but was enhanced by UVB alone or UVB irradiation and arsenite treatment. We also saw upregulation of several G2/M regulatory genes such as cyclin B1, CDC2, CDC2-related protein kinase (PISSLRE),

CDC2-related protein kinase CHED, CDC10, and CDC 25B by 400 nM arsenite, but expression of these genes was not induced by UVB or UVB + arsenite. Expression of three CDK inhibitors (CDKN1A, p16-INK4, and p19-INK4D) was increased in UV irradiated cells. Three extracellular signal-regulated kinases, MAPK p38, ERK3 and ERK6 were also increased by arsenite, but not by UVB irradiation alone. Proliferating cyclic nuclear antigen (PCNA), a component of DNA polymerase □, was slightly induced in all three-treatment conditions. Figure 24 also shows that cyclin A was down-regulated by the combination of arsenite and UV.

ii. Wnt signaling pathway genes (Figure 25)

Of genes representing components of Wnt signaling pathway, most of the cadherins seem to be affected very little by either arsenite or UV. Frizzled and its' homologs were slightly induced in the presence of both arsenite and arsenite + UV irradiation, but not by UV alone. Amoung several Wnts detected in the array, Wnt-2 showed strong increase by arsenite, UVB irradiation and arsenite plus UVB. Expression of the other Wnts (5A, 8B, 10B/12, and 13) was slightly increased in arsenite or UVB irradiation while Wnt-10B/12 and Wnt-13 were significantly induced by 2.5- and 2.8- fold in the UVB/arsenite cells.

Expression of β-catenin exhibited a slight increase in arsenite treated cells but not in UV and UV/arsenite samples.

Expression of the integrins was increased at 400 nM arsenite. Integrins α4, αE, β1, and β6 showed strong induction while the others exhibited only a slight increase in arsenite treated NHEKs. On the contrary, expression of integrins in UVB irradiated NHEKs remained unchanged or decreased. The combination of UV with arsenite also lowered the expression of most integrins. Integrin linked kinase (ILK) and the disheveled (DVL) genes were induced about 3 and 2 fold in arsenite treated cells while adenomatous polyposis coli protein (APC) only increased about 1.2 fold. UVB also increase the expression of ILK but not APC and DVL.

iii. Growth factor/Receptors (Figure 26)

The expression of a number of growth factor and growth factor receptors was found to be modulated by arsenite treatment alone. The expression of ERBB-3 (an EGF receptor) was mainly up-regulated by arsenite but unaffected by UV or UV + arsenite. The expression of vascular endothelial growth factor receptor 1 (VEGFR1) was upregulated in all three treatments conditions while VEGF-C

was only slightly increased by arsenite only and was decreased by UV and the combination of UV and arsenite. The insulin-like growth factor binding protein (IGFBP) related gene, insulin-like growth factor-binding protein 3 (IGF-binding protein 3), early growth response protein 1 (hEGR1), and colon carcinoma kinase 4 precursor (CCK4), were induced in cells treated with arsenite + UV. Expression of the retinoic acid receptor, SL cytokine precursor, and stromal cell derived factor 1 precursor (SDF1) were somewhat down regulated by UV or "UV + arsenite". Expression of B-cell growth factor 1 precursor (BCGF1) and replication factor C 37-kDa subunit (RFC37) was not changed in the arsenite-treated cells but was decreased after UV irradiation and in cells exposed to aresnite + UV.

iii. Apoptosis related genes (Figure 27)

In this group, a retinoblastoma-binding protein RBQ-3 which is part of the transcriptional coactivator ASCOM complex was up-regulated by 400 nM arsenite (Figure 27; Goo, Y. H., *et. al.* 2003). Exposure to UV alone or arsenite + UV treatments didn't enhance the expression of RBQ-3 gene. Interleukin-1 beta convertase precursor (IL-1BC), a protease that cleaves at (W/L) EHD motif to convert

interleukin-1 beta was enhanced if cells were treated with arsenite or both arsenite and UVB.

As shown in figure 27, expression of FAS soluble protein, p53-associated mdm2 and CD40 receptor-associated factor 1 (CRAF1) was slightly induced by arsenite + UV. On the other hand, several other apoptosis related genes such as caspase-10 and death-associated proteins (DAP kinase 1) and death receptor 5 were mostly down-regulated by UVB irradiation. In the presence of arsenite with UVB seemed to eliminate the effects of UVB irradiation on these death-related genes.

v. Other genes (Figure 28)

Expression of several scaffold proteins such as tenacin-R, vitronectin, and caveolin-1 was increased in cells treated with 400 nM arsenite (Figure 28). Tenacin-R was induced in UV- or arsenite+UV- treated cells while vitronectin and caveolin-1 were largely unaffected by UV irradiation. CD59 glycoprotein, interferon gamma precursor (IFN-gamma), and neurotrophin-4 (NT4) also exhibited slight increases in arsenite treated NHEKs. In cells treated with arsenite + UV, neurotrophin-4 was highly induced. Expression of DNA topoisomerase I (TOP1), DNA and topoisomerase II alpha (TOP2A) were inhibited by UVB, while

TOP2A was induced by arsenite alone. Expression of matrix metalloproteinases (MMP 9, 10, and 12) was mostly decreased by UVB while arsenite or arsenite + UV also caused some degree of down-regulation.

Discussion:

I. Microarray profiles of NHEK treated with sub-micromolar arsenite

A. Stress induced genes:

In our gene expression profiles, treatment of NHEK cells with sub-micromolar arsenite altered the expression of many genes. In figure 9 and 10, gene expression of stress response and growth signals were compared in 4, 24, and 72 hours time points. For signaling pathways that respond to stress caused by arsenic, heat shock proteins were expected to be induced in response to many stress signals. Arsenite is believed to cause oxidative stress and may enhance the risk of DNA damage indirectly (Kessel, M. *et.al.* 2002). Therefore, the induction of DNA repair related genes such as Ataxia telangiectasia (ATM), heat shock proteins, DNA repair proteins, GST-A1 and growth arrest and DNA damage induced genes (GADDs) was anticipated. We observed increases in gene expression of all these genes after short treatment times. Induction of some genes was maintained over long periods (eg, ATM and GST-A1); while some went back to normal or less than control by 72 hour (eg. HSPs). Others showed an increase-decrease-increase pattern on the

4-24-72 hour time points (eg. DNA repair proteins and GADDs).

ATM kinase is known to play a key role for cells to respond to DNA damage caused by ionizing radiation. It can phosphorylate p53 and other downstream proteins in order to arrest the cell cycle to permit DNA repair. GADD 45, one of the p53 targets, can bind to, and dissociate the cdc2/cyclin B complex and cause cell cycle arrest (Mak, S.K. *et. al*. 2004). The observation that DNA repair proteins XRCC1, ERCC3 and ERCC6 were induced at early time points may indicate that DNA was damaged by arsenic treatment. GADD153 is a reactive oxygen species (ROS) inducible gene mainly responding to endoplasmic reticulum (ER) stress (McCullough, K.D. *et. al*. 2001., Ikeyama, S. *et. al*. 2003.). Glutathione S-transferase A1 is a GST that provides protection against cellular oxidative stress (Sarkar, D. *et. al*. 2001).

MAPKK3 (MKK3) and Ikappa B kinase complex-associated protein (IKAP) were also induced at this arsenite concentration. IKAP is involved in the regulation of the activation of stress response through c-jun N-terminal kinase (JNK) signaling pathway (Holmberg, C. *et. al*. 2002). MKK3/MKK6 and JNK are known to be involved in MAPK stress response signals. (Gross, E. A. *et. al*. 2002). There are

at least three major MAP kinase pathways which have been well characterized: the extracellular signal regulated kinase (ERK1/2), c-jun N terminal kinase (JNK1/2), and p38 kinase pathways. Generally, activation of the ERK pathway is related to cell proliferation while the JNK and p38 pathways are associated with cell death induced by physical and chemical stressors (Muscarella, D. E. *et. al*. 2002). There are some reports showing that JNK and p38 pathways are activated by arsenite (Muscarella, D. E. V. *et. al*. 2002).

B. Cell cycle regulation:

We also observed changes in expression of several genes that regulate cell growth. Cyclin D1 is an effector of the G_1/S transition. Our microarray and western blot analyses showed upregulation of cyclin D1 expression over fairly long periods of *in vitro* exposure. This result indicates that cyclin D1 expression was induced by sub-micromolar arsenite as a later consequence suggesting there may be other upstream regulations to initiate the induction of cyclin D1.

In the microarray results, proteins required for DNA replication such as MCM2 DNA replication licensing factor, DNA topoisomerase 1, and replication factor C 38-KDa

subunit were altered by submicromolar concentrations of arsenite. We also observed an increase in c-mos and MMP15 in our microarray studies. Proto-oncogene c-mos is known to be involved in meiotic division through the MAPK cascade. Matrix metalloproteinase 15 is known to promote tumor invasion and may be involved in metastasis and apoptosis-resistance (Abraham, R. *et. al*. 2005).

From these findings, it appears that sub-micromolar levels of arsenic may cause oxidative damage in NHEKs. Stress response genes were induced quickly. However, this low dose of arsenite can also be a growth stimulus. GADDs, HSPs, ATM, HOs, and DNA repair enzymes were rapidly induced possibly in response to DNA damage caused by arsenite. At day 3 the induction of growth signals like cyclin D1, cdk4, MCM2 and MMP15 may indicate growth stimulation after cells counteracted stress damage.

II. Stimulation of cell growth and induction of cyclin D1 by sub-micromolar arsenite:

Here, we have studied the effects of submicromolar concentrations of arsenite on gene expression in arsenite-treated NHEK. The experiments described were instigated partly by microarray studies which showed that exposure of cultured human keratinocytes to submicromolar levels of

arsenite led to a marked induction of D type cyclins (Figure 7). The microarray findings also showed that arsenite treatment induced elements of signaling pathways known to activate the cyclin D promoter, including the cyclic AMP response element binding protein (CREBP) and various tyrosine kinases and serine/threonine kinases involved in MAP kinase signaling (figures 9, 10,and 19). Earlier reports had also demonstrated the induction of D type cyclins by arsenic in other systems (Zhao, S *et. al.* 2002; Vogt, B.L. and Rossman, T.G. 2001). D type cyclins are G1 cyclins whose long-term overexpression is thought to be oncogenic by acting to abrogate G1 checkpoint controls. In the experiments described here, we employed human epithelial cells because of the observation that arsenic exposure has been clearly linked to the occurrence of skin carcinomas (Tseng, W.P. 1977). Most in vitro studies of arsenic employ supramicromolar concentrations although concentrations in the submicromolar range more closely simulate the conditions generally associated with chronic exposure in arsenic polluted areas (Gomez-Caminero, A. *et. al.* 2001). Low concentrations of arsenic have been found to be growth stimulatory while higher concentrations induce apoptosis (Liao, W.T. *et. al.* 2004) and these opposing effects are thought to bear a direct relationship to the

paradoxical effects of arsenic as both a carcinogen and as a chemotherapeutic agent. Although there is some evidence that arsenic may be weakly mutagenic (Hei, T.K. *et. al.* 1998; Li, J.-H. and Rossman, T.G. 1991; Moore, M.M. *et. al.* 1997; Noda, Y. *et. al.* 2002) or act as a comutagen (Li, J.-H. and Rossman, T.G. 1989a, 1989b; Hamadeh, H.K. *et. al.* 2002; Vogt, B.L. and Rossman, T.G. 2001), its oncogenic properties are generally thought to derive from epigenetic mechanisms that ultimately effect the cell cycle. Previous reports have implicated activation of a variety of signaling pathways including those that regulate levels of D type cyclins as important targets of arsenic (Hyun Park, W. *et. al.* 2003; Li, X. *et. al.* 2003; Rossman, T.G. 2003; Zhao, S. *et. al.* 2002) that may be related to oncogenesis. Induction of D type cyclins fits well with models based on mechanisms of oncogenesis that involve abrogation of the cell cycle checkpoints at the G1/S interface and which allow the fixation of unrepaired, oncogenic mutations following DNA replication. Here we found significant induction of cyclin D1 and, using real-time PCR, we showed that cyclin D1 expression was, in fact, upregulated at the transcriptional level by arsenite treatment. In addition, the EMSA experiments shown in figure 22 indicate that the stimulation of cyclin D transcription by arsenite derives

mainly from induction of elements of the MAP kinase pathway that ultimately activate AP1. Previous reports have described enhanced binding of nuclear factors to AP-1 binding motifs in arsenite-treated HEL30 cells (Corsini, F. *et. al.* 1999), rat LEC cells (Lau, A.T.Y. *et. al*. 2004) and immortalized mesencephalic cells (Felix, K. *et. al*. 2005). To a lesser, but significant extent, arsenite also brought about induction of CRE binding elements. Stimulation of the cyclin D1 promoter via CRE binding elements by arsenite does not seem to have been previously reported and therefore appears to represent a novel finding. Induction of promoter binding elements was maximal after about 3 days of arsenite exposure which also corresponded to the period of time when cyclin D1 transcription was also induced to maximal levels. Interestingly, the correlation between cellular levels of cyclin D and cyclin D transcription was evident only during the time when cells were in exponential growth (~days 1–5) but not when cells reached confluence at day 7. Translation of cyclin D1 mRNA into protein may be modulated by a number of factors including the activity of eukaryotic initiation factor 4E (Rosenwald, I.B. *et. al.* 1993) or cyclin D. cyclin D1 protein degradation is mediated via GSK-3β (Mori, J. *et. al.* 2005). In the latter study in particular, cyclin D1 levels in cells in G0 were

found to be modulated by degradation of cyclin D1 resulting from phosphorylation. Altered turnover of cyclin D1 in quiescent cells could account for the increase in cyclin D1 levels at day 7 which do not appear to be clearly related to levels of transcription in the confluent cells.

Recently, Rossman and Burns (Rossman, T.G. *et.al.* 2001, Burns, F.J. *et. al.* 2004) reported a mouse model of carcinogenesis in which arsenic appeared to function as a cocarcinogen in the induction of skin carcinomas brought about by ultraviolet irradiation. This report also suggested that the oncogenic properties of arsenic might stem from upregulation of cyclin D. This would result in abrogation of normal checkpoint controls which would, in turn, allow epidermal cells containing UV-damaged DNA to transit abnormally into S phase. Our microarray results also show that sub-micromolar arsenite enhances the expressions of stress response genes and cyclin D1 at about the same pace (Figure 10). The consequence may be that cells may pass the G1/S transition without complete check.

III. Synergistic/additive effects of arsenite and UVB irradiation:

Gene expression was also examined using samples treated with 400 nM arsenite, 27 mJ/cm^2 UVB irradiation and 27 mJ/cm^2 UVB plus 400 nM arsenite. Patterns of altered expression of genes involved in cell cycle regulation, Wnt signaling, growth factors, and apoptosis are described below.

A. G1 cell cycle controls:

Our results showed that all three D type cyclins were induced by arsenite while their binding partners CDK4/CDK6 showed only slightly above normal induction. The possible reason is that unlike D cyclins which have short half-lives, the activities of CDK4/CDK6 do not rely on their mRNA levels. The pre-existing CDK4 is not active itself until it binds to newly synthesized cyclin D1. The complex can then phosphorylate retinoblastoma protein (RB) and E2F transcription factor can be released to transcribe downstream genes such as cyclin E and cyclin A for cell proliferation (Bartek, J., and Lukas, J. 2001). Cyclin A showed an expression pattern similar to the D type cyclins in this profile. (Figure 24.) The G type cyclins have been shown to respond to DNA damage caused by actinomycin-D treatment and their expression was found to be p53 dependent (Bates, S. *et. al*.1996., Horne, M.C. *et. al*.

1996). This may explain why it is strongly induced in UVB irradiated and UVB + arsenite groups.

B. G2 cell cycle controls:

In our cDNA human cancer array, we observed some G2/M regulatory genes whose expression was significantly modulated by 400 nM arsenite. The major players in G2/M phase control, cyclin B and CDC2 (CDK1 p34) were both up-regulated by arsenite alone. The cyclin B/cdc2 complex is activated by phosphorylation of Thr160 and dephosphorylation of Thr 14 and Thr 15. The phosphorylation of Thr 160 is catalyzed by cyclin activating kinase (CAK, cdk7/cyclin H), Phosphorylated Thr 15 can be dephosphorylated by CDC25 phosphatase. The activity of CDC25 is regulated by a checkpoint-activated kinase (Chk1; Smits, V.A. *et. al*.2001.).

C. MAPK signals:

In addition to the G1, G2 phase controls, our cDNA microarray analyses also detected two extracellular signal regulated kinases (ERK3 and ERK6) whose expression was upregulated by arsenite. Also, MAPK p38 and PCNA were increased by arsenite in our cDNA microarray data. ERK3 shares ~50 % identity with ERK1 and ERK2 (Zheng, C. F. and

Guan, K. L. 1994). ERK6 was thought to be activated through MLK-related kinase (MRK) via MKK3/MKK6 and JNK (Gross, E. A., Callow, M. G., Waldbaum, L., Thomas, S., and Ruggieri, R. 2002.). The EGFR-Shc-Grb2-MEK1/2-ERK1/2 pathway stimulated by arsenite has been reported in several studies (Tanaka-Kagawa, T. *et. al*.2003., Lau, A.T. *et. al*. 2004). However, some reports also showed that JNK and p38 pathways were activated by arsenite (Muscarella, D. E. *et. al*. 2002). The cytotoxic and mitogenic effect of arsenite depends on the concentration and time that we treated cells.

D. Apoptosis genes:

Expression of most of the apoptosis related genes represented on the microarrays employed was altered by the UVB irradiation. However, we can still see several death related proteins (FAS, death-associated protein kinase 1, death domain receptor 3, and death receptor 5) whose expression was down regulated by arsenic treatment. This decrease of apoptotic signals probably does not account for much of the stimulation of cell proliferation, but rather suppresses cell growth by increasing the fraction of cells undergoing apoptosis. It has been shown that high levels of arsenite (200 μM) suppress JB6 mouse epidermal cell

transformation while low dose (<25 μM) stimulateed colony formation in soft agar (Huang, C. *et. al*. 1999). The inhibition of cell transformation by high concentration of arsenite was found to be regulated by a JNK-dependent, p53 independent cell death pathway. Our results showed that the apoptosis signals were decreased by the low concentration of arsenite suggesting that the submicromolar arsenite didn't enhance or even lower the signals for cell death.

E. Other genes:

There were also several other genes/proteins altered by arsenic from our cDNA microarrays. For example, Tenascin-R, vitronectin precursor, caveolin-1 were up regulated by arsenite, but not by UV irradiation. Some matrix metalloproteinases such as MMP9, MMP10, and MMP3, were lowered by either arsenite or arsenite+UV. Tenascin-R is an extracellular matrix (ECM) protein which is able to enhance neurite growth by the binding to the neural EGF family member CALEB (Schumacher, S., and Stube, E. M. 2003). Vitronectin is an important component of tissue extracellular matrix (ECM) which may bind to IGFBP-5 and modulate IGF-1 action to stimulate cell migration (Nam, T., Moralez, A., and Clemmons, D, 2002). Caveolin-1 was known

to modulate the functions of many signal transducers such as epidermal growth factor receptor (EGFR), platelet-derived growth factor receptor (PDGFR), insulin receptor, Shc, Grb-2, mSOS-1, and ERK1/2 (Shaul, P. W. *et. al*.1998). Caveolin-1 was also thought to activate the PI3-kinase/Akt pathway and increase the cytotoxicity of arsenite (Shack, S. *et. al*.2003.). Interleukin-1 is a potent activator of immune and inflammatory responses which could rapidly activate some transcription factors including, nuclear factor-κB (NF-κB) and activator protein-1 (AP-1). NF-κB and AP-1 are important regulators of many cytokine genes such as IL-6, IL8, monocyte chemotactic protein-1 (MCP-1). It is also known that the interaction of TNF receptor associated factor 6 (TRAF6) with c-Src can synergistically induce AP-1 activation and its downstream pathway: PI3-kinase-Akt-JNK (Funakoshi-Tago, M. *et. al*.2003). Therefore, it is possible that changes in interleukin gene expression may be involved in the signal responses effected by sub-micromolar arsenite treatment.

In summary, we have employed cultured human keratinocytes exposed to submicromolar concentrations of arsenite as an *in vitro* model system to study changes in cyclin D1 expression and other genes that may be related to

the oncogenic processes that are known to be associated with arsenic exposure in human skin. Our findings suggest that arsenic-induced changes in transcription of the cyclin D1 gene is effected, at least partly, via binding of elements to the AP1 and CREB transactivation site in the cyclin D1 promoter. Our cDNA microarray studies directed our research focus on enhanced cyclin D1 expression and related gene regulation. The gene expression profiles will also serve as a basis for future studies of arsenic induced carcinogenesis.

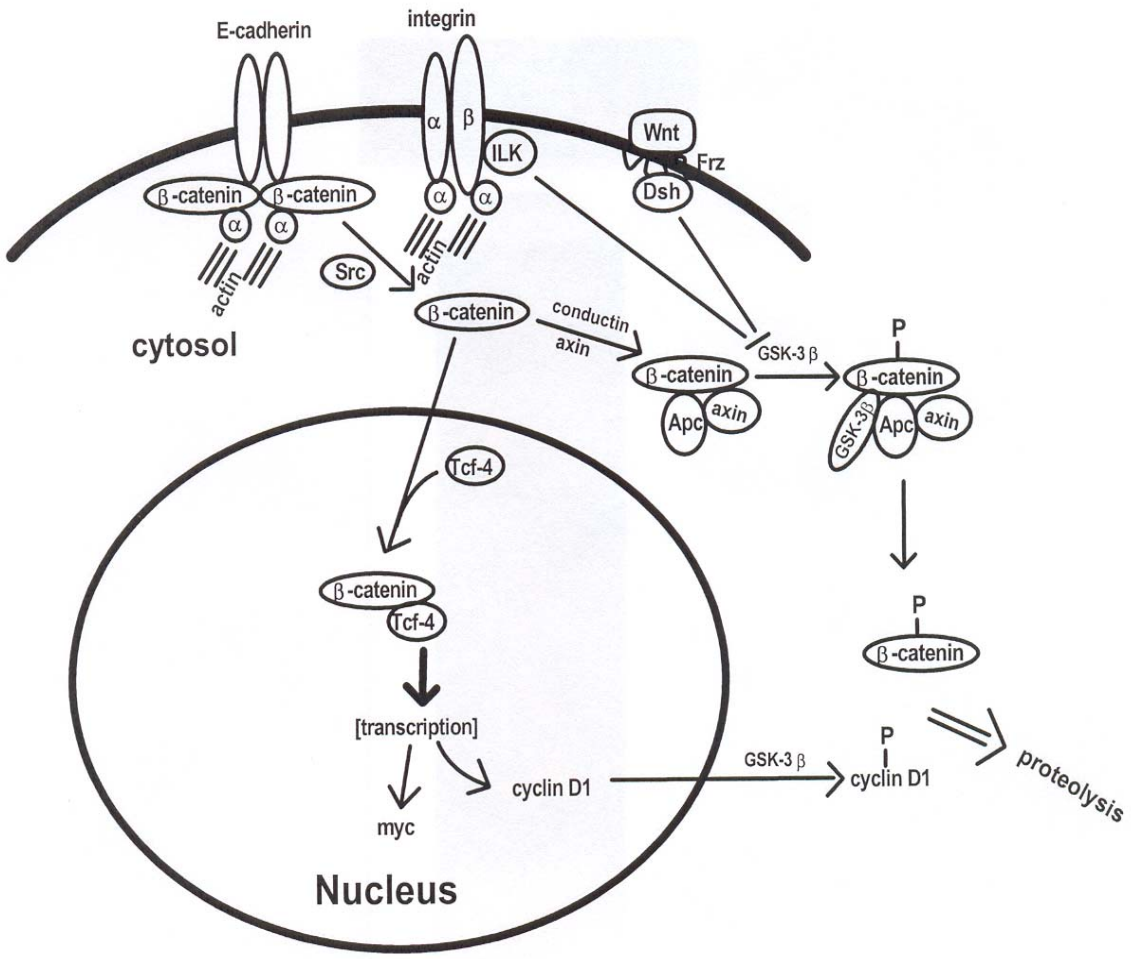

Figure 1. The Wnt signaling pathway.

The cyclin D1 and c-myc transcriptions are regulated by β-catenin/Tcf-4 complex. The activity of β-catenin is controlled by its complex partners and the degrees of phosphorylation. The inactive β-catenin is bound by axin and Apc. This complex will be phosphorylated by GSK-3β and proteolyzed by ubiquitination. When the Wnt signal transduced through Frz receptor, GSK-3β will be blocked and β-catenin will be released from the complex. The free β-catenin can then bind to Tcf-4 in the nucleus and mediate the transcription of cyclin D1 and c-myc. Src-mediated tyrosine phosphorylation causes the release of β-catenin from cytosolic domain of E-cadherin and integrin associated ILK participates the inhibition of GSK-3β.

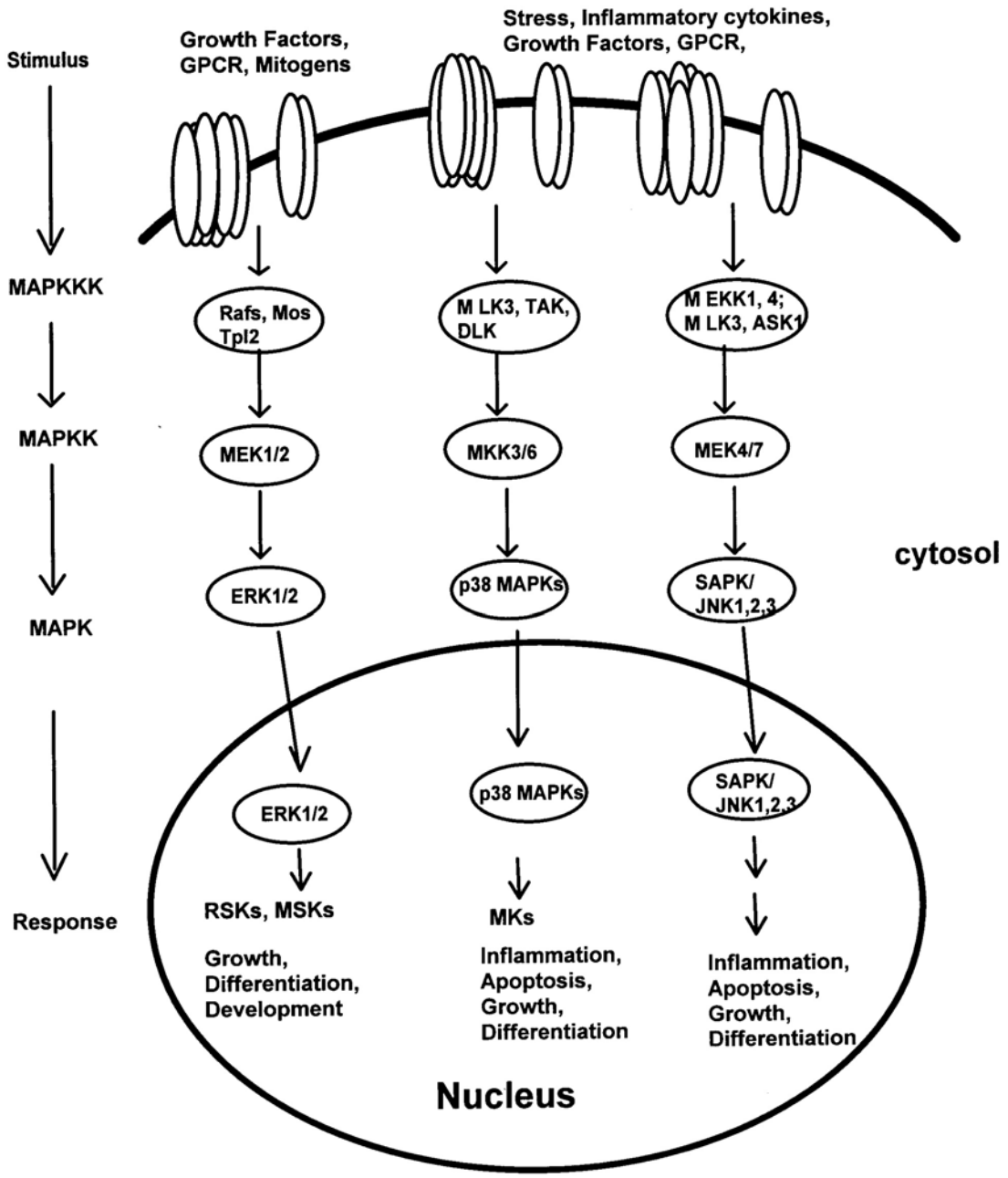

Figure 2. The MAP kinase pathway.

Three major groups of MAPKs were classified as ERK1/2, JNKs, and p38 kinase signals. Basically, ERK1 and 2 are activated in response to growth factors and phorbol esters. JNKs and p38 kinase are more related to stress stimuli. Each family of MAPKs is composed of a set of three evolutionarily conserved kinases: MAPK, MAPK kinase (MAPKK), and MAPKK kinase (MAPKKK).

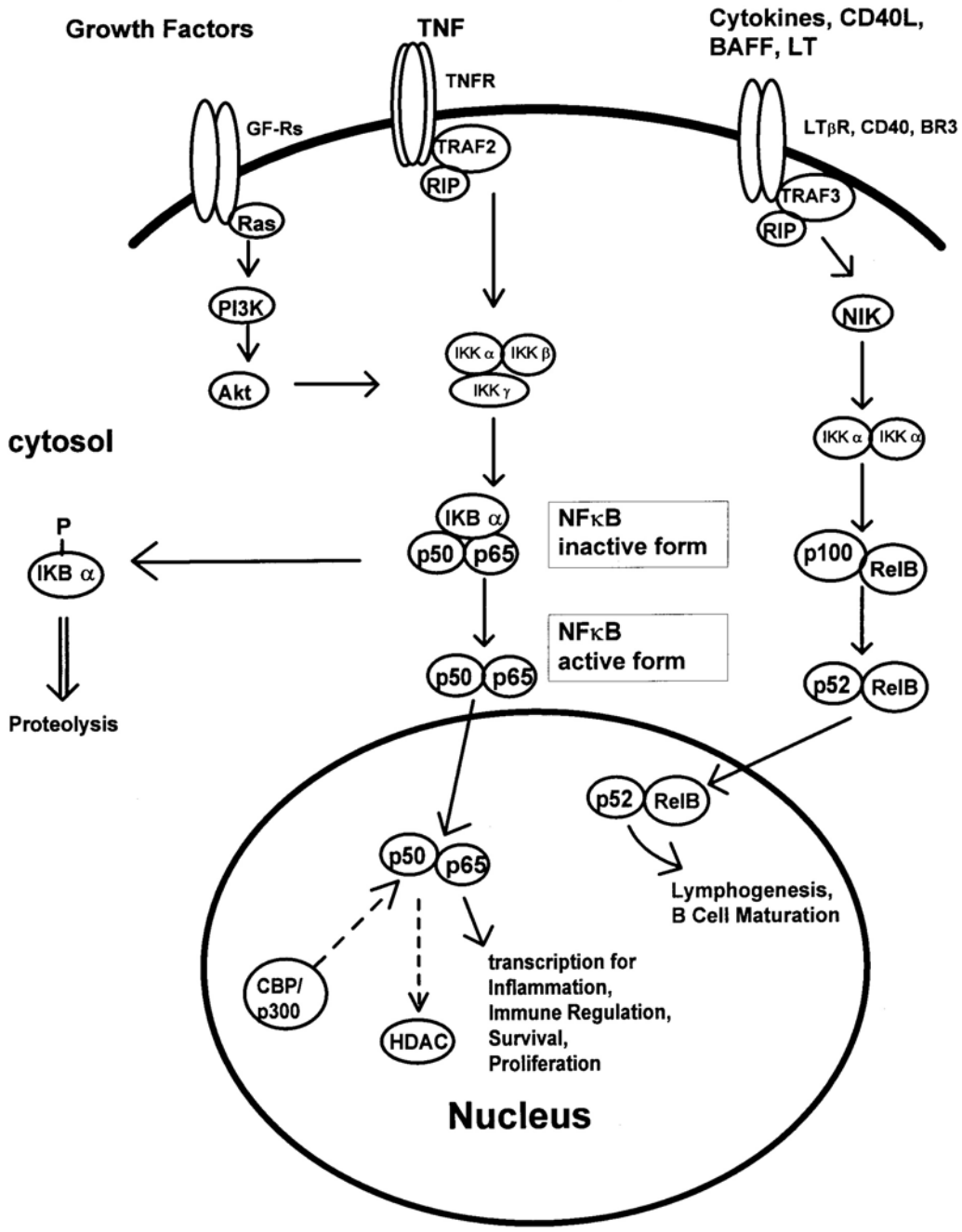

Figure 3. The NFκB signaling pathway.

NFκB members are normally sequestered by their natural inhibitor IκBs in cytoplasm Figure 3). The environmental stimuli can then activate IκB kinase complex and cause the phosphorylation on I□Bs and release the NFκBs. The free NFκBs will then translocate into nucleus and form homo- or hetero- dimmers to activate different gene expression.

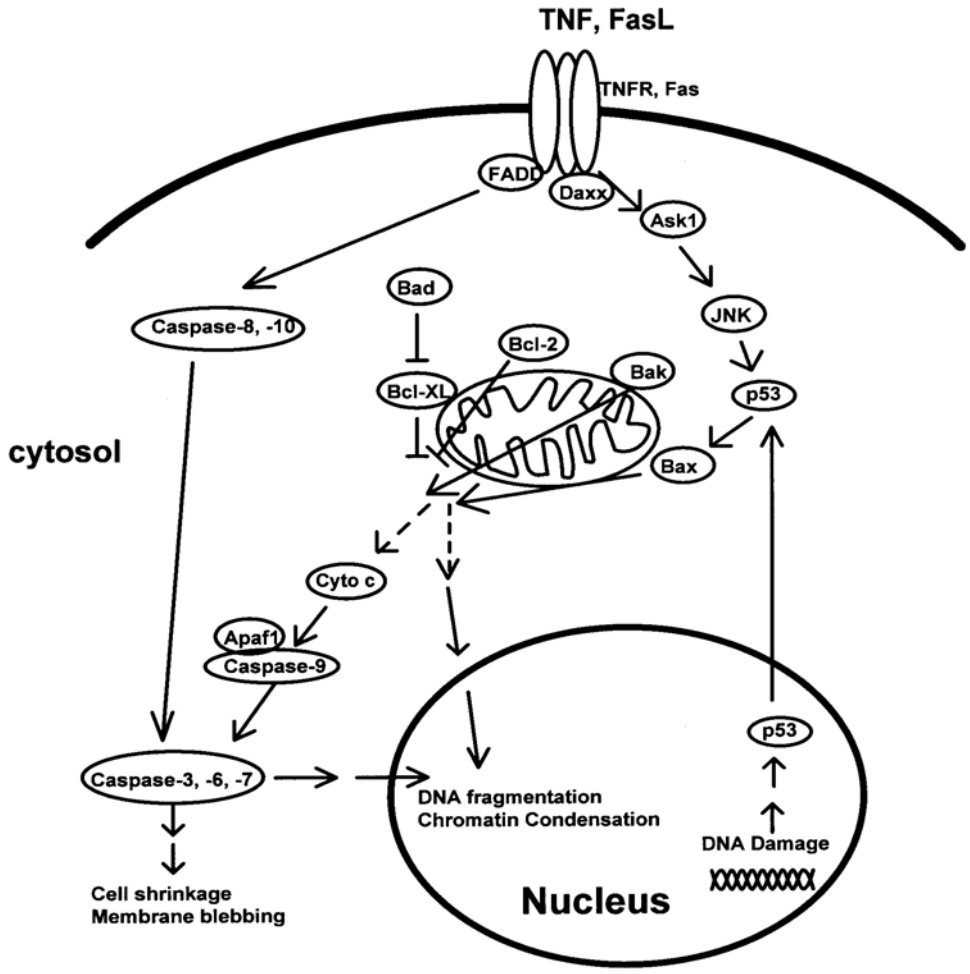

Figure 4. Apoptosis

The apoptotic pathway can be regulated by the interplay of proapoptotic and antiapoptotic proteins of the Bcl-2 family. The α-helical BH3 death domain on proapoptotic proteins such as Bax and Bad allows them to interact with the antiapoptotic proteins Bcl-2 and Bcl-XL. The heterodimer will block the antiapoptotic activity of Bcl-2 and Bcl-XL. The proapoptotic proteins then act at the mitochondrial membrane and promote leakage of cytochrome c. The released cytovhrome c then interacts with Apaf-1, causing self-cleavage and activation of caspase-9. Many members in caspase family are involved in apoptosis for activating downstream events such as cell shrinkage, membrane blebbing, DNA fragmentation, and chromatin condensation. The downstream caspase -3, -6, and -7 can be activated by the activation of caspase-9 from Apaf-1 or caspase-8 from activation of FASL/TNF-R.

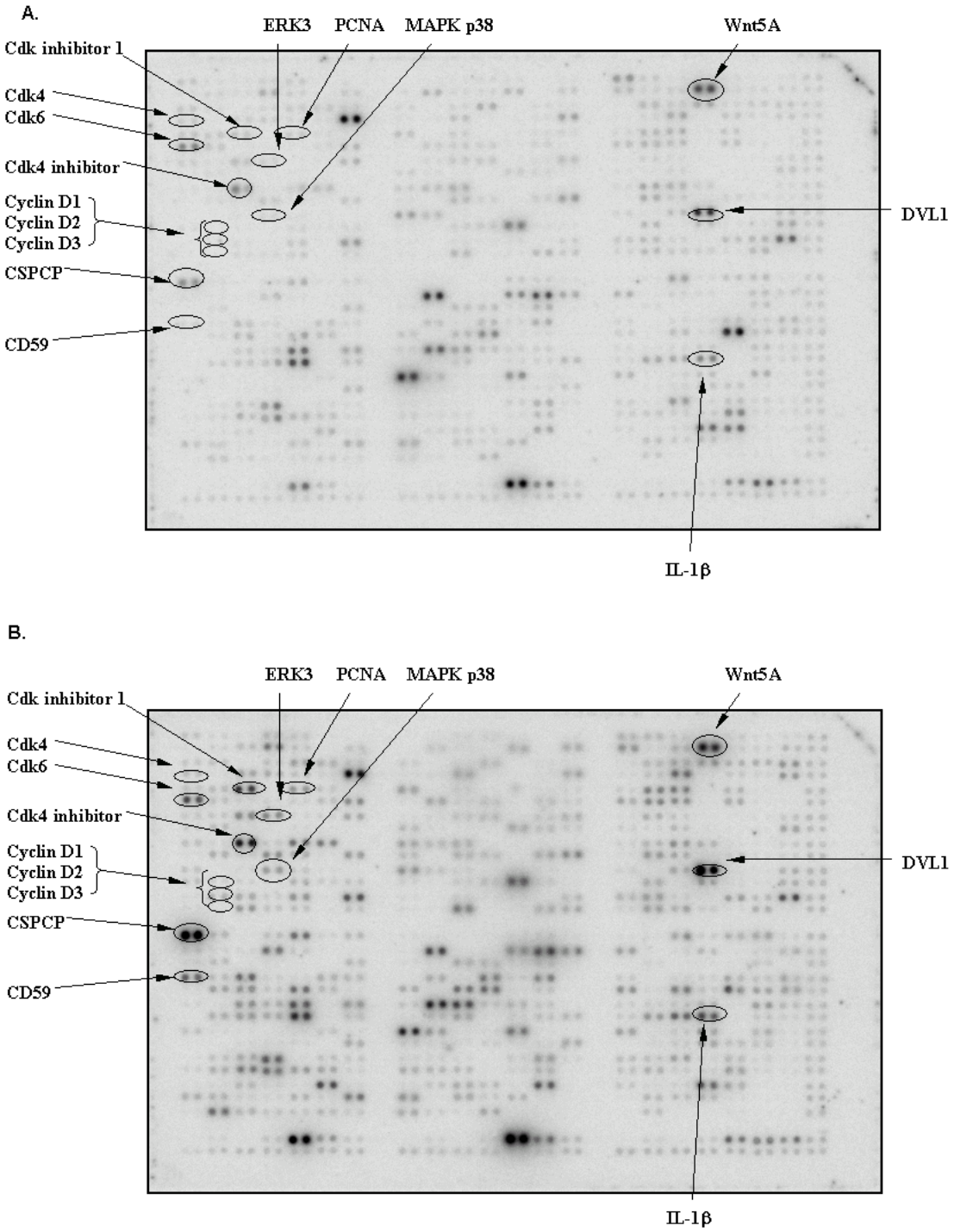

Figure 5. An example of cDNA Microarray image of a human cancer array.

Upper: untreated NHEKs, and lower: 400 nM sodium arsenite treated.

A1: Untreated control

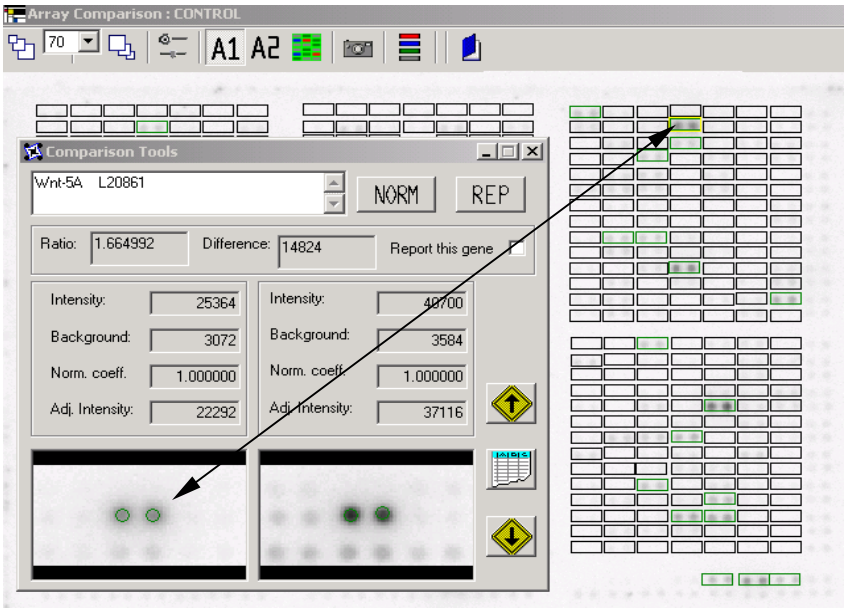

A2: 400 nM arsenite treated

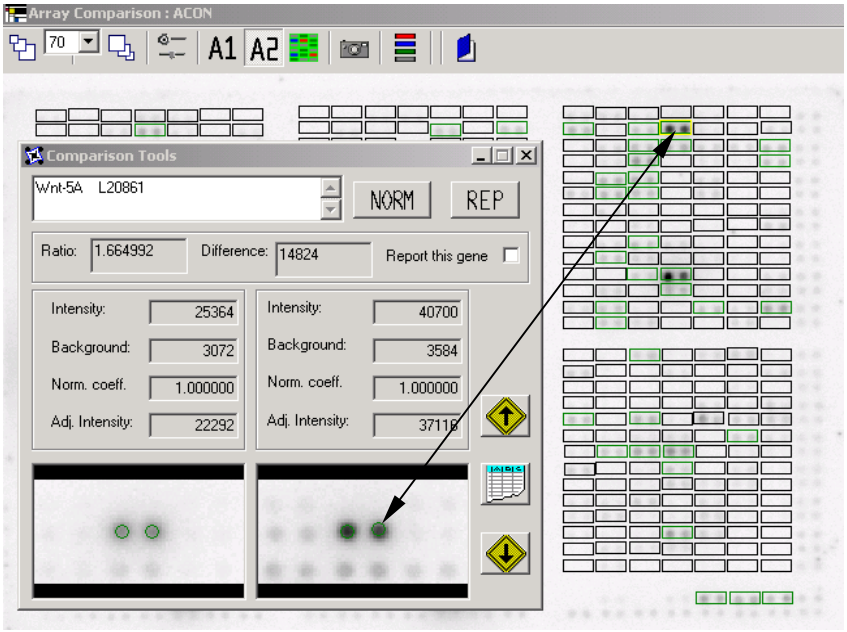

Figure 6. Comparison of gene expression using AtlasImage 2.0 software.

Examples of the results from two array membranes.

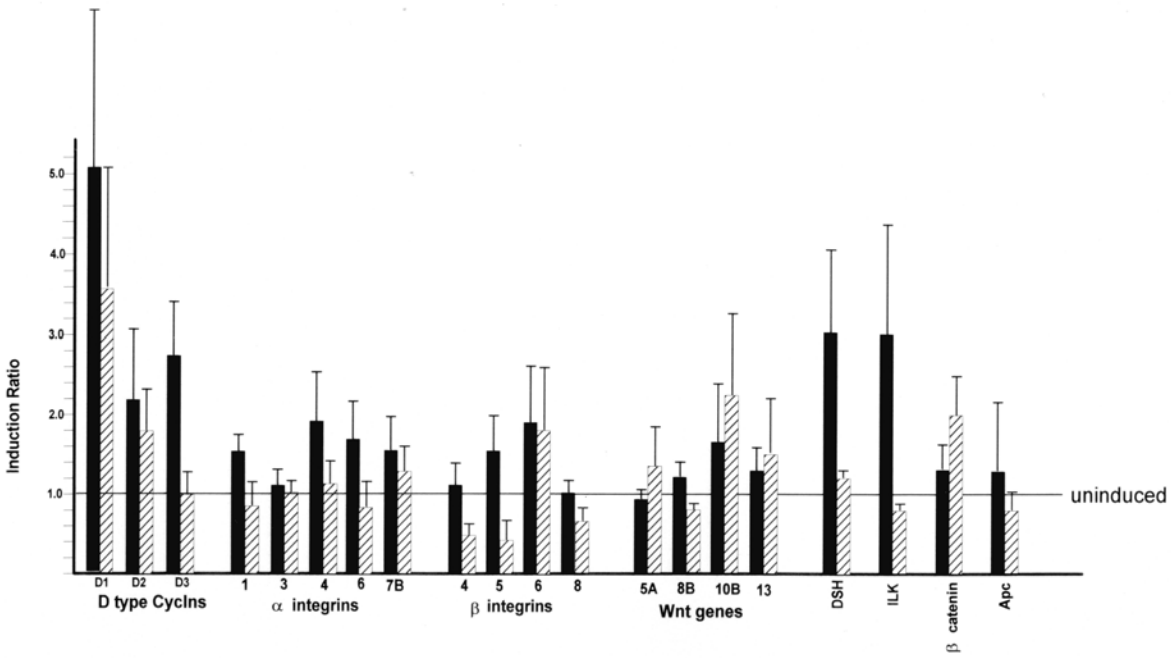

Figure 7. Induction of genes in the Wnt signaling pathway in arsenite treated NHEK.

Microarray analyses were carried out using RNAs isolated from NHEK cells treated for 3 days with 200 and 400 nM sodium arsenite as described in Materials and Methods. Bars represent the average induction ratios (arsenite treated/untreated); uninduced genes show an induction value of 1.0. Average values from five microarrays +/- SEM. (■, 400 nM arsenite, ▨ , 200 nM arsenite)

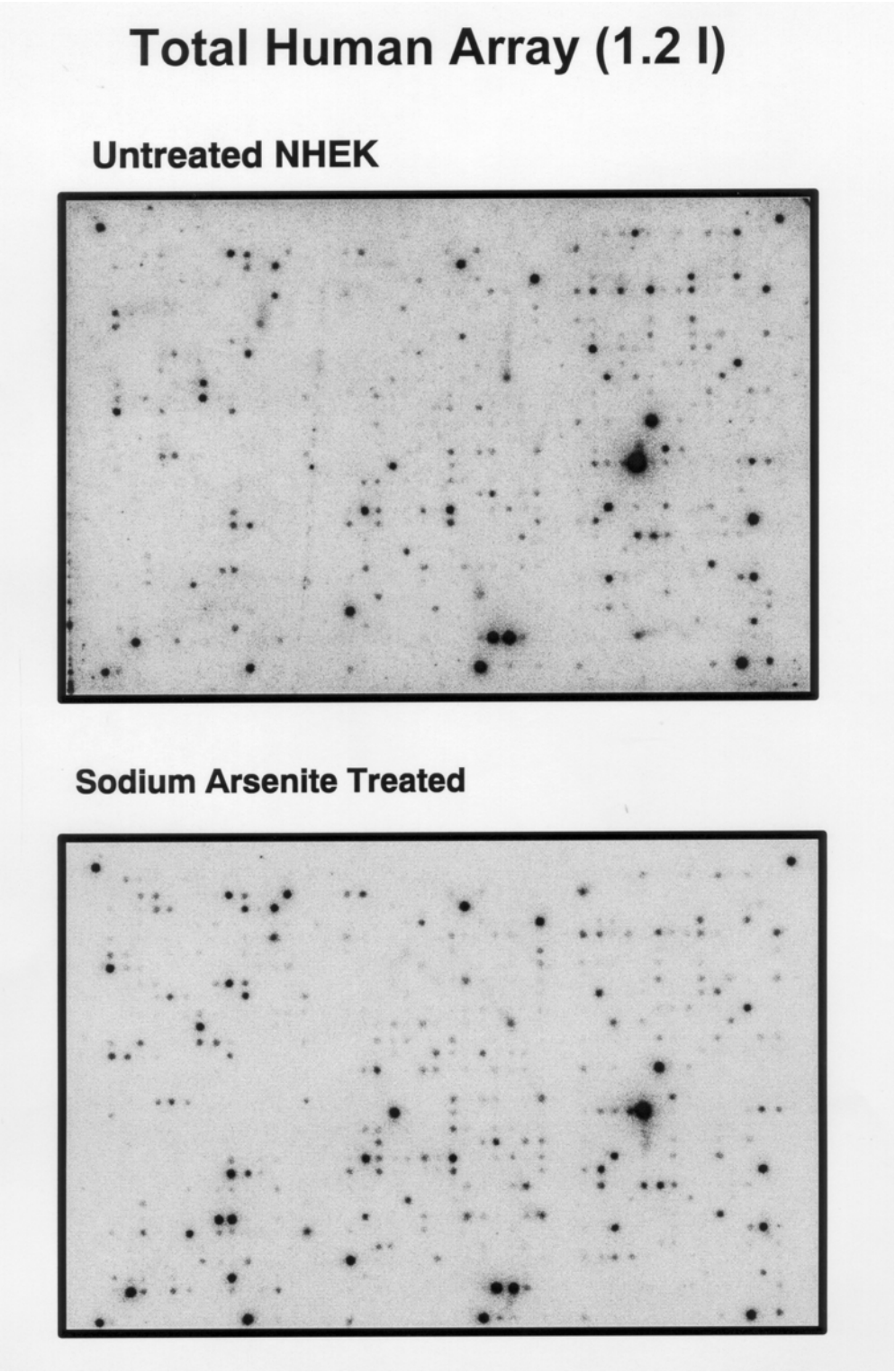

Figure 8. Microarray image of a human 1.2 array

Upper: untreated cells, and lower: 200 nM sodium arsenite treated.

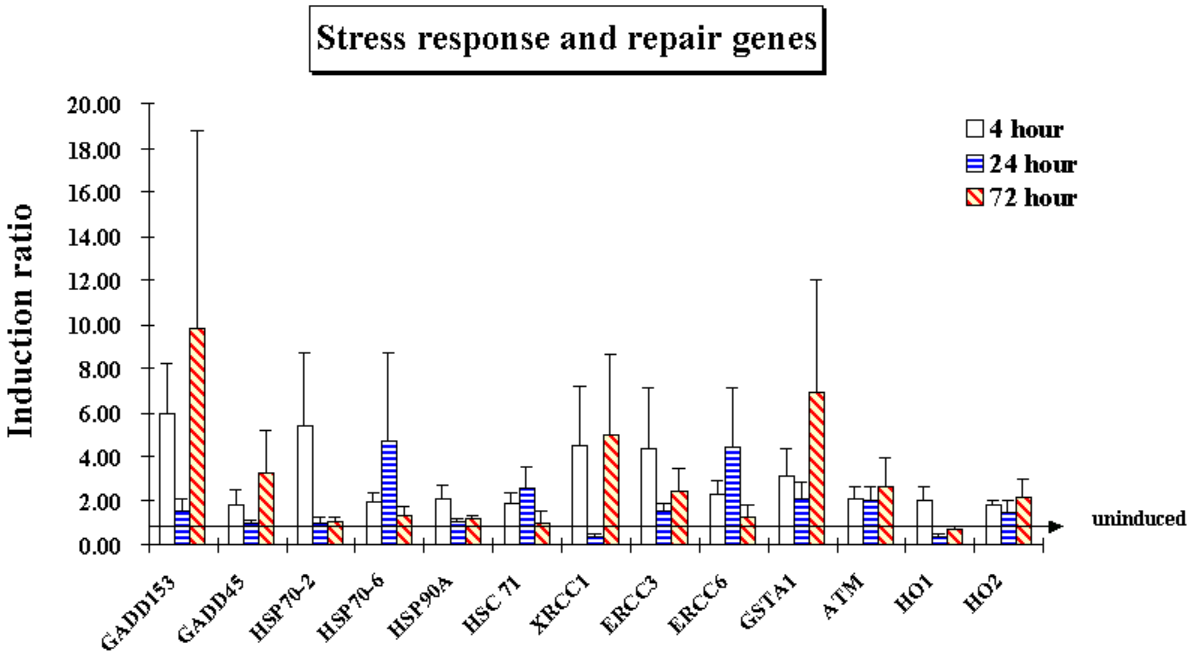

Figure 9. Stress response signals altered by submicromolar arsenite.

NHEKs were treated with 400 nM arsenite for 4, 24 and 72 hourss. Total RNAs were isolated for cDNA microarray analysis. Bars represent the average induction ratios (arsenite treated/untreated); uninduced genes show an induction value of 1.0. Average values from five microarrays +/- SEM.

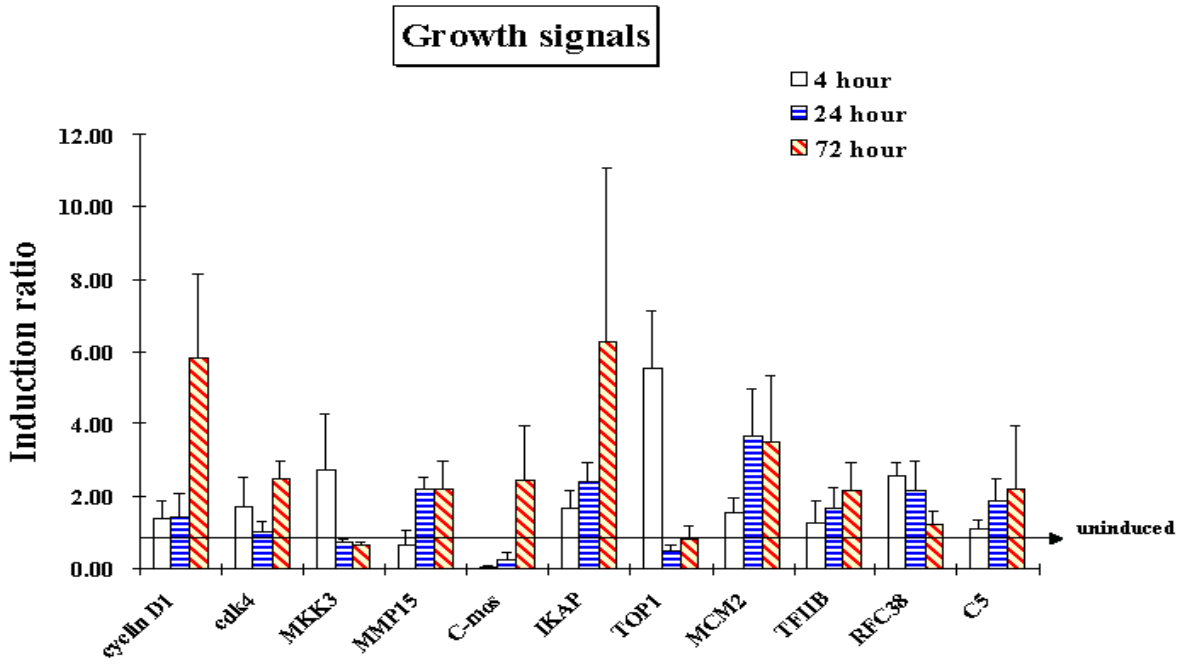

Figure 10. Growth signals altered by submicromolar arsenite.

NHEKs were treated with 400 nM arsenite for 4, 24 and 72 hourss. Total RNAs were isolated for cDNA microarray analysis. Bars represent the average induction ratios (arsenite treated/untreated); uninduced genes show an induction value of 1.0. Average values from five microarrays +/- SEM.

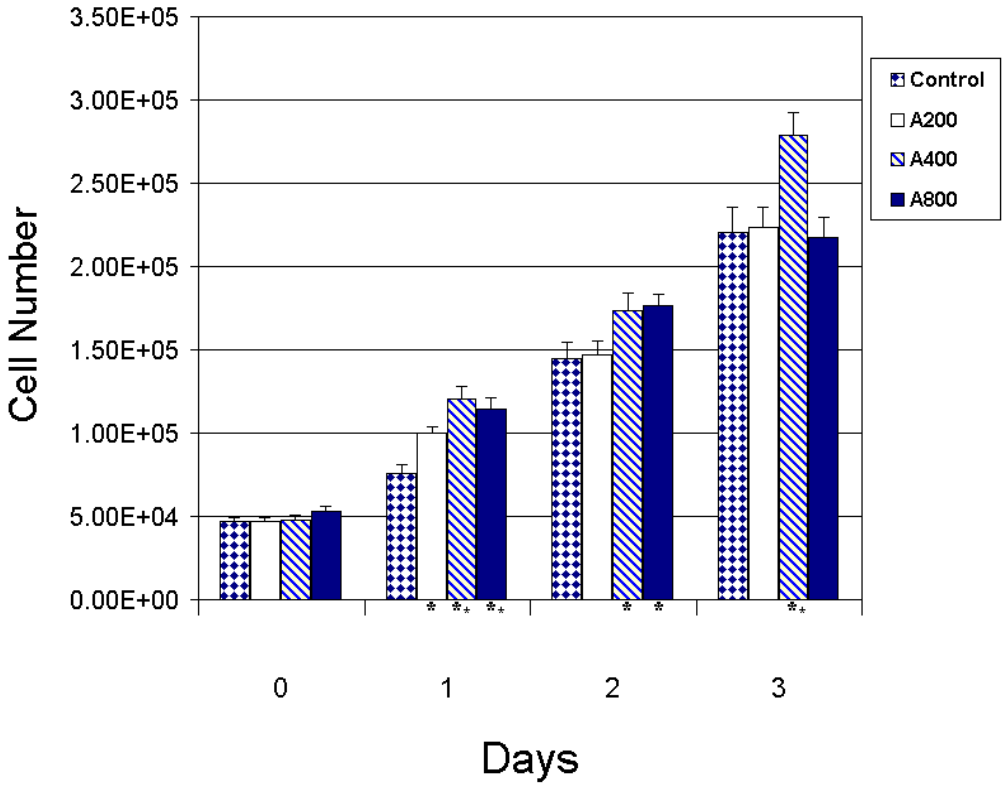

Figure 11. Stimulation of cell growth by arsenite in NHEKs

Cells were grown in 35 mm dia. wells in 6 well tissue culture trays and exposed to arsenite at the indicated concentrations when cultures were approximately 30% confluent (day 0) and cell counts were taken on subsequent days. Points represent the average of cell counts on 4 separate cell cultures carried in triplicate at each time point (+/- SEM). Statistical significance of change in arsenite treated samples compared to time-matched controls (n=4) at p values <0.05 and for $p<0.01$ are indicated by * and *$_*$ respectively.

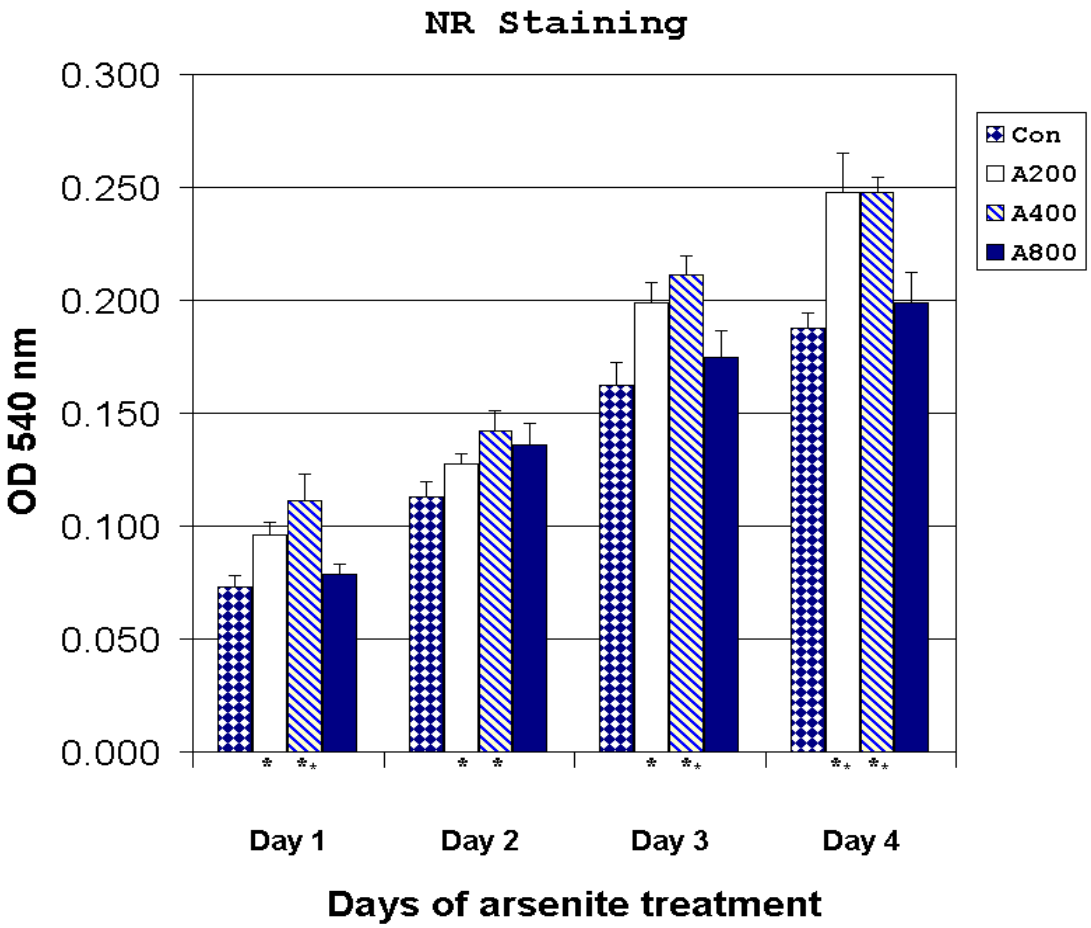

Figure 12. Uptake of neutral red by arsenite treated NHEK.

NHEK cells were grown in the presence of 200, 400 and 800 nM sodium arsenite for 1,2,3 and 4 days after which neutral red uptake was measure as described in Materials and Methods. Values are the average of measurements on five separate cell cultures at each time point (+/- SEM). Mean values significantly different from controls at levels at $p<0.05$ and for $p<0.01$ are indicated by * and *$_*$ respectively.

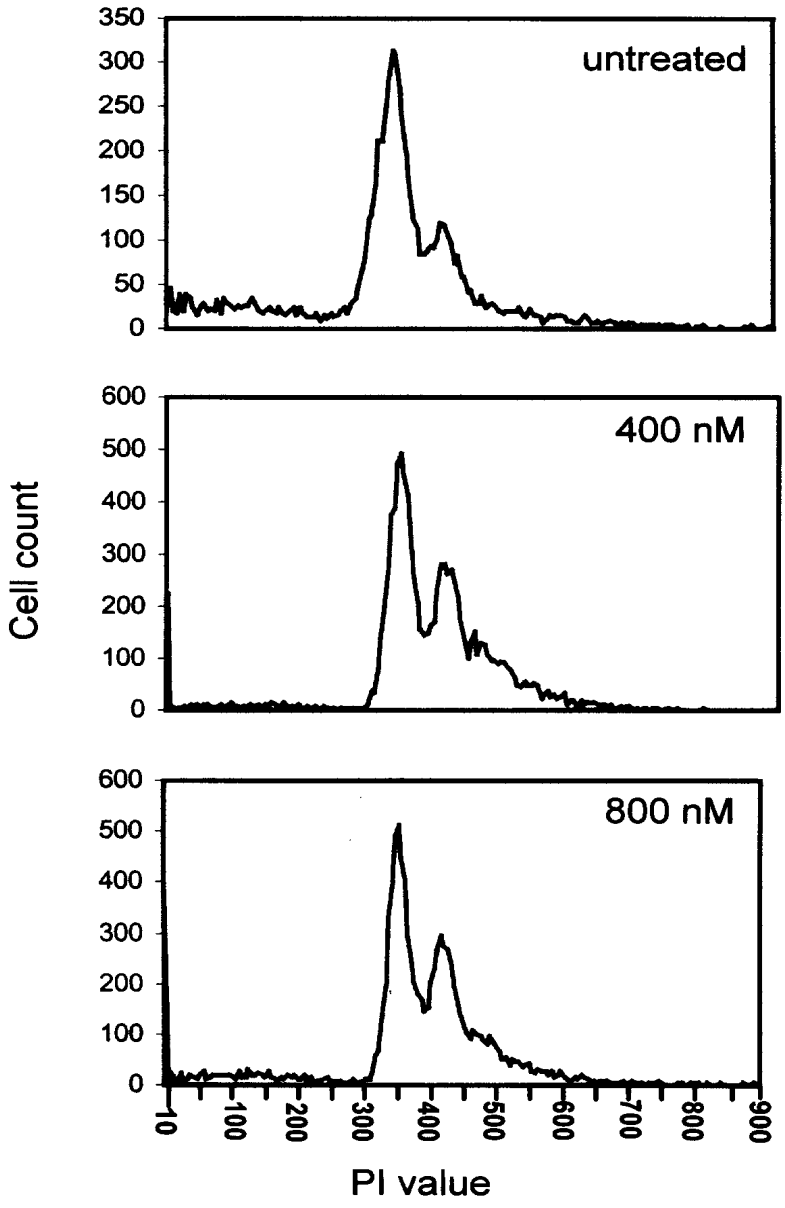

Figure 13. FACS analysis of the cell cycle in arsenite-treated NHEK.

NHEK were exposed to sodium arsenite at the indicated concentrations for 2 days and then harvested for FACS analysis. Histograms were constructed from the raw data. Peaks corresponding to G_0/G_1 and G_2 can be seen at propidium iodide (PI) values of about 330 and 405 respectively.

Table 1. Effect of arsenite treatment of NHEK cells on the distribution of cells in the G_1 and G_2/S compartments.

The relative percentages of cells in the G0/G1 and G2+S compartments in NHEK treated for 2 days with 400 or 800 nM sodium arsenite were calculated from Gaussian approximations of the corresponding peaks in the FACS histograms as described in Materials and methods. The mean values and standard errors (SEM) are shown for all treatment conditions; the *p* values for 400 and 800 nM treated cells relative to untreated controls are shown in the last column.

		Experiment							
		I	II	III	IV	V	Mean	SEM	Probability
Untreated	G1 fraction	65.5	67.4	61.4	71.5	61.4	66.4	1.9	
	G2/S fraction	34.5	32.6	38.6	28.5	38.6	33.6		
400 nM	G1 fraction	54.1	67.7	54	51	56.6	56.7	2.9	*p*=0.034
	G2/S fraction	45.9	32.3	46	49	43.4	43.3		
800 nM	G1 fraction	44.1	58.3	56.6	53.9	ND	53.2	3.2	*p*=0.009
	G2/S fraction	55.9	41.7	43.4	46.1	ND	46.8		

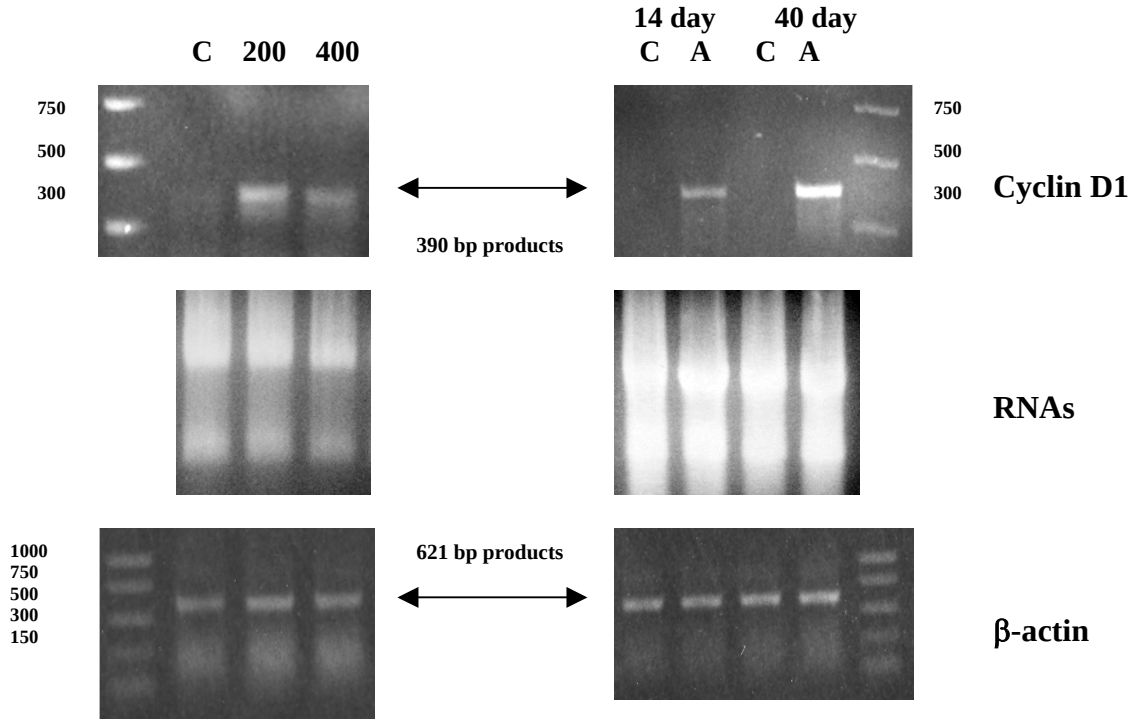

Figure 14. Agarose gels of RT-PCR products of cyclin D1 expression in arsenite treated NHEK.

Left hand panel: NHEKs either untreated (C) or treated with 200 or 400 nM sodium arsenite for a period of 3 days. Right hand panel: RT-PCR of untreated NHEK cells (C) or NHEK treated continuously with 400nM sodium arsenite (A) for 14 and 40 days. Arrowheads show the expected 390 bp PCR product. Lower panels show the RNAs used as templates in the respective RT-PCR reactions. Agarose gels of loaded RNA and RT-PCR for β-actin were shown in the middle and bottom images as endogenous control.

Cyclin D1

β-actin

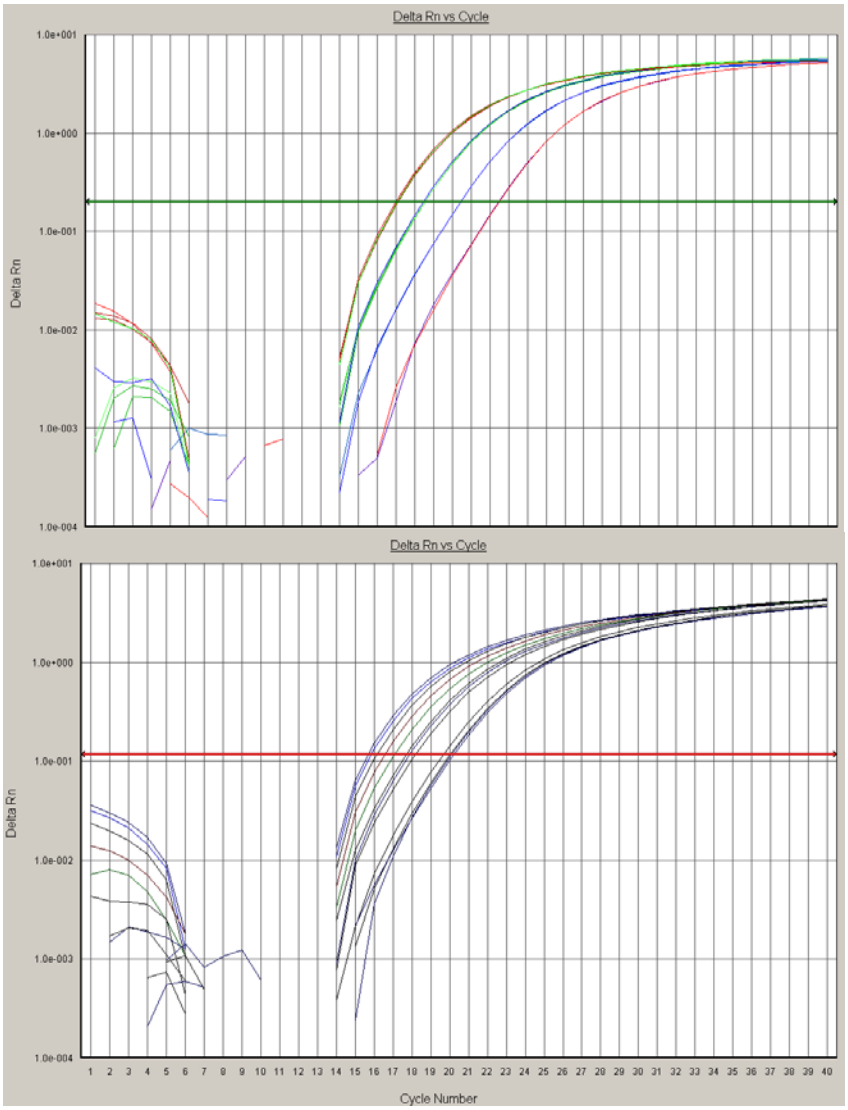

Figure 15. Sample image of Real-time PCR quantitation of cyclin D1 RNA.

Upper: cyclin D1. Lower: beta-actin.

RNAs from arsenite treated and untreated NHEKs were reverse transcribed into cDNA and used as templates for real time PCR analysis. FAM-labeled probes were employed to report the increase of specific genes and a set of primers and a probe for β-actin were used in the same manner as endogenous control. All samples were duplicated and average values were taken. The thresholds were selected in linearly increasing ranges for analysis.

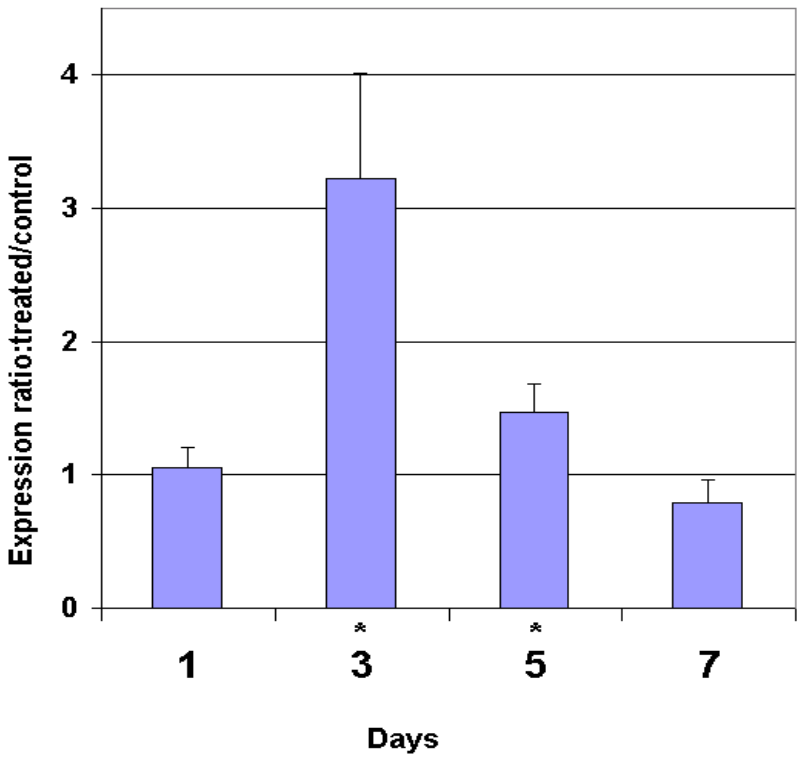

Figure 16. Real-time PCR quantitation of cyclin D1 RNA.

Cyclin D1 cDNA templates were quantitated as described in Materials and methods using total RNAs from NHEK cells treated with 400 nM arsenite. Values shown are the average of measurements on replicate cell cultures (±SEM). For days 1, 3, 5, 7; =3, 7, 5 and 4, respectively. Absence of induction is represented by an expression ratio of 1.0. Mean values significantly different from day 1 values at $p<0.05$ are indicated by *.

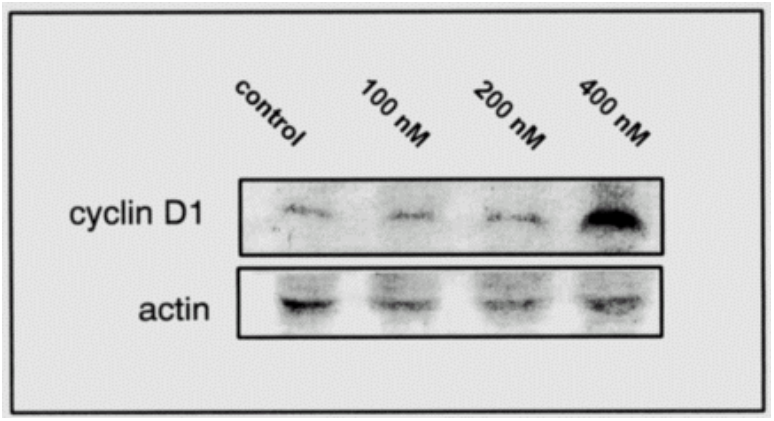

Figure 17. Western blot of cyclin D expression

Western blot of cyclin D expression in NHEK treated with 100, 200 and 400 nM sodium arsenite for 3 days.

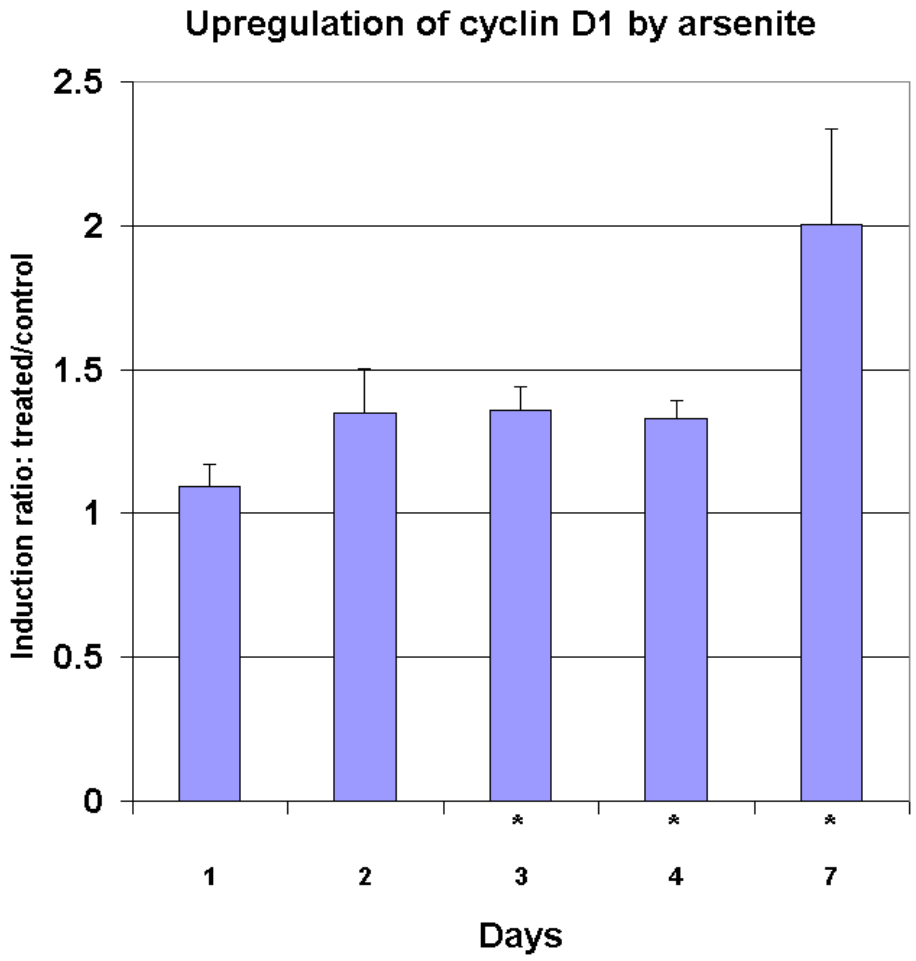

Figure 18. Time course of induction of cyclin D by arsenite.

cyclin D levels in Western blots of extracts of cells treated with 400 nM arsenite for the indicated times were quantitated as described in Materials and methods. Averaged values of replicate measurements (n=5 for days 1, 3, 4; n=3 for day 2 and n=6 for day 7) of induction ratios of cyclin D values in arsenite-treated NHEK divided by those in untreated controls (±SEM). Absence of induction is represented by an induction ratio of 1.0. Mean values significantly different from day 1 cyclin D levels at $p<0.05$ are indicated by *.

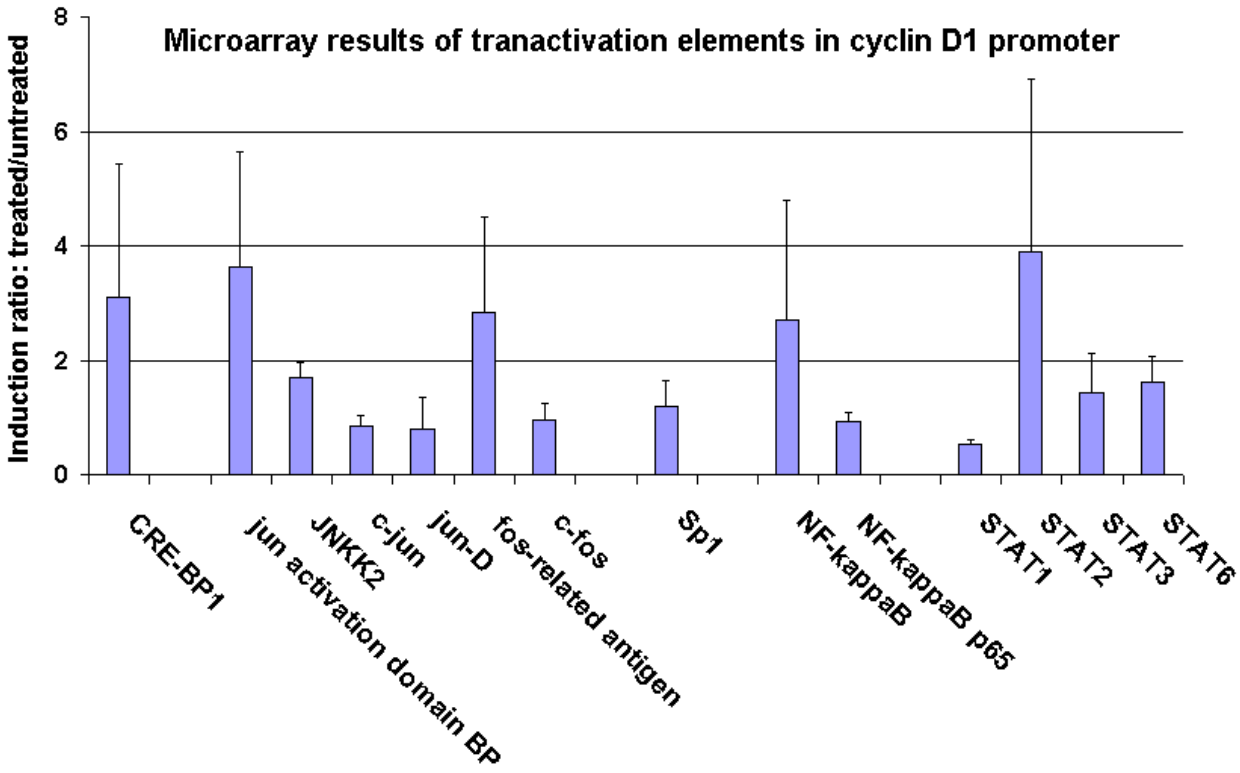

Figure 19. Microarray results of tranactivation elements in cyclin D1 promoter

NHEK cells were grown up to 70% confluence and treated with 200 nM sodium arsenite for 3 days. Microarray analyses were carried out as described in Materials and Methods. Bars represent the average induction ratios (arsenite treated/untreated); uninduced genes show an induction value of 1.0. Average values from six microarrays +/- SEM.

Table 2. EMSA probes specific to individual DNA binding element designed for cyclin D1.

Binding motifs for the indicated transcription factors are underlined.

	Sites on Cyclin D1 promoter
NFκB (-39)	cggactaca**ggggagtttt**gttg
Tcf4 (-80)	ccgg**gctttgatc**tttgc
CRE (-58)	caacag**taacgtca**cacggat
AP1 (-952)	tccga**tgagtcag**ttctagagga
SP1 (-102)	ggcgc**ccgcg**cccccc**ccccc**tgc
SP1 (-122)	tgc**gcccg**cccccg**ccccc**ctcc
STAT (-480)	tgagat**tctttggcc**gtc
	cgtggcg**ttct**tggaaatg

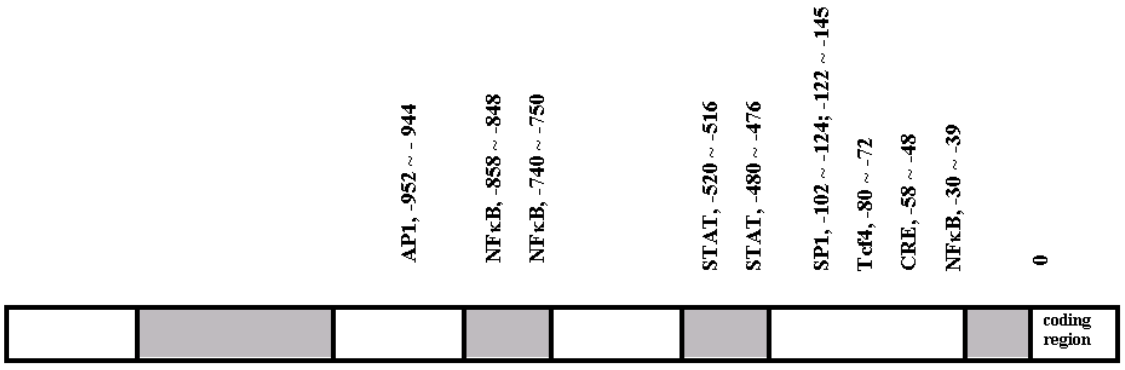

Figure 20. Diagram of probes in cyclin D1 promoter region

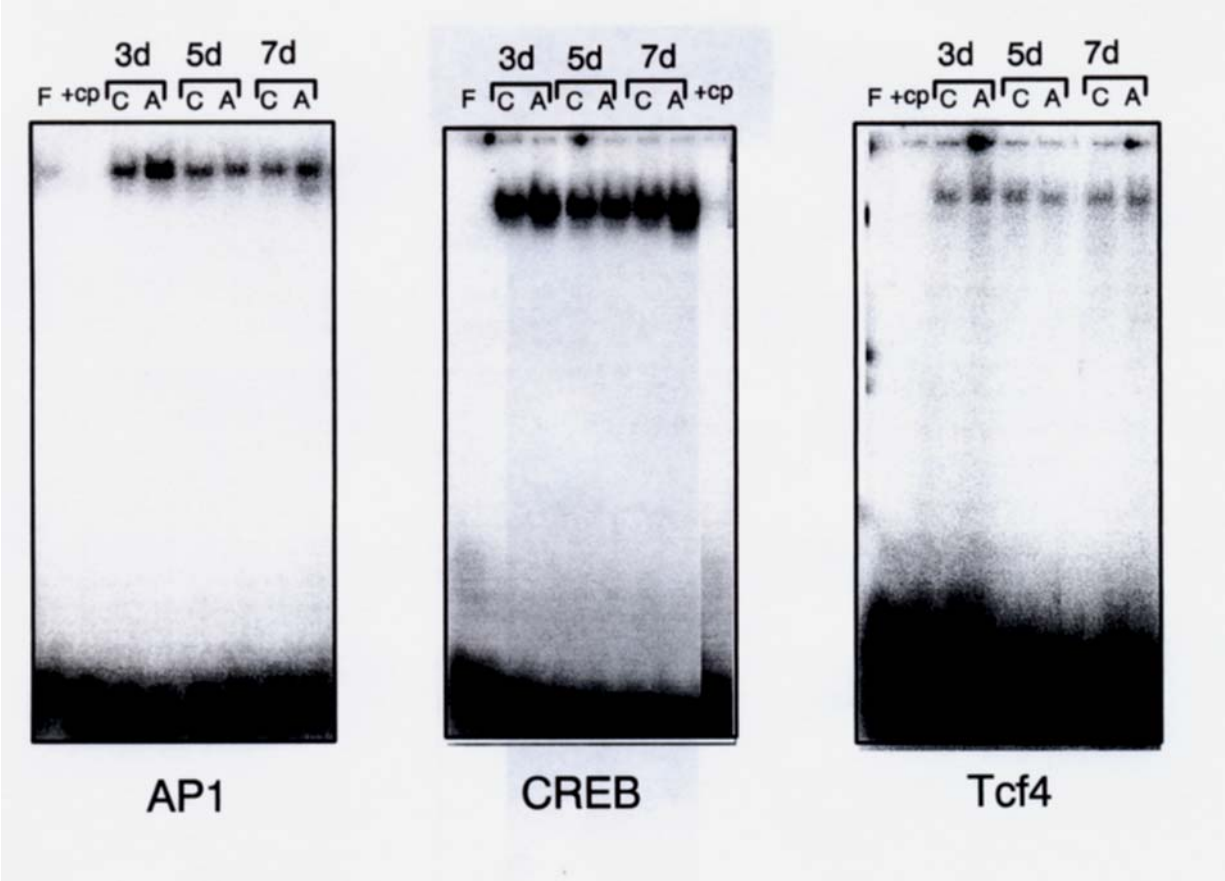

Figure 21. Electrophoretic mobility shift assays for AP1, CREB, and Tcf4.

NHEK cells were grown in the presence of 400 nM sodium arsenite for 3, 5 and 7 days. Binding of nuclear factors from untreated (C) and arsenite treated (A) to end labeled double stranded probes representing segments of the cyclin D1 containing the binding motifs for Tcf4, AP1 and CREB was visualized on polyacrylamide gels. Free probe (F) and reactions run in the presence of a 20-fold excess of unlabeled probe are indicated (+CP).

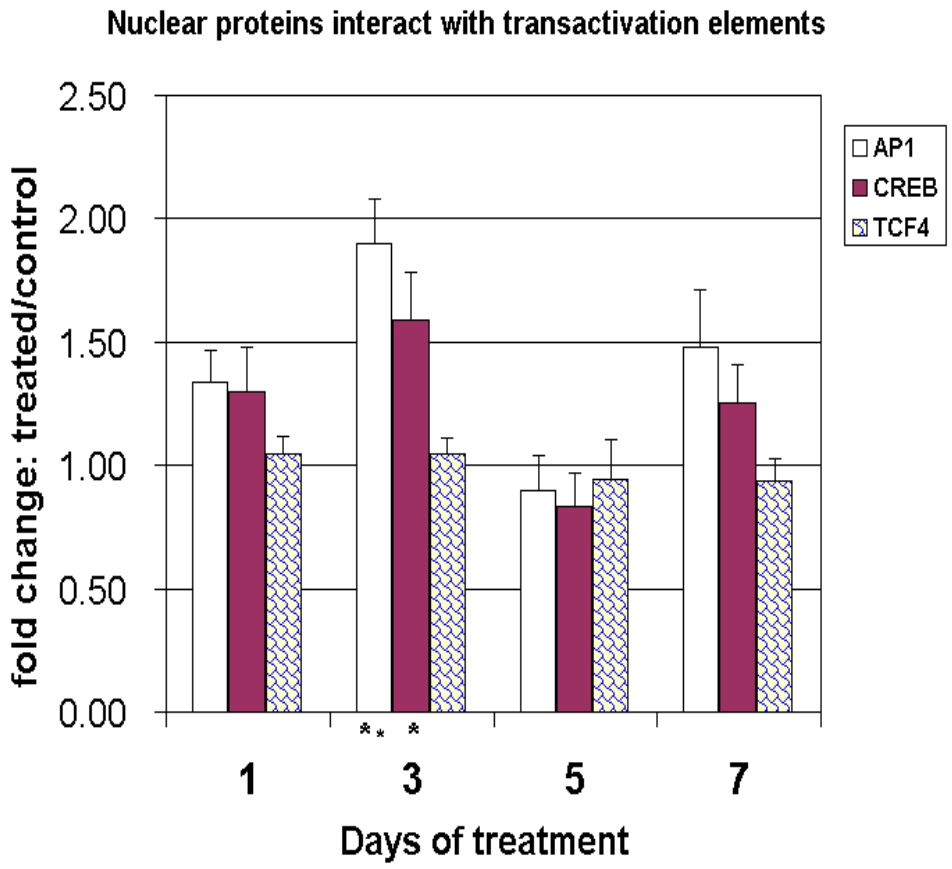

Figure 22. Electrophoretic mobility shift assays.

Bar graph showing the binding activities of the various transcription factors at various times after exposure to arsenite as determined from measurements of relative signal intensities from the bands representing bound probes using ImageQuant software. Averaged measurements from 3 experiments ±SEM are shown. Values for AP1 and CREB binding significantly different from Tcf4 levels at $p<0.05$ and for $p<0.01$ are indicated by * and **, respectively.

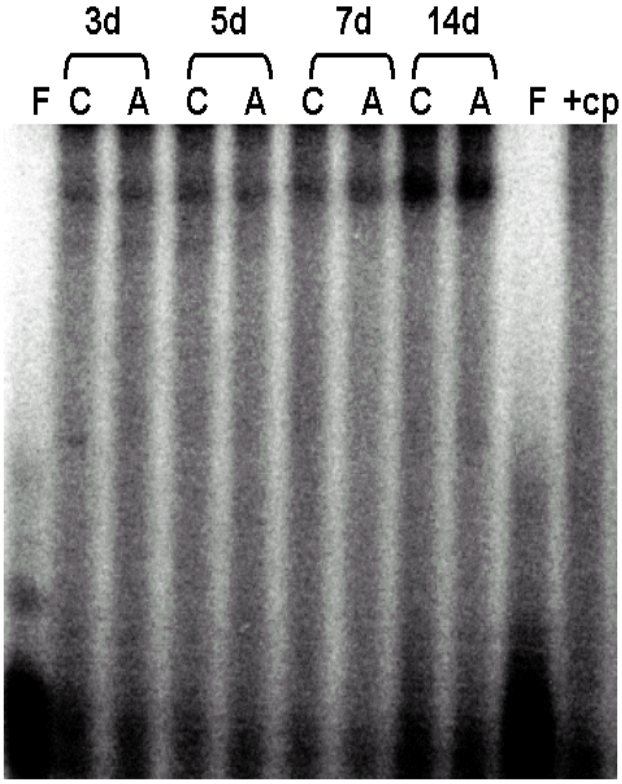

Figure 23. Electrophoretic mobility shift assays for SP1.

NHEK cells were grown in the presence of 400 nM sodium arsenite for 3, 5 and 7 days. Binding of nuclear factors from untreated (C) and arsenite treated (A) to end labeled double stranded probes representing segments of the cyclin D1 containing the binding motifs for SP1 was visualized on polyacrylamide gels. Free probe (F) and reactions run in the presence of a 20-fold excess of unlabeled probe are indicated (+CP).

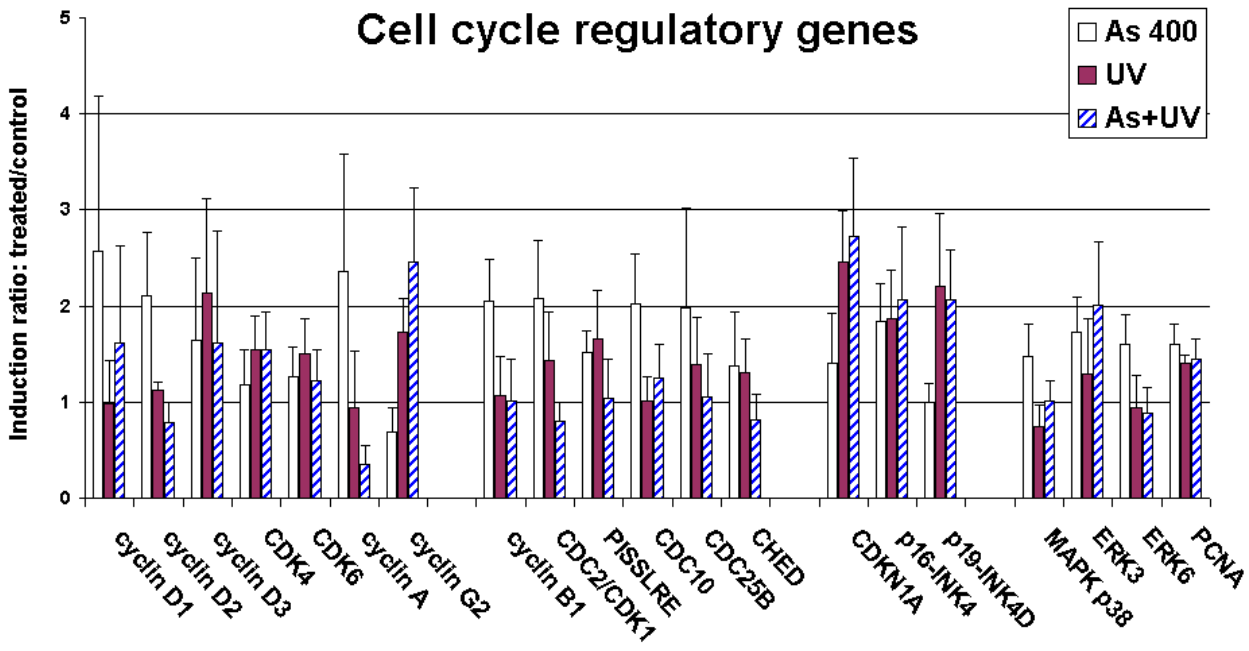

Figure 24. Cell cycle regulatory genes affected by arsenite, UVB irradiation, and arsenite + UVB treated NHEK cells.

NHEK cells were grown up to 70% confluence and treated with 400 nM sodium arsenite for 2 days before the irradiation. Cells were irradiated through a thin layer of PBS with 36 mJ/cm^2/min UVB for 45 seconds. Microarray analyses were carried out as described in Materials and Methods. Bars represent the average induction ratios (arsenite treated/untreated); uninduced genes show an induction value of 1.0. Average values from six microarrays +/- SEM.

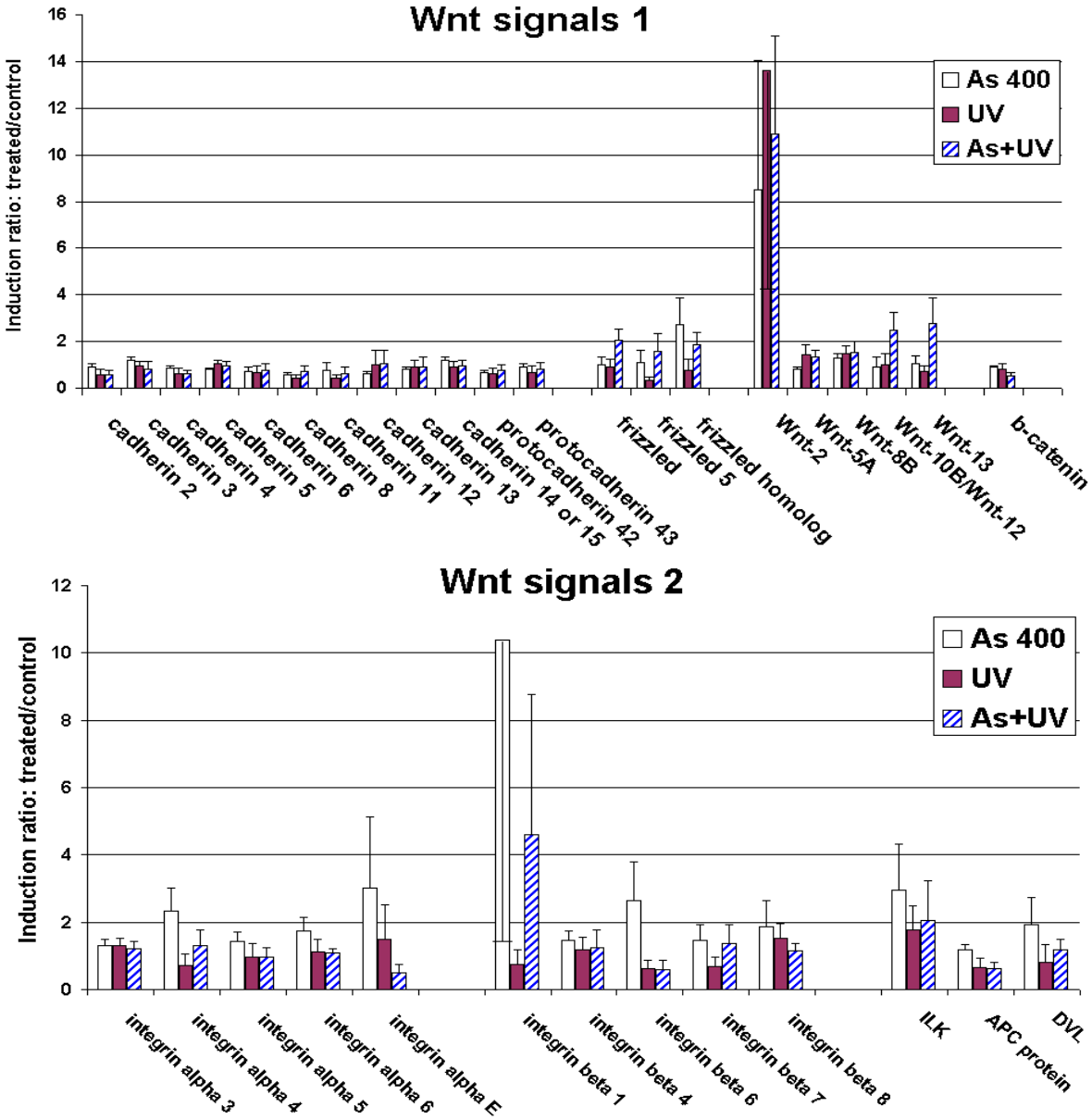

Figure 25. Genes in Wnt signaling pathway affected by arsenite, UVB irradiation, and arsenite + UVB treated NHEK cells.

NHEK cells were grown up to 70% confluence and treated with 400 nM sodium arsenite for 2 days before the irradiation. Cells were irradiated through a thin layer of PBS with 36 mJ/cm^2/min UVB for 45 seconds. Microarray analyses were carried out as described in Materials and Methods. Bars represent the average induction ratios (arsenite treated/untreated); uninduced genes show an induction value of 1.0. Average values from six microarrays +/- SEM.

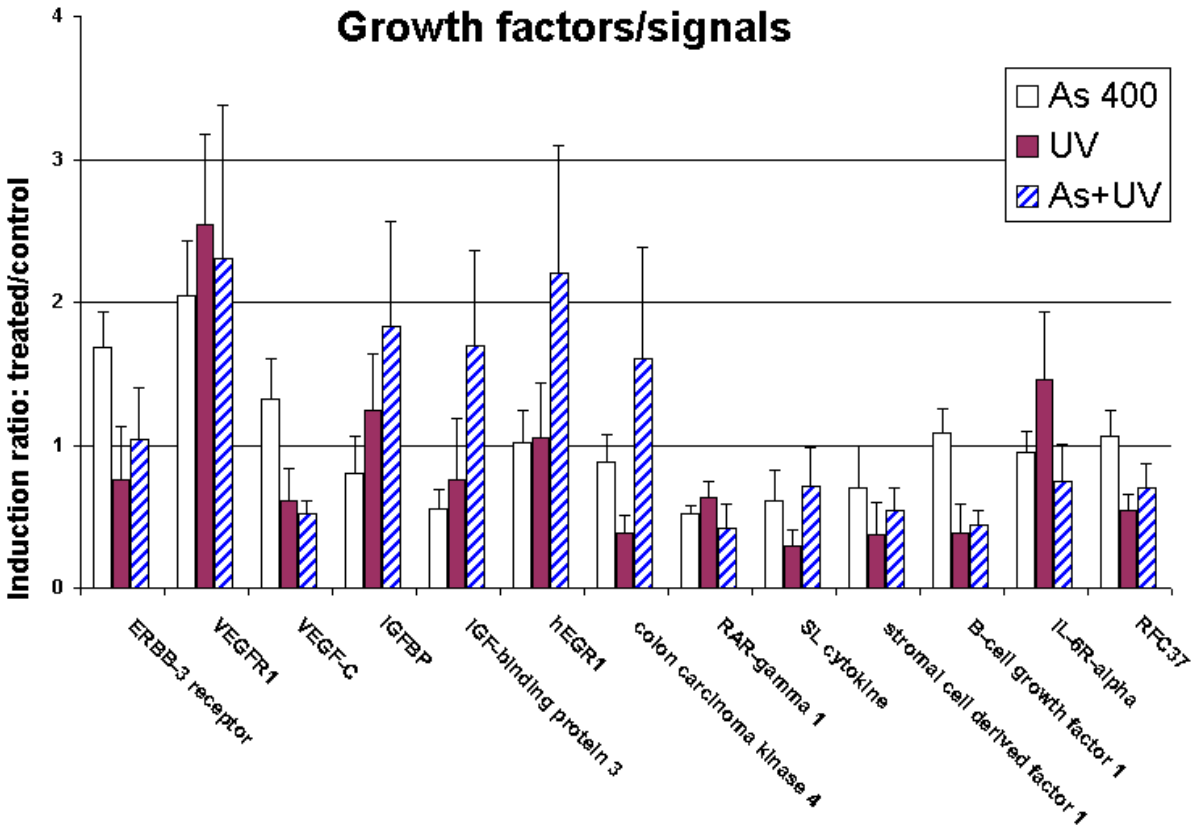

Figure 26. Other growth signals affected by arsenite, UVB irradiation, and arsenite + UVB treated NHEK cells.

NHEK cells were grown up to 70% confluence and treated with 400 nM sodium arsenite for 2 days before the irradiation. Cells were irradiated through a thin layer of PBS with 36 mJ/cm^2/min UVB for 45 seconds. Microarray analyses were carried out as described in Materials and Methods. Bars represent the average induction ratios (arsenite treated/untreated); uninduced genes show an induction value of 1.0. Average values from six microarrays +/- SEM.

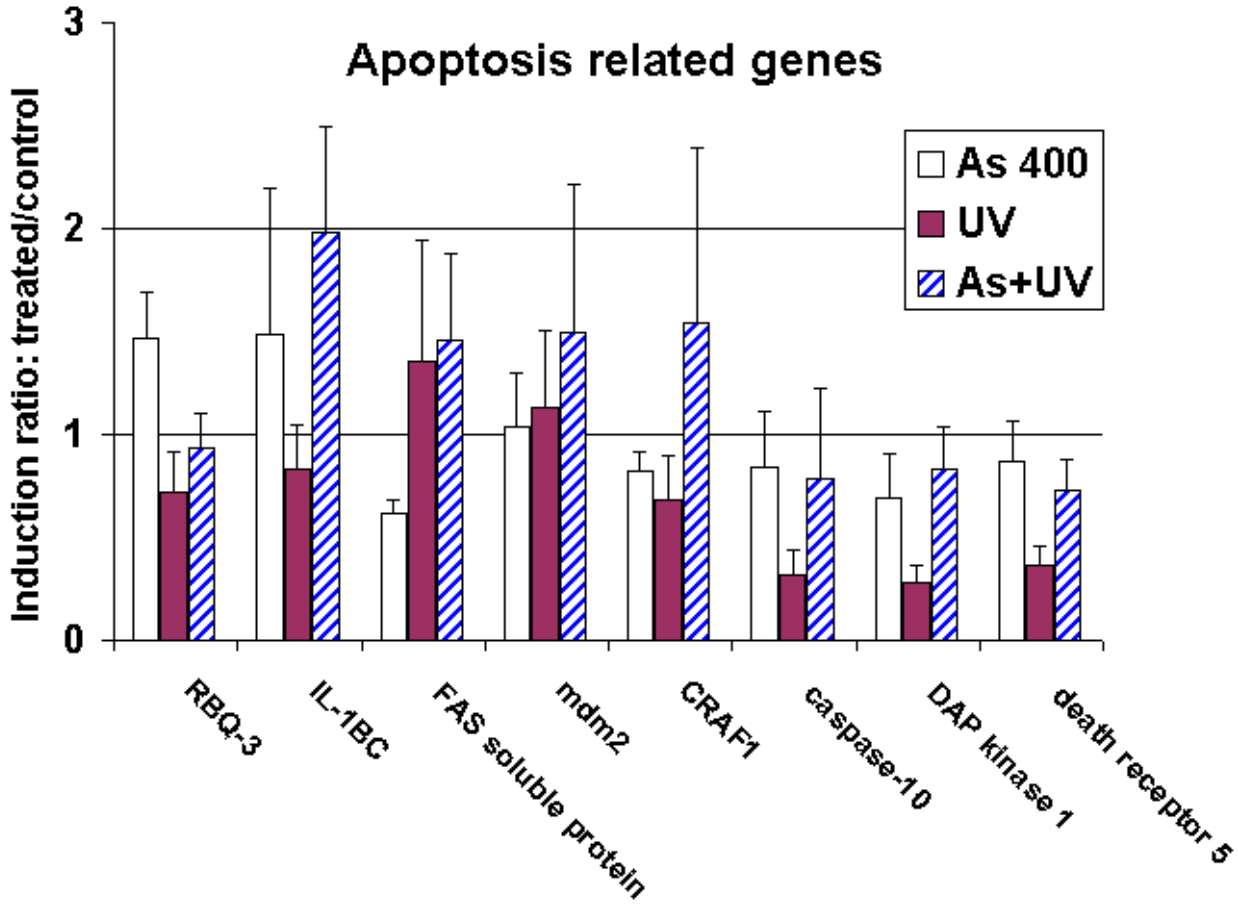

Figure 27. Apoptosis related genes affected by arsenite, UVB irradiation, and arsenite + UVB treated NHEK cells.

NHEK cells were grown up to 70% confluence and treated with 400 nM sodium arsenite for 2 days before the irradiation. Cells were irradiated through a thin layer of PBS with 36 mJ/cm^2/min UVB for 45 seconds. Microarray analyses were carried out as described in Materials and Methods. Bars represent the average induction ratios (arsenite treated/untreated); uninduced genes show an induction value of 1.0. Average values from six microarrays +/- SEM.

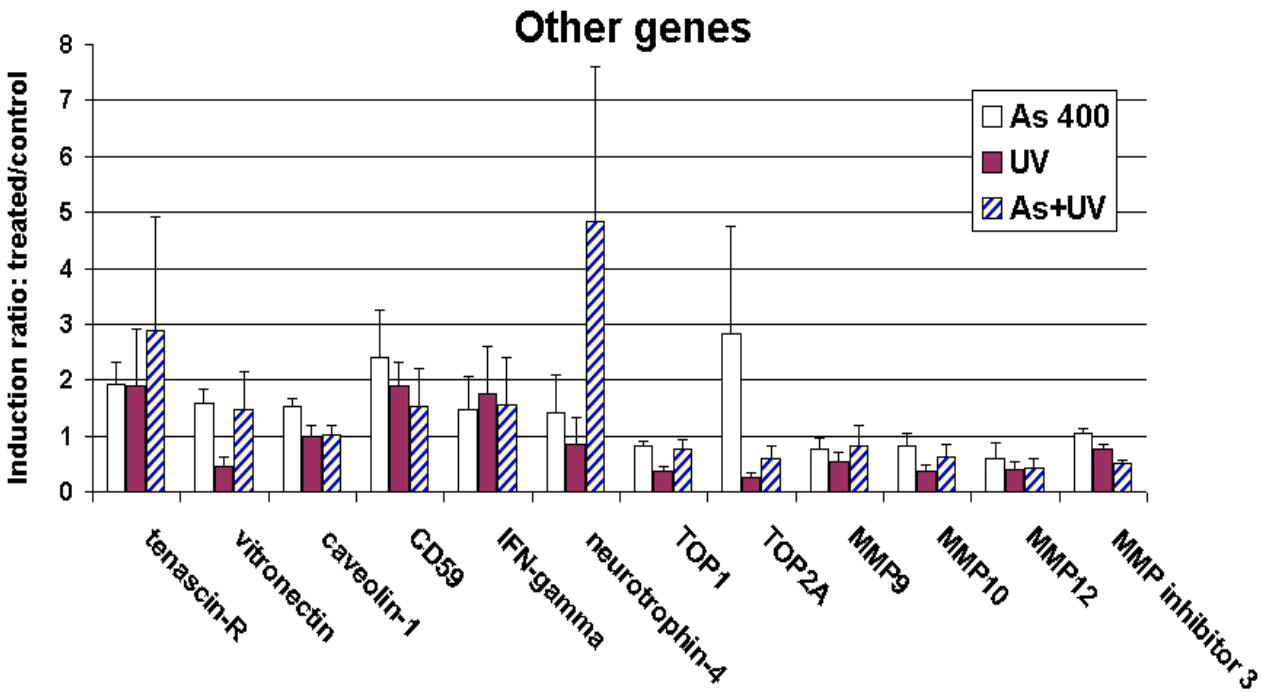

Figure 28. Other genes affected by arsenite, UVB irradiation, and arsenite + UVB treated NHEK cells.

NHEK cells were grown up to 70% confluence and treated with 400 nM sodium arsenite for 2 days before the irradiation. Cells were irradiated through a thin layer of PBS with 36 mJ/cm^2/min UVB for 45 seconds. Microarray analyses were carried out as described in Materials and Methods. Bars represent the average induction ratios (arsenite treated/untreated); uninduced genes show an induction value of 1.0. Average values from six microarrays +/- SEM.

Appendix I: Primers for RT PCR of cyclin D1 and beta actin

Primer Information:			
Name	**Primer sequence**	**GC %, Tm**	**Reference (from gene ID)**
			X59798:
cd1 3R	ctggcattttggagaggaag	50%,59.8°C	638 ← 657
cd1 4L	ccctcggtgtcctacttcaa	55%,60.1°C	267 → 286
Note:	Primer 4L is located in exon 1 (mRNA/genomic DNA: 267/2918). Primer 3R is in exon3 (mRNA/genomic DNA: 657/5411).		
4L + 3R, 390 bp	Therefore, if DNA contamination in RNA sample, the PCR product will be 5411-2918 = 2493 bp.		
			M10277:
ActinF	acactgtgcccatctacgagg	57%,72.8 °C	2147 → 2167
ActinR	aggggccggactcgtcatact	62%,74.7 °C	2954 ← 2974
Note:	The 621-bp fragment spans exon 3 through exon 5. (Intron 4: 95 bp; Intron 5: 112 bp)		
	Annealing temp: 59.6 °C, If genomic DNA contamination, the products would be 828 base pairs.		
Reference:	Cancer Epidemiol. Biomarkers Prev., Sep 1999; 8: 801.		

Appendix II: Oligonucleotides for EMSA probes:

Oligonucleotide information: for EMSA with cyclin D1 promoter, Tanscription factor binding site in bold, s: sense; a: antisense.			
Name	**Primer sequence**	**GC %, Tm**	**Reference**
			L09054:
creD1s	caacagtaacgtcacacggat	43%, 68.9 °C	-48~ -58
creD1a	atccgtgtgacgttactgttg	43%, 68.9 °C	-48~ -58
APW1s	tccgatgagtcagttctagagga	50%, 71.8 °C	-947~ -953
APW1a	tcctctagaactgactcatcgga	50%, 71.8 °C	-947~ -953
Tcf4s	ccgggctttgatctttgc	55%, 66.8 °C	-72~ -82
Tcf4a	gcaaagatcaaagcccgg	55%, 66.8 °C	-72~ -82
STATs	gggttcctggaaggg	66.7%,63.8 °C	-520~ -516
STATa	cccttccaggaaccc	66.7%,63.8 °C	
SP1-1s	ggcgcccgcgccccctcccccctgc	91.7%,91.0 °C	-102~ -124
SP1-1a	gcaggggggaggggcgcgggcgcc	91.7%,91.0 °C	-102~ -124
NFkBs	cggactacaggggagttttgttg	52.2%,73.5 °C	-30~ -39
NFkBa	caacaaaactcccctgtagtccg	52.2%,73.5 °C	-30~ -39

Bibliography

Abraham, R., Schäfer, J., Rothe, M., Bange, J., Knyazev, P., and Ullrich, A. **2005**. Identification of MMP-15 as an Anti-apoptotic Factor in Cancer Cells. *J. Biol. Chem.* 280: 34123-34132.

Asmuss, M., Mullenders, L.H., Eker, A., and Hartwig, A. **2000**. Differential effects of toxic metal compounds on the activities of fpg and XPA, two zinc finger proteins involved in DNA repair. *Carcinogenesis.* 21 (11): 2097-2104.

Bates, S., Rowan, S., and Vousden, K.H. **1996**. Characterisation of human cyclin G1 and G2: DNA damage inducible genes. *Oncogene.* 13(5):1103-1109.

Burns, F.J., Uddin, A.N., Wu, F., Nádas, A., and Rossman, T.G. **2004**. Arsenicinduced enhancement of ultraviolet radiation carcinogenesis in mouse skin: a dose–response study. *Environ. Health Perspect.* 112: 599–603.

Boyce, S.T. and Ham, R.G. **1985**. Cultivation, frozen storage, and clonal growth of normal human epidermal keratinocytes in serum-free media. *J. Tissue Cult.* Methods 9: 83–93.

Bröker, L. E., Kruyt, F. A. E., and Giaccone, G. **2005**. Cell Death Independent of Caspases: A Review. *Clin. Cancer Re.* 11: 3155-3162.

Chen, C.-J. and Wang, C.-J. **1990**. Ecological correlation between arsenic level in well water and age-adjusted mortality from malignant neoplasms. *Cancer Research.* 50:5470-5474.

Chen, N.Y., Ma, W.Y., Huang, C., Ding, M., and Dong, Z. **2000**. Activation of PKC is required for arsenite-induced signal transduction. *J. Environ. Pathol. Toxicol. Oncol.* 19 (3): 297-305.

Copenhagen, Denmark. **2000**. WHO Regional office for Europe, Chapter 6.1.

Corsini, E., Asti, L., Viviani, B., Marinovich, M., and Galli, C.L. **1999**. Sodium arsenate induces overproduction of interleukin-1 alpha in murine keratinocytes: role of mitochondria. *J. Invest. Dermatol*. 113 (5): 760-765.

Edelman, B., Steinberg, M.L., and Defendi, V. **1985.** Changes in fibronectin synthesis and binding distribution in SV40-transformed human keratinocytes. *Int. J. Cancer* 35 (2): 219-225.
Edmead, C., Kanthou, C., and Benzakour, O. **1999**. Thrombin activates transcription factors sp1, NF-kappaB, and CREB: importance of the use of phosphatase inhibitors during nuclear protein extraction for the assessment of transcription factor DNA-binding activities. *Anal. Biochem.* 275 (2): 180-186.

Engel, R., Hopenhaynrich, C., Receveur, O., and Smith, A. **1994.** Vascular effects of chronic arsenic exposure: A review. *Epidemology Review*. 16:184-209.
Environmental health criteria for arsenic and arsenic compounds. *The International Programme on Chemical Safety (IPCS).* 224: Chapter 1: Summary, Section 4. *The World Health Organization Press*, Geneva.

Fawell, J.K., and Mascarenhas, R. **2003.** Arsenic in Drinking-water: Background document for development of WHO Guidelines for Drinking-water Quality.

Feinglass, E.J. **1973.** Arsenic intoxication from well water in the United States. *New England Journal of Medicine,* 288: 828-830.

Felix, K., Manna, S.K., Wise, K., Barr, J., and Ramesh, G.T. **2005.** Low levels of arsenite activates nuclear factor-κB and activator-1 in immortalized mesencephalic cells. *J. Biochem. Mol. Toxicol.* 19 (2):67-77.

Germolec, D.R., Spalding, J., Yu, H.S., Chen, G.S., Simeonova, P.P., Humble, M.C., Bruccoleri, A., Boorman, G.A., Foley, J.F., Yoshida, T., Luster, M.I. **1998.** Arsenic enhancement of skin neoplasia by chronic stimulation of growth factors. *American Journal of Pathology.* 153 (6): 1775-1785.

Gomez-Caminero, A., Howe, P., Hughes, M., Kenyon, E., Lewis, D.R., Moore, M., Ng, J., Aitio, A., and Becking, G. **2001.** Environmental health criteria for arsenic and arsenic compounds. The International Programme on Chemical Safety (IPCS). 224: Chapter 1: Summary, Section 4. *The World Health Organization Press*, Geneva.

Goo, Y.-H., Sohn, Y.C., Kim, D.-H., Kim, S.-W., Kang, M.-J., Jung, D.-J., Kwak, E., Barlev, N.A., Berger, S.L., Chow, V.T., Roeder, R.G., Azorsa, D.O., Meltzer, P.S., Suh, P.-G., Song, E.J., Lee, K.-J., Lee, Y.-C., and Lee, J.W. **2003**. Activating Signal Cointegrator 2 Belongs to a Novel Steady-State Complex That Contains a Subset of Trithorax Group Proteins. *Mol. Cell. Biol.* 23: 140 - 149.

Gross, E.A., Callow, M.G., Waldbaum, L., Thomas, S., and Ruggieri, R. **2002**. MRK, a Mixed Lineage Kinase-related Molecule That Plays a Role in γ-Radiation-induced Cell Cycle Arrest. *J. Biol. Chem.* 277: 13873-13882.

Guha Mazumder, D. N. Diagonosis and treatment of chronic arsenic poisoning. WHO, **2000**.

Hallberg, B., Rayter, S. I., and Downward, J. **1994**. Interaction of Ras and Raf in intact mammalian cells upon extracellular stimulation. *J. Biol. Chem.* 269: 3913-3916.

Hamadeh, H.K., Trouba, K.J., Amin, R.P., Afshari, C.A., and Germolec, D. **2002**. Coordination of altered DNA repair and damage pathways in arseniteexposed keratinocytes. *Toxicol. Sci.* 69: 306–316.

Hanahan, D. and Weinberg, R. A. **2000**. The hallmarks of cancer. *Cell.* 100: 57-70.

Hei, T.K., Liu, S.X., and Waldren, C. **1998**. Mutagenicity of arsenic in mammalian cells: Role of reactive oxygen species. *Proc. Natl. Acad. Sci.* 95: 8103-8107.

Holmberg, C., Katz, S., Lerdrup, M., Herdegen, T., Jäättelä, M., Aronheim, A., and Kallunki, T. **2002**. A Novel Specific Role for IB Kinase Complex-associated Protein in Cytosolic Stress Signaling. *J. Biol. Chem.* 277: 31918-31928.

Horne, M.C., Goolsby, G.L., Donaldson, K.L., Tran, D., Neubauer, M., and Wahl, A.F. **1996**. Cyclin G1 and cyclin G2 comprise a new family of cyclins with contrasting tissue-specific and cell cycle-regulated expression. *J Biol Chem.* 271(11):6050-6061.

Huang, C., Ma, W-. Y., Li, J., and Dong, Z. **1999.** Arsenic Induces Apoptosis through a c-Jun NH2-Terminal Kinase-dependent, p53-independent Pathway. *Cancer Res.* 59: 3053 - 3058.

Huang, R.N., and Lee, T.C. **1996.** Cellular uptake of trivalent arsenite and pentavalent arsenate in KB cells cultured in phosphate-free medium. *Toxicol Appl Pharmacol.* 136(2): 243-249.

Hyun Park, W., Hee Cho, Y.,Won Jung, C., Oh Park, J., Kim, K., Hyuck Im, Y., Lee, M.H., Ki Kang,W., and Park, K. **2003.** Arsenic trioxide inhibits the growth of A498 renal cell carcinoma cells via cell cycle arrest or apoptosis. *Biochem. Biophys. Res. Commun.* 300 (1): 230–235.

IARC IARC Monographs on the Evaluation of Carcinogenic Risk of Chemicals to Man. **1980.** Some Metals and Metallic Compounds, Vol. 23, *Internatiomnal Agency for Research on Cancer, Lyon.*

Ikeyama, S., Wang, X.-T., Li, J., Podlutsky, A., Martindale, J.L., Kokkonen, G., Huizen, R., Gorospe, M., and Holbrook, N.J. **2003.** Expression of the Pro-apoptotic Gene gadd153/chop Is Elevated in Liver with Aging and Sensitizes Cells to Oxidant Injury. *J. Biol. Chem.* 278: 16726-16731.

Kessel, M., Liu, S.X., Xu, A., Santella, R., and Hei, T.K. **2002.** Arsenic induces oxidative DNA damage in mammalian cells. *Mol. Cell. Biochem.* 234-235: 301-308

Lau, A.T.Y., Li, M., Xie, R., He, Q.Y., and Chiu, J.F. **2004.** Opposed arsenite-induced signaling pathways promote cell proliferation or apoptosis in cultured lung cells. *Carcinogenesis*, 25 (1): 21-28.

Liao, W.T., Chang, K.L., Yu, C.L., Chen, G.S., Chang, L.W., and Yu, H.S. **2004.** Arsenic induces human keratinocyte apoptosis by the FAS/FAS ligand pathway, which correlates with alterations in nuclear factor-kappa B and activator protein-1 activity. *J. Invest. Dermatol.* 122 (1): 125–129.

Li, J.-H. and Rossman, T.G. **1989a.** Mechanism of comutagenesis of sodium arsenite with N-methyl-N-nitrosourea. Biol. *Trace Element Res.* 21: 373–381.

Li, J.-H. and Rossman, T.G. **1989b.** Inhibition of DNA ligase activity by arsenite: a possible mechanism of its comutagenesis. *Mol. Toxicol.* 2: 1–9.

Li, J.-H. and Rossman, T.G. **1991.** Comutagenesis of sodium arsenite with ultraviolet radiation in Chinese hamster V79 cells. *Biol. Met.* 4: 197–200.

Li, X., Ding, X., and Adrian, T.E. **2003.** Arsenic trioxide induces apoptosis in pancreatic cancer cells via changes in cell cycle, caspase activation, and GADD expression. *Pancreas* 27 (2): 174–179.

Lin, S., Cullen, W.R., and Thomas, D.J. **1999.** Methylarsenicals and arsinothiols are potent inhibitors of mouse liver thioredoxin reductase. *Chem Res Toxicol.* 12(10): 924-930.

Liu, Z., Shen, J., Carbrey, J.M., Mukhopadhyay, R., Agre, P., and Rosen, B.P. **2002.** Arsenite transport by mammalian aquaglyceroporins AQP7 and AQP9. *Proc Natl Acad Sci.* 99(9): 6053-6058.

Lynn, S., Lai, H.T., Gurr, J.R., and Jan, K.Y. **1997.** Arsenite retards DNA breat rejoining by inhibiting DNA ligation. *Mutagenesis.* 12 (5): 353-358.

Mak, S.K. and Kültz, D. **2004.** Gadd45 Proteins Induce G2/M Arrest and Modulate Apoptosis in Kidney Cells Exposed to Hyperosmotic Stress. *J. Biol. Chem.* 279: 39075-39084.

McCullough, K.D., Martindale, J.L., Klotz, L.-O., Aw, T.-Y., and Holbrook, N.J. **2001.** Gadd153 Sensitizes Cells to Endoplasmic Reticulum Stress by Down-Regulating Bcl2 and Perturbing the Cellular Redox State. Mol. Cell. Biol. 21: 1249-1259.

Moore, M.M., Harrington-Brock, K., Doerr, C.L. **1997.** Relative genotoxic potency of arsenic and its methylated metabolites. *Mutat. Res.* 386: 279–290.

Mori, J., Takahashi-Yanaga, F., Miwa, Y., Watanabe, Y., Hirata, M., Morimoto, S., Shirasuna, K., Sasaguri, T. **2005.** Differentiation-inducing factor-1 induces cyclin D1 degradation through the phosphorylation of Thr286 in squamous cell carcinoma. *Exp. Cell Res.* 310: 426–433.

Muscarella, D.E. and Bloom, S.E. **2002.** Differential Activation of the c-jun N terminal kinase pathway in arsenite-induced apoptosis and sensitization of chemically resistant compared to susceptible B-lymphoma cell lines. *Toxicological sciences.* 68: 82-92

Nagata, D., Suzuki, E., Nishimatsui, H., Satonaka, H., Goto, A., Omata, M., and Hirata, Y., **2001.** Transcriptional activation of the cyclin D1 gene is mediated by multiple cis-elements, including SP1 sites and a cAMP-responsive element in vascular endothelial cells. *J. Biol Chem.* 276: 662–669.

National Research Council, Arsenic in drinking water. **2000.** *National Academy Press*, Washington, DC.

Noda, Y., Suzuki, T., Kohara, A., Hasegawa, A., Yotsuyanagi, T., Hayashi, M., Sofuni, T., Yamanaka, K., and Okada, S. **2002.** In vivo genotoxicity evaluation of dimethylarsinic acid in MutaMouse. *Mutat. Res.* 513 (1–2): 205–212.

Ouyang, W., Ma, Q., Li, J., Zhang, D., Liu, Z.-G., Rustgi, A.K., and Huang, C. 2005. Cyclin D1 Induction through IκB Kinase ß/Nuclear Factor-B Pathway Is Responsible for Arsenite-Induced Increased Cell Cycle G1-S Phase Transition in Human Keratinocytes. *Cancer Res.*65 (20): 9287 - 9293.

Porter, A.C., Fanger, G.R., and Vaillancourt, R.R. **1999.** Signal transduction pathways regulated by arsenate and arsenite. *Oncogene.* 18 (54): 7794-7802.

Pott, W.A., Benjamin, S.A., and Yang, R.S. **2001.** Pharmacokinetics, metabolism, and carcinogenicity of arsenic. *Rev. Environ. Contam. Toxicol.* 169: 165-214.

Roux, P. P. and Blenis, J. **2004.** ERK and p38 MAPK-activated protein kinases: a family of protein kinases with diverse biological functions. *Microbiol. Mol. Biol. Rev.* 68(2): 320-344.

Rosenwald, I.B., lazaris-Karatzas, A., Sonenberg, N., Schmidt, E.V. **1993.** Elevated levels of cyclin D1 protein in response to increased expression of eukaryotic initiation factor 4E. *Mol. Cell. Biol.* 13 (12): 7358–7363.

Rossman, T.G., Uddin, N., Burns, F.J., and Bosland M.C. **2001.** Arsenite is a cocarcinogen with solar ultraviolet radiation for mouse skin: an animal model for arsenic carcinogenesis. *Toxicol. Appl. Pharmacol.* 176 (1):64-71.

Rossman , T. G. **2003.** Mechanism of arsenic carcinogenesis: an integrated approach. *Mutat. Res./Fundamental and Molecular Mechanisms of Mutagenesis*. 533 (1-2): 37-65.

Samet, J.M., Silbajoris, R., Wu, W., and Graves, L.M. **1999**. Tyrosine phosphatases as targets in metal-induced signaling in human airway epithelial cells. *Am. J. Respir. Cell. Mol. Biol.* 21 (3): 357-364.

Sarkar, D., Imai, T., Kambe, F., Shibata, A., Ohmori, S., Hayasaka, S., Funahashi, H., and Seo, H. **2001.** Overexpression of Glutathione-S-Transferase A1 in Benign Adrenocortical Adenomas from Patients with Cushing's Syndrome. *J. Clin. Endocrinol. Metab.* 86: 1653-1659.

Schaumloffel, N. and Gebel, T. **1998.** Heterogeneity of the DNA damage provoked by antimony and arsenic. *Mutagenesis.* 13 (3): 281-286.

Schwerdtle, T., Walter, I., Mackiw, I., and Hartwig, A. **2003.** Induction of oxidative DNA damage by arsenite and its trivalent and pentavalent methylated metabolites in cultured human cells and isolated DNA. *Carcinogenesis.* 24(5): 967-974.

Shack, S., Wang, X.-T., Kokkonen, G.C., Gorospe, M., Longo, D.L., and Holbrook, N.J. **2003.** Caveolin-Induced Activation of the Phosphatidylinositol 3-Kinase/Akt Pathway Increases Arsenite Cytotoxicity. *Mol. Cell. Biol.* 23: 2407-2414.

Simeonova, P.P., Wang, S., Toriuma, W., Kommineni, V., Matheson, J., Unimye, N., Kayama, F., Harki, D., Ding, M., Vallyathan, V., and Luster, M.I. **2000.** Arsenic mediates cell proliferation and gene expression in the bladder epithelium: association with activating protein-1 transactivation. *Cancer Res.* 60 (13): 3445-3453.

Steinberg, M.L., Chen, G.T., Vazquez, R., Ruml, T., and Kas, J. **1999.** SV40-immortalized human keratinocytes as an in vitro model system for studying environmental carcinogens. *International Biodeterioration & Biodegradation.* 44, 7-16.

Steinberg, M.L. and Defendi, V. **1982**. Fusion induced differentiation of SV40 transformed human keratinocytes. *Exp. Cell Res.* 139: 369–375.

Styblo, M., Serves, S.V., Cullen, W.R., and Thomas, D.J. **1997**. Comparative inhibition of yeast glutathione reductase by arsenicals and arsenothiols. *Chem Res Toxicol.* 10(1): 27-33.

Tanaka-Kagawa, T., Hanioka, N., Yoshida, H., Jinno, H., and Ando, M. **2003**. Arsenite and arsenate activate extracellular signal-regulated kinases 1/2 by an epidermal growth factor receptor-mediated pathway in normal human keratinocytes. *Br J Dermatol.* 149(6):1116-27.

Thomas, D.J., Styblo, M., and Lin, S. **2001**. The cellular metabolism and systemic toxicity of arsenic. *Toxicol. Appl. Pharmacol.* 176(2): 127-144.

Tseng, W.P. **1977**. Effects and dose response relationships of skin cancer and blackfoot disease with arsenic. *Environ. Health Perspect.* 19: 109–119.

Tully, D.B., Collins, B.J., Overstreet, J.D., Smith, C.S., Dinse, G.E., Mumtaz, M.M., and Chapin, R.E. **2000**. Effects of arsenic, Cadmium, chromium, and lead on gene expression regulated by a battery of 13 different promoters in recombinant $HepG_2$ cells. *Toxicol. Appl. Pharmacol.* 168 (2): 79-90.

Vahter, M. **1999**. Methylation of inorganic arsenic in different mammalian species and population groups. *Sci Prog.* 82 (Pt 1): 69-88.

Vogt, B.L. and Rossman, T.G. **2001**. Effects of arsenite on p53, p21 and cyclin D expression in normal human fibroblasts—A possible mechanism for arsenite's comutagenicity. *Mutat. Res.* 478 (1–2): 159–168.

Welch, A.H., Lico, M.S., and Hughes, J.L. **1988**. Arsenic in ground water of the western United States. *Ground Water,* 26:333–347.

WHO, **2006**. Guidelines for drinking-water quality, third edition.

Wu, W., Graves, L.M., Jaspers, I., Davlin, R.B., Reed, W., and Samet, J.M. **1999.** Activation of the EGF receptor signaling pathway in human airway epithelial cells exposed to metals. *Am. J. Physiol.* 277 (5) L924-931.
Zhao, C.Q., Young, M.R., Diwan, B.A., Coogan, T.P., and Waalkes, M.P. **1997.** Association of arsenic-induced malignant transformation with DNA hypomethylation and aberrant gene expression. *Proc. Natl. Acad. Sci.* 94 (20): 10907-10912.

Zhao, S., Tsuchida, T., Kawakami, K., Shi, C., and Kawamoto, K. **2002.** Effect of As_2O_3 on cell cycle progression and cyclins D1 and B1 expression in two glioblastoma cell lines differing in p53 status. *Int. J. Oncol.* 21 (1): 49-55.

Part II. UVB-induced Mitochondrial DNA deletions in NHEK exposed to arsenite.

Abstract:

The study was started with a FS20 UVB irradiation on detecting the mitodhondiral DNA deletion and later sub-micromolar arsenite was employed for examining the synergistic effects. The formation of mitochondrial deletions brought about by FS20 irradiation was first examined in a line of SV40 immortalized human epithelial cells. In this system, MtDNA deletions were found to be induced within 24 h following a single irradiation as low as 1.4 mJ/cm2 from an FS20 light source. We observed at least two distinct FS20-induced Mt deletions: the widely observed 4977 bp common deletion (CD) and a novel 5128 bp deletion flanked by TAGG repeats at nt 8247–8250 and 13,375–13,378 that has not, to our knowledge been previously described. While glutathione (GSH) at concentrations between 50 and 200 μM was found to block the formation of the CD in a dose-dependent manner, GSH at higher concentration induced the CD even in unirradiated cells. This is consistent with the idea that low dose GSH inhibits CD formation via reductive elimination of

peroxides while higher concentrations may act as an electron donor to produce reactive oxygen species. Interestingly, in irradiated cells, GSH at intermediate concentrations (50 μM) induced a second, shorter, deletion similar to the novel deletion induced by FS20 alone but involving a different TAGG repeat spanning nt 13,175–13,178.

Based on the preliminary results of the UVB induced mtDNA deletion and our microarray experiments of NHEKs treated with sub-micromolar arsenite (part I), another series of studies was carried out with the aim of examining the possible role of arsenic in potentiating the DNA damaging effects of FS20 ultraviolet B (UVB) radiation. For this purpose the formation mitochondrial DNA (mtDNA) deletions in arsenite treated NHEK was studied. The goals of the studies in this part were: (1) characterization of arsenic and UVB induced mtDNA deletions. (2) Quantitation of deletions and the production of reactive oxygen species (ROS) in UVB and arsenite+UVB treated cells.

We have identified several more different mtDNA deletions in arsenite-treated and UVB irradiated human epithelial keratinocyte using both normal keratinocyte (NHEK) and SV40 transformed cell lines as model systems. The relative levels of deletions were quantitated through

real time PCR. Arsenite treated cells with UVB irradiation appear to exhibit more deletions, especially in arsenite-treated NHEKs exposed to higher levels of UVB irradiation (4, and 8 minutes; or 5.7 mJ/cm^2 and 11.4 mJ/cm^2 respectively). We also observed that the reactive oxygen species (ROS), as measured flourescently by ROS-reactive dyes, were induced by UVB irradiation (2.9, 5.7, and 11.4 mJ/cm^2) but reduced in NHEKs treated with 400 nM arsenite.

Introduction:

It has been shown that arsenic induces chromosome aberrations and inhibits DNA repair in mammalian cells (Moore, L.E. *et. al.*1997). At least one study has shown that the genotoxic effects of arsenite may be caused by the generation of hydroxyl radicals (Liu, S.X. *et. al.*2001). Reactive oxygen species (ROS) and other organic free radicals, such as ubisemiquinone and flavosemiquinone, are generated through the electron transport chain as byproducts (Agarwal, S. *et. al.*1994). These ROS are normally detoxified by antioxidants and free radical-scavenging enzymes such as manganese superoxide dismutase, catalase and glutathione peroxidase, inside mitochondria. Therefore, if mitochondria are damaged by chemicals which cause a decrease in the activity of these detoxification systems, cellular levels of ROS will increase. ROS will then cause mtDNA mutations and lipid peroxidation of mitochondrial membranes. (Wei, Y.H. 1998). The damaged membranes may then cause leakages of ROS into cytoplasm and diffusion of ROS may enhance genotoxicity to cells. Therefore, both ROS activity and mtDNA mutations are indicators of genotoxic processes that may be caused by a variety of stimuli.

Mitochondria contain their own genetic material. Human mtDNA is a 16571 bps circular, double-stranded molecule. There are 37 genes: 2rRNA genes, 22 tRNA genes, and 13 structural genes in human mtDNA (Figure 1, Moraes, C. T. *et. al.* 2003). MtDNA is highly susceptible to environmental stress because of the lack of protective histones, and the constant exposure to reactive free radical species. Trivalent arsenic has been reported to induce multilocus mutations, mostly large deletion mutations, through generation of reactive oxygen species (Hei, T.K. *et. al.* 1998). Other research has also illustrated that the mitochondrion is a primary target of arsenite-induced genotoxic effect in mammalian cells (Hei, T.K. *et. al.* 2005).

MtDNA mutations cause disease when mutations accumulate to a minimum critical number in different tissues (threshold effect). One widely observed mutation, the common deletion (Figure 1), has been associated with diseases of the nervous system (Lane, H. *et. al.* 2003; Gu, G. *et. al.* 2002), eye and heart (Lin, P.H. *et. al.* 2003; Arai, T. *et. al.* 2003; Tabaku, M. *et. al.*1999), thyroid, (Maximo, V. *et. al.* 2002; Rogounovitch, T.I. , *et. al.* 2002) kidney (Niaudet, P. *et. al.* 1994; Hirayama, K. *et. al.* 2002) and skin (Ray, A.J. *et. al.* 2000; Berneburg, M. *et. al.*

2004). However, the effect of arsenite on the formation of deletions in human mtDNA has been little studied. A possible mechanism for the generation of common deletion has been proposed by Berneburg's group (Figure 2, Berneburg, M., et. al. 1999). In this model deletion is mediated by two 13-base-pair direct repeat (DR) sequences ACCTCCCTCACCA in 8471 and 13460 in Cambridge mitochondrial DNA reference sequence (Gen-Bank no. NC_001807. [gi:17981852]). When mtDNA replicates asymmetrically from the origin of heavy strand (O_H), the single stranded segment (ss) generated from the replication fork will form a D-loop containing one direct repeat (DR1). Then, as the replication fork progresses, the SS DR1 can anneal to DR2 on the complementary strand. If the D-loop on heavy strand of mtDNA is attacked by UV-generated ROS, the nicked, unpaired single stranded DNA is subject to degradation by exonucleases. Degradation proceeds up to the double stranded segment containing the base paired repeats. Recombination within the repeats followed by ligation results in a mtDNA heavy strand containing the 4977 bp deletion.

In our laboratory, we have studied mitochondrial DNA deletions caused by ultraviolet radiation in cells treated with arsenite. We have also characterized several types of novel deletions other than common deletion that may also be associated with these environmental toxicants. We have designed primers and probes for quantification of specific types of mtDNA deletions to examine the effects of arsenite and UVB on NHEK cells.

Materials and methods:

A. PCR study for Mitochondrial DNA deletion:

Line 22 and 130 SV40 immortalized human epidermal keratinocytes (IHEKs) were used for some of the experiments. Cells were grown in DMEM supplemented with 15% fetal bovine serum and 4□g/ml hydrocortisone. NHEK (Normal human epithelial keratinocyte from Cambrex Corp.) cells were grown in culture medium supplied by Cascade Biologics Company. Cells were treated with sodium arsenite when they were at about 30 % confluence. Cells were irradiated from the bottom with an FS20 lamp (Light Source, Inc.) (Figure 4) at a distance of 35 cm for various times as indicated. The FS20 covers the UVB range (290–320 nm) with an emission spectrum between 272 and 390 nm and a λmax of 312.5 nm. Absorption of light by the plastic wall of the culture flask (Figure 5) was measured using a Cary 500 spectrophotometer (Varian, Inc.); the flask absorbed more than 85% at wavelengths below 295 nm and about 51% of the light at λmax. The irradiation dosage cells received ranged between 2 and 8 minutes were approximately 1.4 to 11.4 mJ/cm^2. Total cellular DNAs were isolated using DNeasy blood and tissue kit (QIAGEN, cat. no. 69504). DNA concentrations were determined by reading the absorbance 260/280 nm in spectrophometry.

Deletion analysis was carried out by the PCR-based technique of Soong and Arnheim (Soong, N.-W., and Arnheim, N. 1996**)** using the amplimer pair MT2 and MT1C for amplification of non-deleted sequences (nt 13,175–13,500; revised Cambridge reference sequence, Gen-Bank no. NC 001807). The nested amplimers MT3 and MT2 paired with MT1A were used to detect mitochondrial fragments representing deletions within the segment spanning nt 8224 and 13,500 (Figure 3). By employing a short 2-segment amplification protocol in which primer annealing and DNA polymerization segments at 60 ^{o}C for 20 seconds were combined, we were able to specifically amplify the few hundred base-pair mtDNA fragments; the large undeleted mtDNA require at least 5 minutes to complete an amplification cycle. For sequencing, PCR products were precipitated for 1 hour with 1 volumes of 4M ammonium acetate and 2 volumes of ethanol. The precipitate was pelleted and the pellet was washed with 70% ethanol, air dried and resuspended in TE buffer and sequenced in the RCMI sequencing facility at City College using the amplimers as a sequencing primers. The locations of the deletion(s) boundaries were determined by alignment of the PCR product sequence with the Cambridge mitochondrial DNA reference sequence (Gen-Bank no . NC_001807. [gi:17981852]).

We have characterized several novel mtDNA deletions caused by UVB irradiation in IHEK line 22, and proposed possible mechanisms for their formation (Figure 8 and 10 Fang, J. *et. al*. 2006). We have now discovered a number of other deletions and designed primers MLs (ML1~ML6) and MRs (MR1~MR5), UV1, and UV2 (Figure 11) for further studies on specific types of deletions.

B. Real time PCR for common deletion and type II deletion:

For real time PCR of Common deletion and Δuv, the Roche LightCyler for Real-Time PCR was used to measure total mitochondria and the common deletion. Each capillary contained 1X LightCycler® FastStart DNA Master HybProbe, 300nM each forward and reverse primer, 200 nM probe and 0.1 unit heat-labile uracil-DNA glycosylase (Roche Applied Science) in a total volume of 10 μl. The probe for the ensuing amplicon is located at nucleotides 13,461–13,480 of the Cambridge sequence and is tagged with the reporter FAM (6-carboxy fluorescein, λmax 518 nm) at the 5′ end and the quencher BHQ1 at the 3′ end. Pogozelski (Pogozelski W.K. *et al.* 2003) designed two plasmids, one that contains the amplicon for the common deletion and the other that contains the amplicon for total mitochondria. In each run, as appropriate, the plasmids were run as external controls.

For common deletion, copy number per cell was determined from the plasmid control copy number and its threshold cycle.

For the experiments with arsenite and UVB, we designed a FAM (6-carboxy fluorescein, λmax 518 nm)-labeled probe for the common deletion (FAM- tggcagcctagcatt-MGB) which have been tested in real time PCR using the appropriate primer pairs. Primers MT1C and UV2 were used for endogenous control which will amplify a 229 base-pair product from undeleted mitochondria. For reactions using a FAM-labeled probe, 300 nM of probe, forward and reverse primers were mixed with Taqman universal PCR master mix (ABI, cat. no. 4304437) and the mixture was added to reaction tubes containing 20 ng of the indicated DNA samples. For endogenous controls, the reactions were performed in a similar way with 0.2 ng sample DNAs and without the addition of probe but using power SYBR green PCR master mix (ABI, cat. no. 4368577). Type II deletions were detected in the real time PCR in the presence of Sybr Green. Primers ML2, MR1 (300 nM each), dNTP (400 nM), and 0.5X sybr green (Invitrogen/Molecular Probes, S7563) were mixed with PCR reaction mixture and added to optical tubes containing 20 ng of DNA templates isolated from treated NHEKs. The tubes of endogenous controls were set in a

similar manner 2 with 0.2 ng DNA templates. Data was then collected and analyzed using relative quantification method (RQ method) in SDS v1.3.1 software from Applied Biosystems for relative levels of gene expression.

C. Reactive oxygen species detection:

NHEKs were grown on cover slips and treated with arsenite. To examine oxyradical production, NHEKs were grown either with or without 400 nM arsenite and irradiated with different doses of UVB 24 hours later. One day later, cells were incubated with 2 μM 5′, 6′-carboxy-2′, 7′-dichlorodihydrofluorescein diacetate (carboxy-DCFDA) for 40 minutes. Cells were then trypsinized and washed three times with PBS and fluorescent signals were measured in FACS.

Results:

1. Mitochondrial deletions induced by FS20 in vitro

We used the technique described by Soong and Arnheim (Soong, N.-W. and Arnheim, N. 1996) to study the formation of mitochondrial deletions in vitro after FS20 irradiation of a line of human epithelial cells. This analysis makes use of the fact that large deletions result in the fusion of normally distal DNA segments so that PCR products from primers located within these distal segments generate aberrantly short products. In these experiments, we found that irradiation of line 22 keratinocytes with an FS20 light source lead to the induction of mitochondrial deletions within 24 h after a single exposure (Figure 6). Irradiated cells were found to exhibit at least two distinct mitochondrial deletions that generated corresponding PCR products of about 300 and 150 bp with the MT1A and MT2 amplimer pair (Figure 6, upper and middle panels). These experiments also showed that induction of the deletions increased in a manner related to irradiation dosage over exposure times ranging between 1 and 8 minutes (1.4–11.4 mJ/cm2) although maximal band intensities were generally seen after 4 minutes of irradiation (5.7 mJ/cm2) and all subsequent experiments were carried out using an

irradiation time of 4 minutes. Figure 6 also illustrates that, in the in vitro system, the intensity of the PCR bands corresponding to each deletion varied independently from one another and from one experiment to the next but were consistent within each experiment. We generally observed that one type of deletion predominated in a given experiment although in some experiments PCR products for both deletions were present in about equal quantity (one example is shown in Figure 8, lower panel). PCR products corresponding to mitochondrial genomes carrying deletions could only be seen in the nested PCR reactions indicating that they represent only a small fraction of the total mitochondrial pool.

Real time PCR showed that the common deletion was present even in non-irradiated cells but only at a level of about 0.003 copies/cell or in about 0.04% of the total mitochondrial genomes. After 4 minute-irradiation, this increased to 0.013 copies/cell or about 0.12% of mitochondrial genomes. A dose-dependent increase in deletion formation was seen in cells irradiated for 1, 2 and 4 minutes (1.4, 2.9, and 5.7, mJ/cm^2 respectively, Figure 9).

Mitochondrial deletions are widely believed to involve strand breaks caused by reactive oxygen species such as

superoxides or hydroxyl radicals. If the FS20-induced mitochondrial deletions involve ROS, then their formation ought to be suppressed by antioxidants, particularly those that act directly to eliminate ROS via reductive mechanisms. In order to determine whether ROS production plays a direct role in the formation of deletions in the FS20 irradiated cells, we examined the effects of the antioxidant, glutathione (GSH) on mitochondrial deletions in the in vitro system. When cells were pretreated 24 h prior to irradiation with GSH at concentrations ranging from 50 to 200 μM the antioxidant was found to block formation of the deletions in a dose-dependent manner (Figure 7). However, irradiated cells treated with GSH at 100 and 200 μM also displayed two additional small MT1A/MT2 PCR bands of about 150 and 100 bp, respectively. Surprisingly, we also observed a PCR product of about 300 bp in cells treated with 1mM GSH alone.

Sequence analyses carried out on the gel purified PCR bands in figure 6 showed that the PCR product of about 300 bp represented the well characterized 4977 bp deletion referred to as the common deletion (CD) that is generated from complementary cuts within two perfect 13 bp repeats that flank the deletion (Pogozelski, W.K. *et. al.* 2003). The smaller band was found to contain a fusion product

derived from a larger deletion of 5128 bp (Δuv) with cut sites within the flanking tetramer; TAGG (mitochondrial nt 8247–8250) and its inverted complement ATCC (nt 13,375–13,378; Figure 8) and appears to represent a novel deletion not previously described. In several cases, we were able to detect low levels of spontaneous deletion in control cultures. The spontaneous deletions all proved to be the 5128 bp deletion seen in FS20 irradiated cells (Δuv). In the Δuv deleted mitochondrial genomes, the fragments of the cut sites were present in the fusion sequence, TATCC, indicating a mechanism of deletion involving two possible cut schemes within the TAGG and ATCC motifs, either TA↓GG/A↓TCC or T↓AGG/↓ATCC. Sequence analysis of the PCR product of ~150 bp in irradiated cells treated with 100 μM GSH showed it to be identical with the PCR product corresponding to the novel 5128 bp deletion induced by FS20 alone (Figure. 6, middle panel, and 8). The smaller product of ~100 bp was not seen to exhibit homology to any mitochondrial sequences in an NCBI BLAST search. We also found that, in FS20 irradiated cells pretreated with GSH at the two higher concentrations (500 and 1000 μM), the MT1A/MT2 amplimers produced a more intense band with a slightly larger apparent size than the 303 bp product corresponding to the common deletion. The nucleotide

sequence data showed that these bands represented a 4927 bp deletion distinct from either of the deletions produced by irradiation alone. Sequence alignments showed that this new deletion (Δuv+GSH) was generated by cuts within the Δuv upstream TAGG tetramer at nt 8247–8250 and a second TAGG direct repeat at nt 13,175–13,178. Sequence analyses of the PCR product of ~300 bp seen in cells treated with 1mM GSH alone (Figure 7) showed that this product represented induction of the common deletion.

2. Identification of mtDNA deletions generated by arseite and UVB:

Continuous from the UVB induced mtDNA deletions; we are able to design more primers to study the mtDNA deletions (Figure 11). By using recent designed primers and PCR studies described in material and methods, we obtained several more types of mitochondrial deletions caused by UVB irradiation and arsenite treatment (Figure 12). Figure 12 shows different types of deletions found in our laboratory. One group of deletions has direct repeats at both cut sites as shown on the upper image of figure 12. This type of deletion maintains one copy of the repeat sequence after formation of the deletion. We also observed other types of deletions which may utilize the repeat sequences

(underlined) within, or near the deleted regions (strikethrough, on the bottom of figure 12). The repeat sequences are lost after deletion. In one case, we observed inverted repeats at both cut sites and there are an additional 2 bases in the junction (Figure 12, last type). In this case, GAA/CTT seems to be the key element mediating this particular type of deletion.

Figure 13 shows the PCR products for 2 kinds of deletions (Common deletion, and type II, the first 2 with direct repeat sequences "ACCTCCCTCACCA" and "AGCCCACT" figure 12) using the primer set ML4/MR3 for the common deletion and ML2/ML1 for the type II deletion. The corresponding 161 and 155 base-pair PCR products were purified and sequenced for confirmation. Since there are other PCR products that can be observed in agarose gels and the total band intensity does not represent the level of any specific mtDNA deletion in a given sample. We then designed specific probes for real time PCR to study specific deletions.

3. Real time PCR study for two types of deletions

Two types of deletions were examined by real time PCR to study the effects of arsenite and UV irradiation on NHEK

cells. The common deletion was significantly increased by exposure to 400 nM arsenite and UVB irradiation while the type II was induced less in both treatment conditions (figure 14 and Table 1). NHEKs treated with 400 nM arsenite exhibited higher levels of the common deletion, especially in cells exposed to 5.7, and 11.4 mJ/cm^2 UV irradiation, compared with untreated NHEKs. A UVB dose dependent pattern was observed in both untreated and arsenite treated groups for the common deletion. For the type II deletion, UVB irradiation only caused a slight increase in the non-arsenite-treated group. The addition of sodium arsenite tended to accelerate the induction of mtDNA deletion on type II deletion and exhibits a UVB dose-dependent manner on 2.9, and 5.7, mJ/cm^2 UVB irradiation.

4. Reactive oxygen species detection:

We examined oxyradical production induced by sub-micromolar arsenite on NHEK cells. Cells pretreated with 400 nM arsenite for 48 hours and incubated with carboxy-DCFDA showed significant decrease (about 40 %) on the fluorescent signals compared to untreated control. The group of NHEKs irradiated with 2.9, 5.7, and 11.4 mJ/cm^2 UVB one day before ROS detection has about 20 % increase of ROS activity. The NHEKs pretreated with 400 nM and irradiated

with UVB shows some ROS induction by irradiation compared to arsenite treated control. However, if we compare them to the indicated UVB irradiated samples, the arsenite treated cells also had less ROS generation.

Discussion:

1. The novel mtDNA deletions in human epithelial cells irradiated with an FS20 ultraviolet light source.

In this report, we have described an *in vitro* model system of human epithelial cells in which mitochondrial genomic deletions were induced by FS20 irradiation. In addition to the 4977 bp deletion often observed in a wide variety of pathological conditions we also found at least two other deletions produced by FS20 or FS20 in combination with GSH that appear to be novel. The breakpoints of the vast majority of the mitochondrial deletions occur at sites that are within, or just adjacent to, segments that are repeated at or close to the breakpoints of the deletion (summarized on the MITOMAP website, www.mitomap.org). The breakpoints of the two novel deletions occurred either within repeats of the tetrameric sequence TAGG (Δuv+GSH) or within TAGG and its inverted complement, ATCC (Δuv). We found no other reports of deletions occurring at TAGG and/or ATCC sites although there is at least one report of CCTA used as a cut site in a case of mitochondrial myopathy (Larsson, N.-G. and Holme, E. 1992). We were unable to discern any significant features of the sequences flanking the TAGG cut sites nt 8247–8250 and 13,175–13,178 that

might account for why deletions at these TAGG sites might be favored over any of the other 15 TAGG motifs that are present within the MT2/MT1A primer region. It has been suggested that the nucleotide environments surrounding the cut site motifs may play a role in determining site selection, possibly by inducing a favorable local tertiary structure (Hou, J.H. and Wei, Y.H. 1998). The deletions removed segments of the mitochondrial covering complexes I, IV and V but the frequency of the deletions under the conditions tested was too small to cause significant damage to overall electron transport function.

The mechanism by which deletion occurs in mitochondria is generally believed to involve a slipstrand intermediate in which the heavy strand upstream repeat segment mispairs with the complementary sequences of its downstream counterpart; this leads to the formation of a single stranded loop which is subsequently removed to create the deletion (Berneburg, M. *et. al.* 1999). However, the uv deletion cut sites are inverted complements of one another rather than direct repeats. Therefore, a similar slipstrand mechanism would require that the cut site sequences be aligned in parallel and the duplex stabilized by Hoogsteen base pairs. Hoogsteen base pairing is frequently seen in distorted DNA helices, particularly in

triple helical DNA (Frank-Kamenetskii, M.D. and Mirkin, S.M. 1995.) but has also recently been demonstrated in duplexes of short oligonucleotides (Aishima, J. *et. al.* 2002). For the Δuv repeat sequences, it is likely that a parallel duplex could be generated via mispairing of the cut sites either via an intrastrand duplex or in a triple helical intermediate with the double stranded downstream cut site similar to the model proposed by Rocher et al. (Rocher, C. *et. al.* 2002) (Figure 10).

We were also able to use the in vitro system to test the effects of antioxidants on the formation of deletions. Depending upon concentration, glutathione pretreatment both suppressed and induced mitochondrial deletions. At low concentrations the FS20-induced deletions were suppressed by GSH pretreatment as well as other antioxidants including ascorbic acid (not shown) indicating that their formation was mediated by ROS. However, the induction of deletions by GSH alone or in concert with uv radiation was unexpected. The antioxidant effects of glutathione$_{red}$ stem from its ability to carry out the reduction of peroxides and free radicals. However, at the higher concentrations, GSH might, itself, also generate ROS by reduction of oxygen via electron carriers: 2GSH→GSSG +H+ +2e−, e− +O2→O2−.

The majority (22 out of 27) of the FW20-induced deletions that we sequenced were not the 4977 bp common deletion but were rather the novel, 5128 bp deletion (Δuv). Although the reasons for this variability remain unknown, it seems likely that slight differences in ongoing metabolism and/or redox status of the cells in different experiments might produce differing rates of deletion at the different mitochondrial genomic loci. Berneburg et al.(Berneburg, M. *et al.* 2004) studied UVA-induced mtDNA deletions in human fibroblasts. In that system, deletions were only seen after multiple irradiations using >1000-fold higher doses of ultraviolet radiation than used here but, in the keratinocyte system, using FS20, deletions were seen after a single irradiation.

2. Identification of mtDNA deletions in human epithelial cells treated with 400 nM sodium arsenite and ultraviolet.

We have described an *in vitro* model system of human epithelial cells in which mitochondrial genomic DNA deletions were induced by FS20 irradiation. In addition to the 4977 bp common deletion often observed in a wide variety of pathological conditions we also found at least 6 other deletions produced by irradiation with an FS20 UVB

light source or FS20 irradiation in combination with sub-micromolar sodium arsenite. The breakpoints of the vast majority of the mitochondrial deletions occur at sites that are within, or just adjacent to, segments that are repeated at or close to the breakpoints of the deletion. One group of deletions was apparently mediated by recombination involving direct repeat sequences (Figure 12, upper panel) and they were easily identified. For those deletions caused through homologous sequence near the breakpoint, the mechanism may be a little different. However, some of the deletions' cut sites are inverted complements of one another rather than direct repeats. (The third from the bottom of Figure 12, TAGG/ATCC). For the last type of deletion (AAG/CT/TGAA), the upstream AAG end mispairs with the complementary sequence on the downstream side. The breakpoint contains an insertion of two additional bases to become CTT in the middle which is an inverted complementary sequence of AAG.

3. Quantification of mtDNA deletions in normal human epithelial cells treated with 400 nM sodium arsenite and ultraviolet.

In the quantitative studies, our finding of two types of mitochondrial DNA deletion is consistent with the finding that arsenite, together with UVB irradiation seems to

enhance DNA damage caused by ultraviolet irradiation. Arsenite is also believed to act to cause oxidative stress to cells, especially to their mitochondria. Mitochondrial DNA, however, has fewer DNA repair enzymes and histones than is true for chromosomal DNA. Therefore, a variety of mutations can accumulate and persist throughout a lifetime. As people age, they are subjected to ROS stresses from sunlight and environmental chemicals. The accumulation of mtDNA mutations will become significant and lead to diseases associated with mtDNA alterations of various types (Johns, D.R. *et al.*1995). Our real time PCR results showed that submicromolar arsenite enhances the events of DNA recombination/deletion on mtDNA. An increase in mtDNA damage is likely to reflect an increase in overall DNA damage.

4. ROS was induced in NHEKs treated with ultraviolet B, but was reduced by 400 nM arsenite.

Arsenicals have been shown to induce reactive oxygen species (ROS) which can cause DNA damage and other damages in cells (Shi, H. 2004a). Wang's study on CHO-KI cells suggests that arsenite promotes the production of ·OH from H_2O_2 (Wang, T.S., *et. al.* 1996). This report also indicated that $O_2\cdot^-$ is likely the primary ROS induced by arsenic. The

formation of $O_2 \cdot^-$ will then cause a cascade of other ROS species such as H_2O_2 and ·OH. The most possible source of ROS is mitochondria. Evidence shows that ROS induced by arsenate could be completely abrogated by rotenone in HEL 30 cells indicating that mitochondria are involved in the arsenite induced ROS generation (Corsini, E., *et. al.* 1999). Free radical production may be increased by arsenite at the ubiquinone site of the respiratory chain. Even though there might be some other sources of ROS in the cells that may be induced by arsenicals, mitochondria are still considered as the main source of ROS induced by cells (Shi, H. 2004b). Therefore, damage to mitochondria and mtDNA may be important indicators of processes related to arsenite-induced disorders including tumor formation.

Carboxy-DCFDA is a standard probe for ROS. It detects hydrogen peroxide (H_2O_2), hydroxy radical (HO-), hypochlorous acid (HOCl), and peroxyl radical (COO-). For peroxynitrite anion (ONOO-) and superoxide anion (O_2-), other probes such as coelenterazine (for both ONOO- and O_2-), dihydrorhodamine 123 (for ONOO-), or 2-methyl-6-(4-methoxyphenyl)-3,7-dihydroimidazo[1,2-a]pyrazin-3-one (MCLA, for O_2-), should be used. Carboxy-DCFDA is colorless and nonfluorescent until it's oxidized. The hydrolysis of the acetate groups by intracellular esterases generates a more

polar species and allows it to be retained inside the cell. Unlike Hei's studies (Hei, T.K. *et. al.* 1998) which employed micromolar range of arsenite to treat cells and examine ROS in 5~10 minutes, our observations show that 400 nM arsenite reduced ROS while irradiation with UVB increased ROS by about 20 % after 24 hours. The ~20 % ROS induction seems to be less than what we expected and we recently employed two other ROS detection dyes, dihydrorhodamine I23 (for ONOO-, Molecular Probes, #D23806), and MitoSOX Red (for O2-, Molecular Probes, # M36008) to study the induction of ROS for different periods of incubation time after 5.7 mJ/cm^{2}UVB irradiation. These results showed that ROS induction might reach a maximum at about 30 minutes after the irradiation and return back to levels slightly above normal (not shown). We think that ROS formation will follow a similar time course in cells treated with arsenite and our ongoing studies will focus on the same time points in arsenite-treated cells. The reduction of ROS observed in our carboxy-DCFDA staining was performed 2 days after arsenic addition and the oxidative stress induced by arsenite may already be removed. Low dose arsenite has been found to protect against subsequent oxidative stress in WI38 fibroblasts and HaCaT keratinocytes (Snow, E.T. *et. al*. 2005). In these

experiments ROS production was found to be decreased by 0.5 μM arsenite at 24 hour time point. The low dose protective (adaptive) effect against oxidative stress was found to be associated with increased transcription, protein levels and enzyme activity of some base repair genes. Glutathione (GSH) and some major glutathione-related redox enzymes, such as glutathione reductase (GR, exp. with WI-38, PMC42, HaCaT), and glutamete cysteine lyase (GCL, exp. with AG06) were found to be increased in mRNA and activity levels by sublethal dose of arsenite in different cells including keratinocyte (AG06, HaCaT), fibroblast (WI-38) and breast tumor cells (PMC42) (Schuliga, M. *et. al.* 2002). Glutathione S-transferase (GST) however, was only slightly enhanced by the same dose of arsenite in HaCaT keratinocytes. The induction of GSH and GSH related enzymes can be involved in the ROS detoxification and the adaptive response against oxidative stress.

Sub-micromolar concentrations of arsenite are not considered to be strongly mutagenic. However, some studies indicated that in cell cultural systems, arsenite can enhance the mutagenicity of ultraviolet radiation, especially UVB (Lee, T.-C. *et. al.* 1985; Li, J.H. and Rossman, T.G. 1991). Here our mt DNA deletion results also

showed that arsenite enhances UVB induced mtDNA mutations. However, the ROS activity generated by sub-micromolar arsenite after 24 hours seems to be lower than untreated control. Other carcinogenic mechanisms should also be considered. For example, in a study by Hartwig et al (1997) it was suggested that the comutagenic effects of arsenite are caused by the suppression of DNA repair systems after UVR and both nucleotide excision repair and base excision repair activities have been found to be altered by arsenite (Li, J.H. and Rossman, T.G. 1989). DNA ligase III may be inhibited by high concentrations of arsenite and may result in a reduction of DNA strand break rejoining (reviewed in Rossman, T.G. et. al. 2004). Hairless Skh1 mice were employed for the study of arsenic cocarcinogenic effects with UVR (Rossman, T.G. *et. al.*2001, 2002). In this study it was shown that low dose arsenite, which is not mutagenic, can accelerate the carcinogenesis caused by another mutagen like UVR. The results of our real time PCR experiments on the formation of mtDNA deletions are consistent with this hypothesis.

Conclusion:

UVB irradiation of keratinocytes produced novel mitochondrial DNA deletions involving repeats of sequence, TAGG. The finding that the antioxidant, glutathione, at high concentrations induced formation of the common deletion or, in combination with UVB irradiation, enhanced formation of the TAGG-based deletions suggests the possibility that reductive antioxidants might, under certain conditions, actually act to enhance the formation of reactive oxygen species.

Sub-micromolar arsenite treatment and UVB irradiation of keratinocytes produced novel mitochondrial DNA deletions involving direct repeats, invert repeats, and other homologous sequences. Our study indicated the DNA deletion were induced by UVB in a dose dependent manner and arsenite has synergistic effect on it. Reactive oxygen species were observed decreasing by 2-day arsenite treatments and increasing with 2.9, 5.7, and 11.4 mJ/cm^2UVB irradiation.

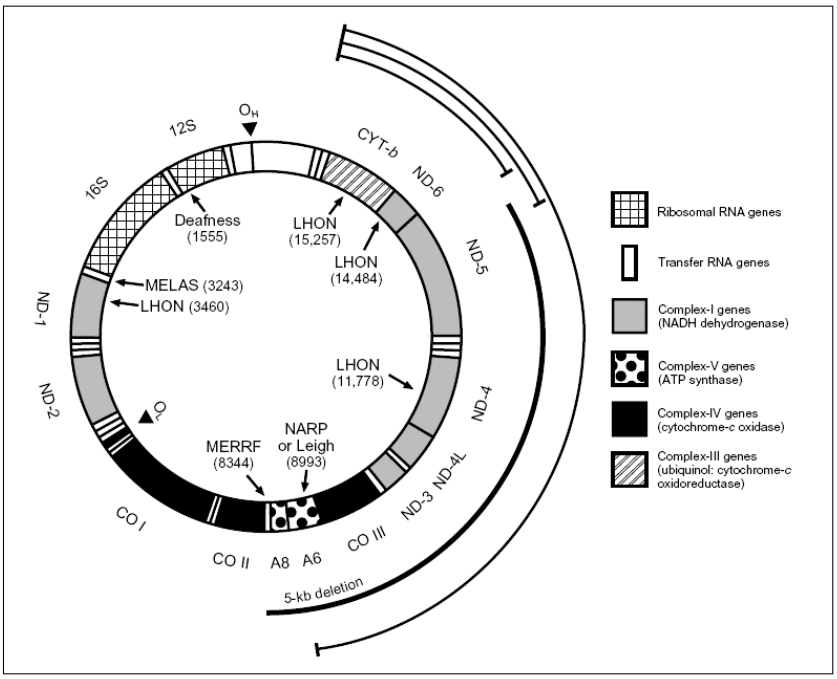

7587~8270	**cytochrome c oxidase II"**
8296~8365	**mitochondrially encoded tRNA lysine**
8367~8573	**ATP synthase 8; ATPase subunit 8**
8528~9208	**ATP synthase 6; ATPase subunit 6**
9208~9988	**cytochrome c oxidase III**
9992~10059	**mitochondrially encoded tRNA glycine**
10060~10405	**NADH dehydrogenase, subunit 3 (complex I)**
10406~10470	**mitochondrially encoded tRNA arginine**
10471~10767	**NADH dehydrogenase, subunit 4L (complex I)**
10761~12138	**NADH dehydrogenase, subunit 4 (complex I)**
12139~12207	**mitochondrially encoded tRNA histidine**
12208~12266	**mitochondrially encoded tRNA serine 2 (AGU/C)**
12267~12337	**mitochondrially encoded tRNA leucine 2 (CUN)**
12338~14149	**NADH dehydrogenase, subunit 5 (complex I)**

Figure 1. Mitochondrial genes in deleted region

MtDNA genes been effected in the deletion region. Two cytochrome c oxidase subunits, 4 NADH dehydrogenase subunits, and 6 tRNAs were possibly effected if the mtDNA deletions occur in between the 8000 and 13000 nt.

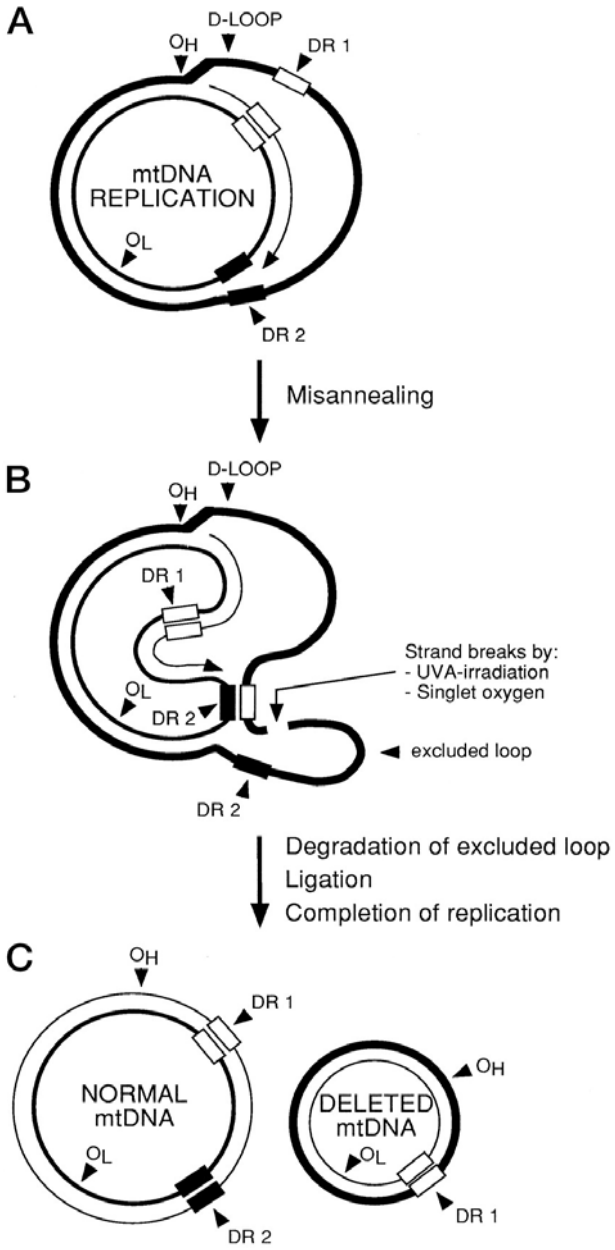

Figure 2. Generation of the 5kB Common Deletion in the presence of ROS (Berneburg, M. *et. al.* JBC 274: 15345-15349, 1999). The common deletion can be started with the misannealing of the two direct repeats (DR1 and DR2). Next, single strand DNA strand is broken by UV irradiation or singlet oxygen attack. Then, the excluded loop is degraded and the two ends of the shortened heavy strand are sealed by ligase. After the replication is completed, a deleted mtDNA is formed.

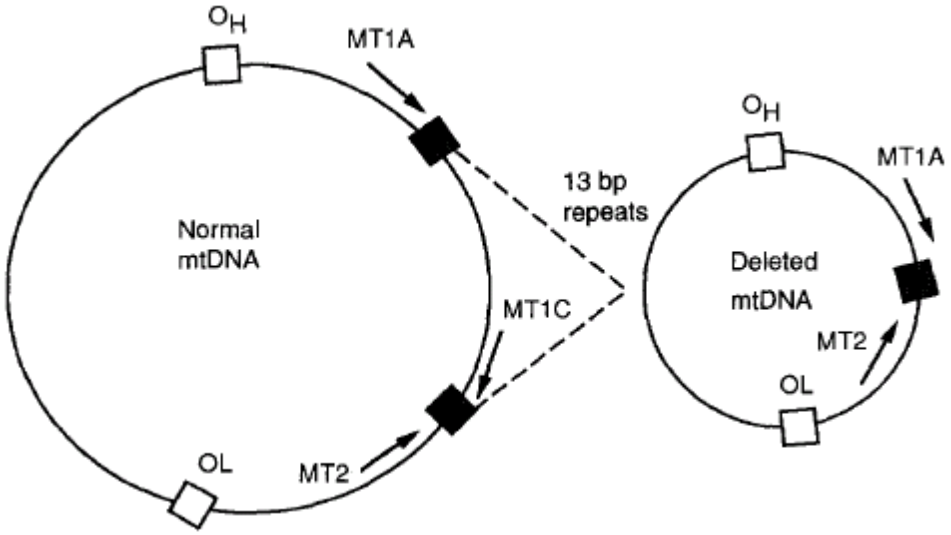

Figure 3. PCR design for common deletion.

A 4977-bp deletion between two 13-bp direct repeats brings primers MTIA and MT2 sufficiently close together to allow preferential amplification under short cycle times. Primers MTIC and MT2 amplify a section of undeleted, wild-type mtDNA and are used for normalization of total mtDNA. OL and OH denote the mitochondrial origins of replication. (N-W Soong and N Arnheim, Methods in Enzymol 264: 421, 1996).

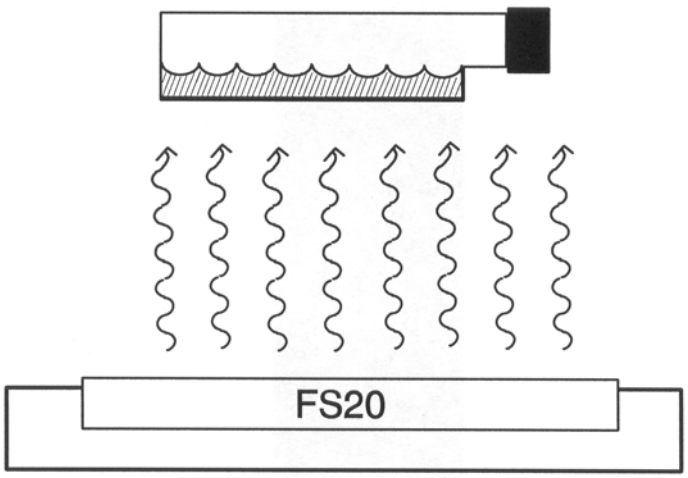

Figure 4. Irradiation illustration.

Human keratinocyte at about 35% confluence were irradiated from the bottom with an FS20 lamp at a distance of 14 inches for 4 minutes (5.7 mJ/cm^2).

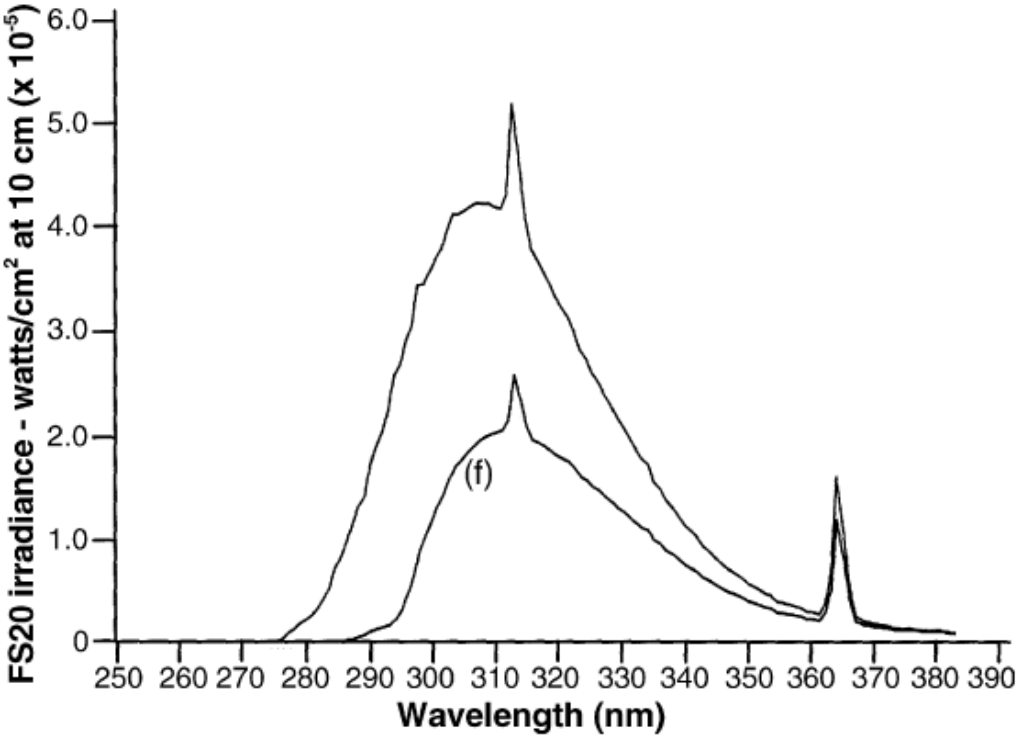

Figure 5. The FS20 irradiation spectrum.

FS20 irradiance in air, and through the wall of the plastic tissue culture flask (f) is shown.

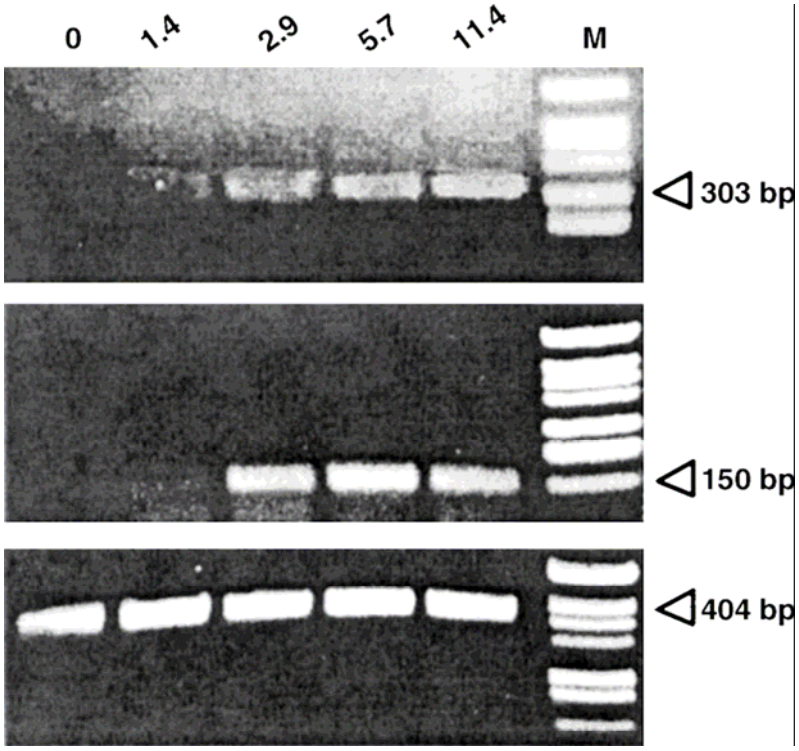

Figure 6. Induction of mitochondrial deletions in cells exposed to an FS20 light source.

T25 culture flasks of immortalized human keratinocyte line 22 cells were irradiated for various times ranging between 1 and 8 min with the FS20 lamp as described in Section 2. Twenty-four hours later, totalDNAwas prepared from the cells and used as a PCR template for deletion analysis using the amplimer pair, MT2/MT1A (upper and middle panels). Numbers represent radiation dosage in mJ/cm^2. Upper panel: dose-dependent appearance of a 303 bp PCR band derived from the 4977 bp common deletion; arrowhead points to the 298 bp marker band. Middle panel: dose-dependent appearance of a 150 bp PCR product corresponding to a novel 5128 bp deletion (Δuv); arrowhead points to the 154 bp marker band. Lower panel: presence of non-deleted mitochondrial sequences in irradiated cells. A 404 bp PCR product generated from the MT3/MT1C amplimer pair is seen in all lanes; arrowhead points to the 394 bp marker band.

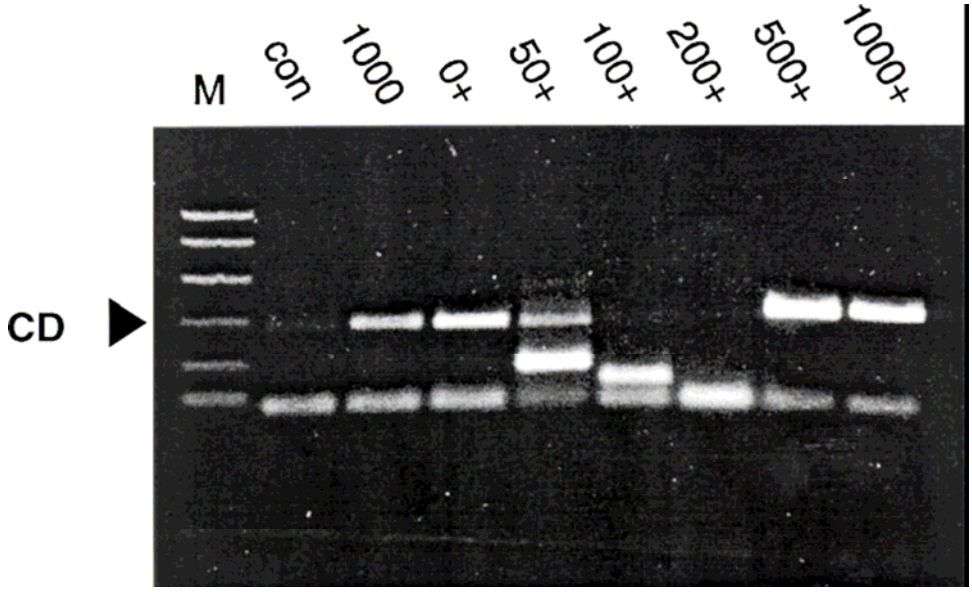

Figure 7. Effect of glutathione pretreatment on formation of the FS20-induced mitochondrial common deletion.

Line 22 cells at about 35% confluence were pretreated with glutathione. Twenty-four hours later cells were uv irradiated with an FS20 lamp for 4 min (5.7 mJ/cm2). DNA was harvested 24 h after irradiation and analyzed for mitochondrial deletions. The numbers indicate the concentrations of glutathione in micromolar. Symbol '+' indicates that the cells were irradiated after pretreatment with glutathione; control cells (con) were neither irradiated nor pretreated. Arrowhead points to the 300 bp marker band; marker bands of 150 and 50 bp are seen below.

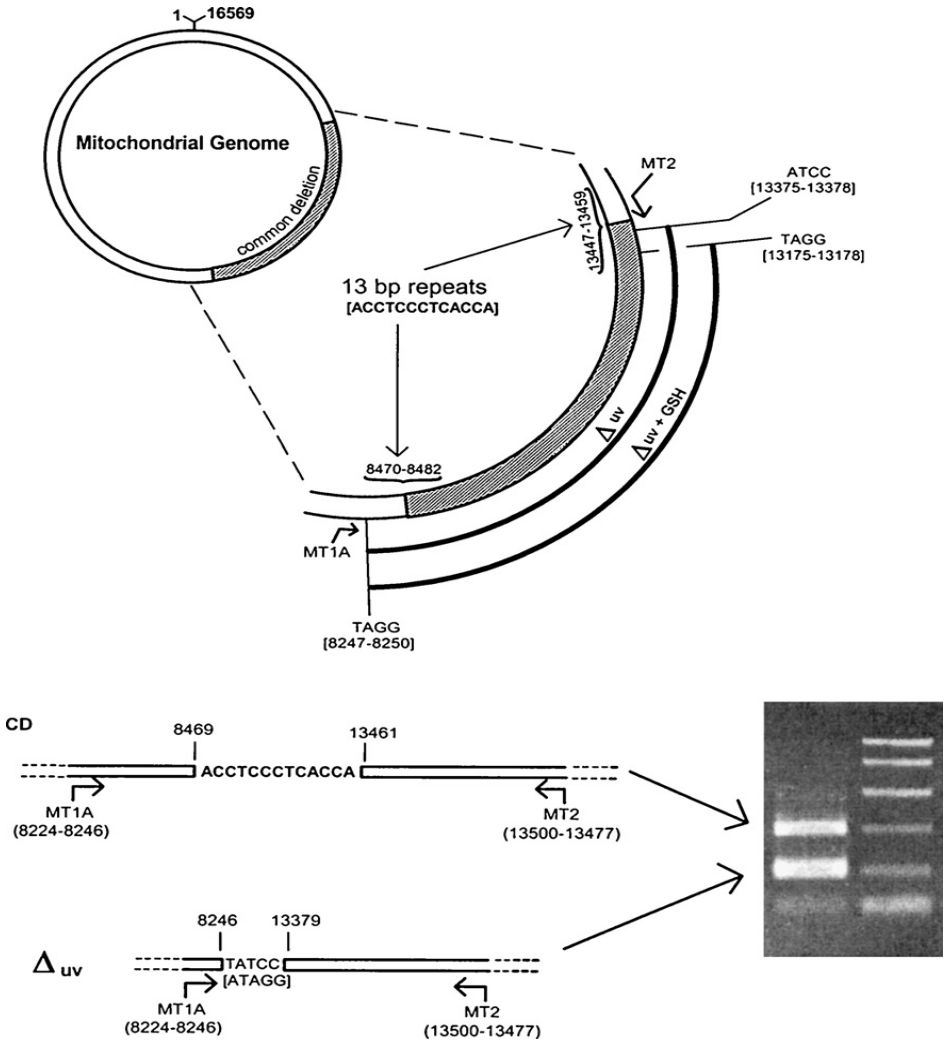

Figure 8. Diagrammatic summary of the deletions induced by FS20 and FS20 + GSH.

Upper panel: the location of the MT1A MT2 PCR primers, and the 13 bp directrepeats flanking the 4977 bp common deletion on the mitochondrial genome are shown. The locations of TAGG and ATCC tetramers that contain the cut sites for the Δuv and Δuv+GSH deletions are shown in the detail. Lower panel: the junctional sequences formed from splicing the cut ends of the common deletion (CD) and Δuv and the corresponding MT1A/MT2 PCR products in an experiment in which both deletions can be seen; the respective PCR products comigrate with the 300 and 150 bp marker (M) bands, respectively.

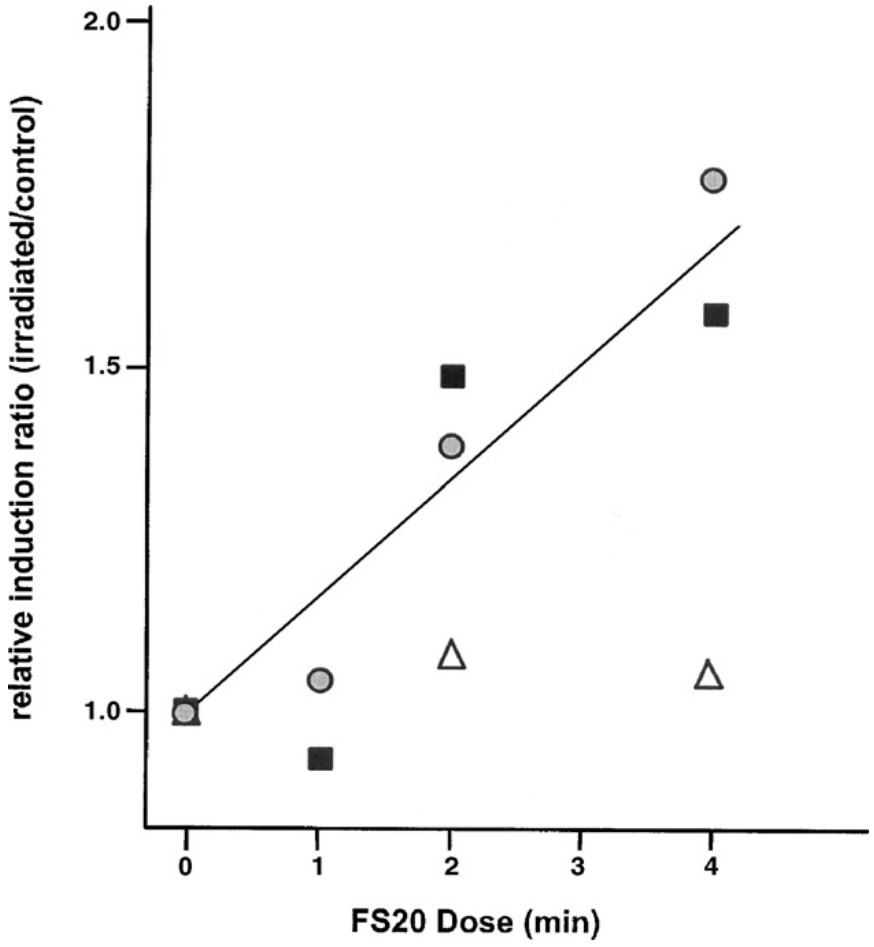

Figure 9. Real-time PCR measurements of the induction of the common deletion in FS20 irradiated keratinocytes using real-time PCR.

Mitochondrial DNA deletions in line 22 keratinocytes irradiated for 1, 2 and 4 min were examined by real-time PCR. Relative levels of deletion in irradiated vs. unirradiated cells are shown for the common deletion (○) and for the Δuv deletion (■). Relative levels of total mitochondria are indicated by symbol 'Δ'. The Δuv deletion was amplified with MT2 and the deletion specific primer TTTGAAATATCCACAACCTT which anneals only to the junctional site created by the deletion.

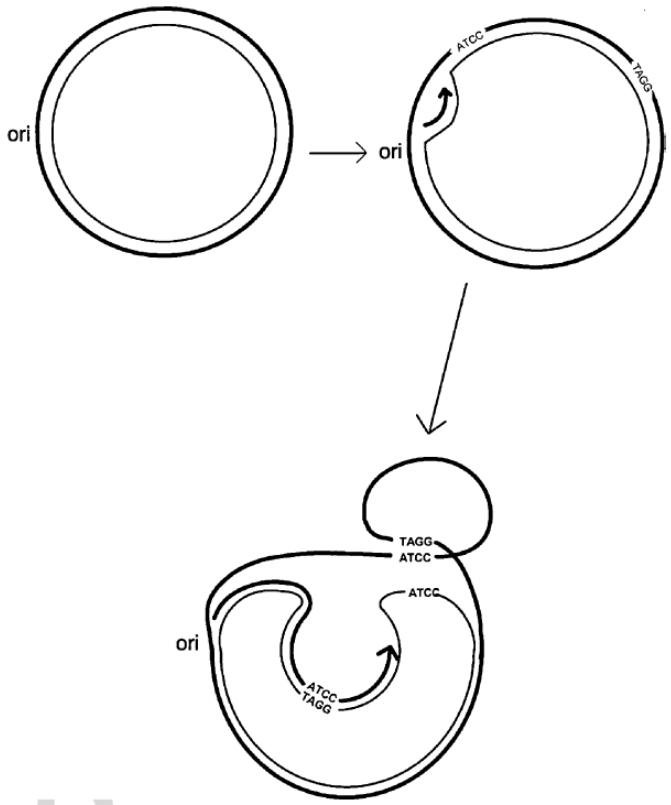

Figure 10. Possible mechanism for the generation of the Δuv deletion.

Replication of the mitochondrial genome proceeds asymmetrically along the L strand from the origin (ori) leaving an unpaired segment of the H strand (thick line) that forms a loop via parallel alignment of the tetrameric sequence, TAGG and its downstream reverse complement, ATCC. Hoogsteen base pairs stabilize the aligned tetramers in a duplex or possibly in a triple helix if the Hand L strands are still base paired at the downstream tetramer. Nicking, followed by degradation of the single stranded loop and ligation of the ends (AT and AGG or A and TAGG) creates the deletion.

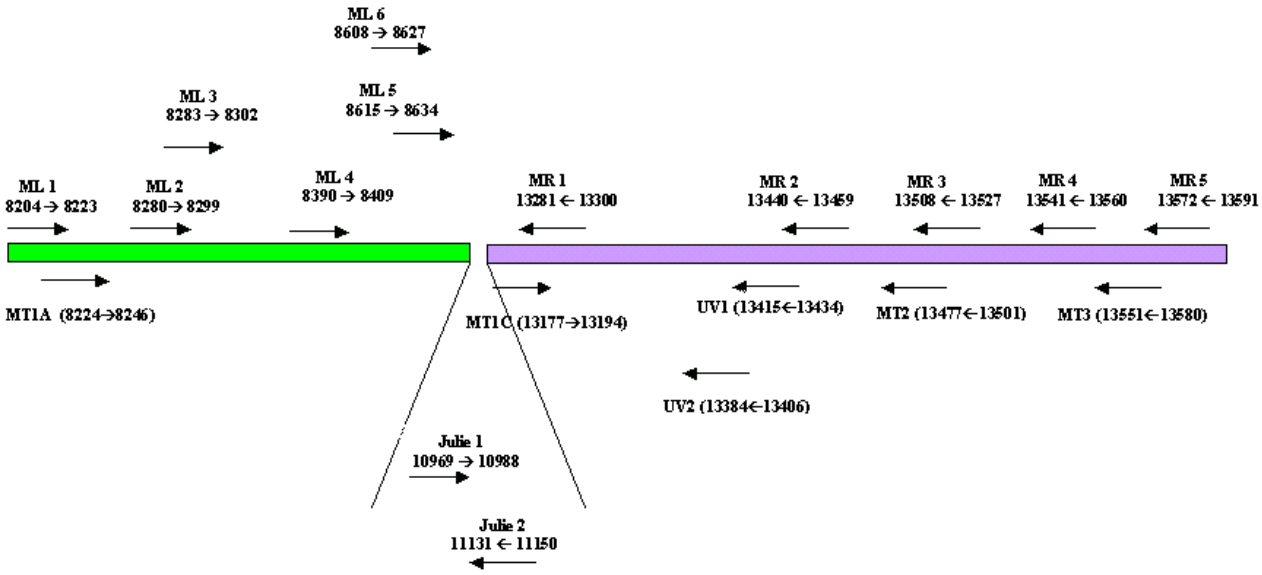

Figure 11. Primer locations for studying mitochondrial deletions.

After more mtDNA deletions in the region 8000~13000 were identified in SV40 immortalized human keratinocytes line 130 and line 22, different sets of primers were designed to specifically amplify different types of deletions.

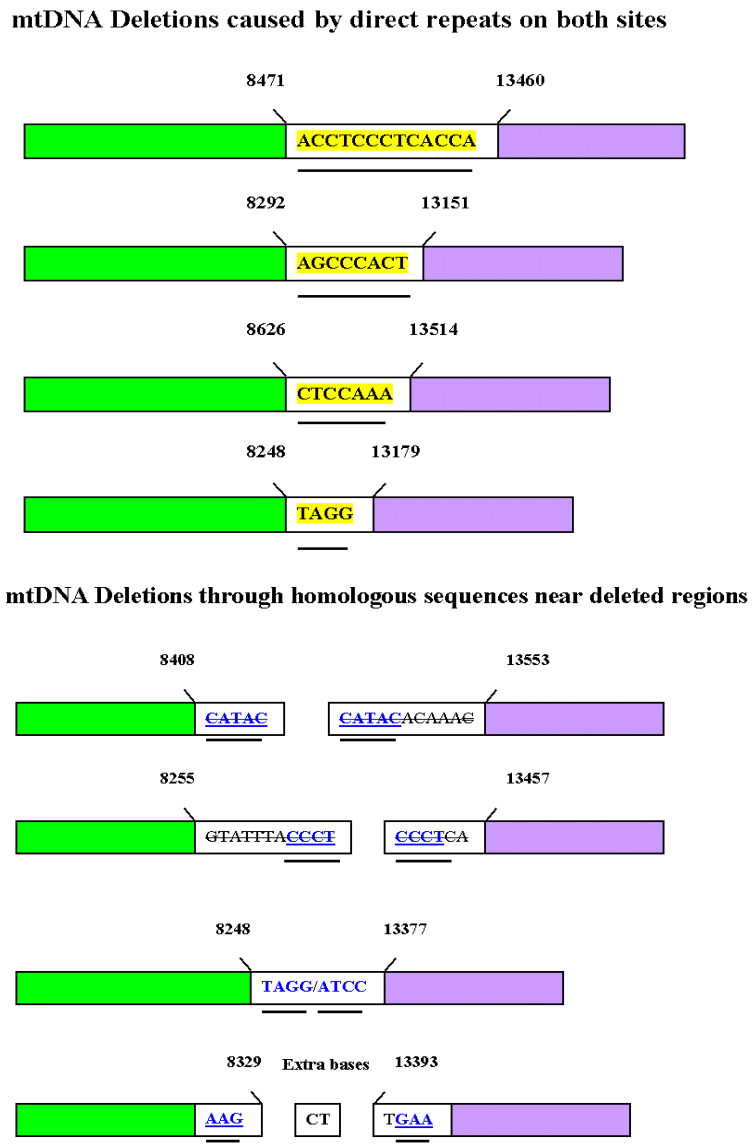

Figure 12. mtDNA deletions observed in our laboratory.

Experiments were carried out on SV40 immortalized human keratinocytes line 130 and line 22, mtDNA deletions were identified by aligning the sequences of PCR products with the reference strain sequence, Gen-Bank no. NC 001807.

Upper: deletions caused through direct repeats on both sites. Lower: deletions through homologous sequences near deleted regions.

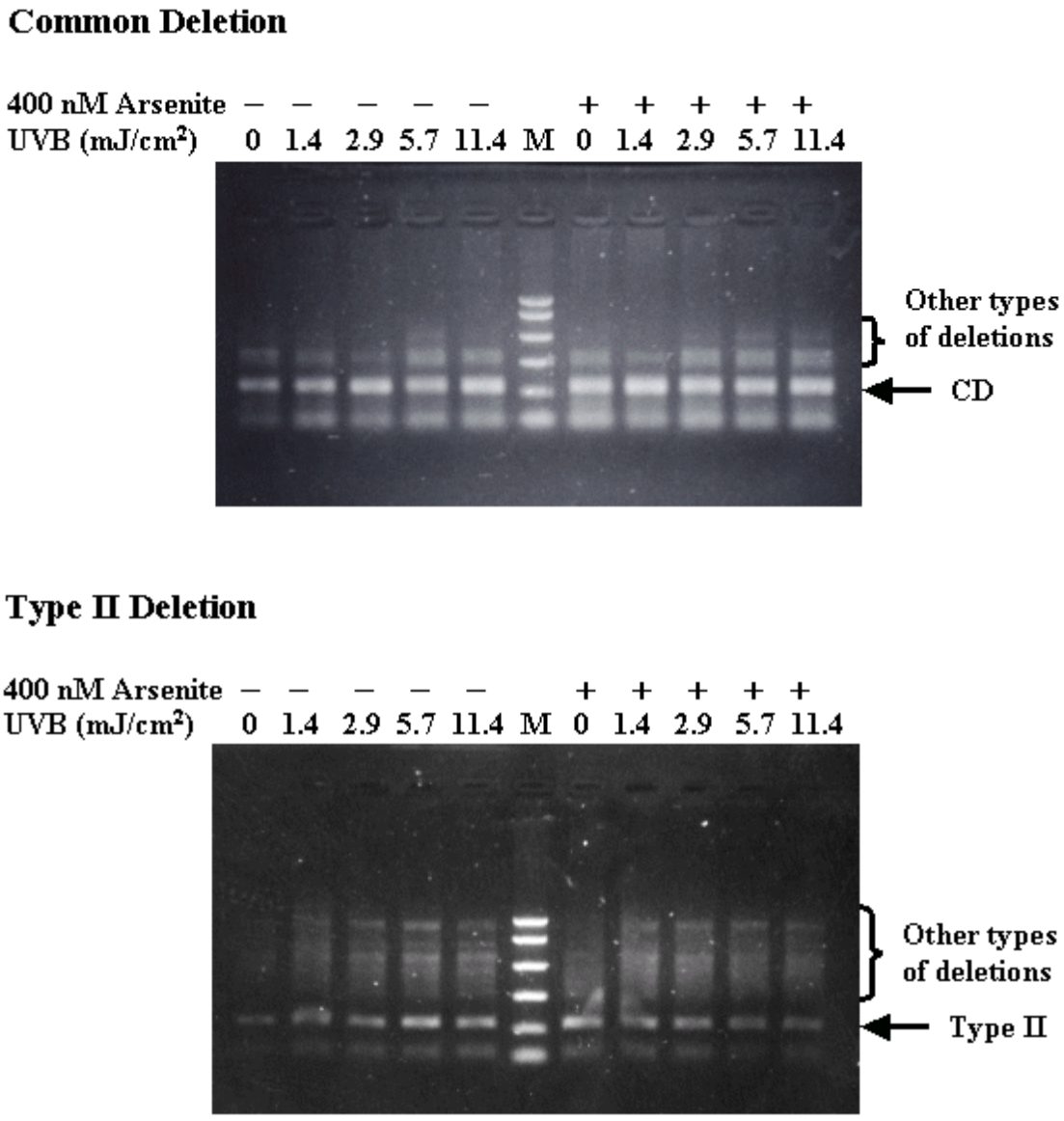

Figure 13. Agarose gel of PCR products from NHEK DNA samples.

NHEK cellular DNAs were isolated from arsenite/UV treated samples as PCR templates.

Upper: PCR products using primers ML4 and MR3. Sequence results confirmed as common deletion.

Lower: PCR products using primers ML2 and MR1. Sequence results confirmed as type II deletion.

Table 1. Real Time PCR results. Cells were divided into two groups: untreated and 400 nM arsenite treated. 24 hours later, both groups of NHEKs were irradiated by FS20 light sourse for 2.9, 5.7, and 11.4 mJ/cm^2.

A. Real time PCR of common deletion of NHEK treated with different dose of UVB and/or 400 nM arsenite.
B. Real time PCR of Type II deletion of NHEK treated with different dose of UVB and/or 400 nM arsenite.

A. Common deletion:

UVR dose (mJ/cm2)	0	2.9	5.7	11.4	As 0	As 2.9	As 5.7	As 11.4
Exp8	1.00	1.97	2.83	0.32	0.27	0.27	5.92	39.59
Exp7	1.00		3.61		7.09		11.30	
Exp6	1.00	0.68	0.52	0.46	0.28	0.95	2.09	2.71
Exp5	1.00	5.61	10.23	1.40	4.85	46.35	99.06	ND
Exp4	1.00	3.99	5.11	12.92	14.96	14.74	8.77	5.96
Exp3	1.00				1.23			
Exp2	1.00				1.17			
Exp1	1.00				2.63			
Average	1.00	3.06	4.46	3.78	4.06	15.57	25.43	16.08
STDEV	0.00	2.18	3.63	6.11	5.01	21.57	41.30	20.42
SEM	0.00	1.09	1.62	3.06	1.77	10.78	18.47	11.79

B. Type II deletion:

UVR dose (mJ/cm2)	0	2.9	5.7	11.4	As 0	As 2.9	As 5.7	As 11.4
Exp 1	1.00	1.05	0.60	1.67	2.95	3.48	12.60	1.67
Exp 2	1.00	6.97	2.81	3.16	0.95	8.14	0.37	1.28
Exp 3	1.00	1.12	0.28	N/A	0.20	0.09	0.30	N/A
Exp 4	1.00	0.41	0.08	1.01	0.67	3.12	2.40	1.05
Exp 5	1.00	0.96	0.94	2.50	1.32	0.81	9.34	1.98
Exp 6	1.00	0.22	0.99	0.98	0.05	0.23	1.94	0.63
Exp 7	1.00	1.60	1.44	1.05	3.77	2.22	7.19	1.16
Exp8	1.00	0.44	1.76	N/A	6.12	0.92	6.67	N/A
Exp9	1.00	N/A	0.59	0.67	0.96	N/A	0.27	0.89
Average	1.00	1.76	1.02	1.73	1.42	2.59	4.88	1.29
STDEV	0	2.34	0.91	0.91	1.42	2.80	4.85	0.48
SEM	0	0.89	0.34	0.41	0.54	1.06	1.83	0.21

Numbers on the tables represent the induction ratio compared to the untreated control.

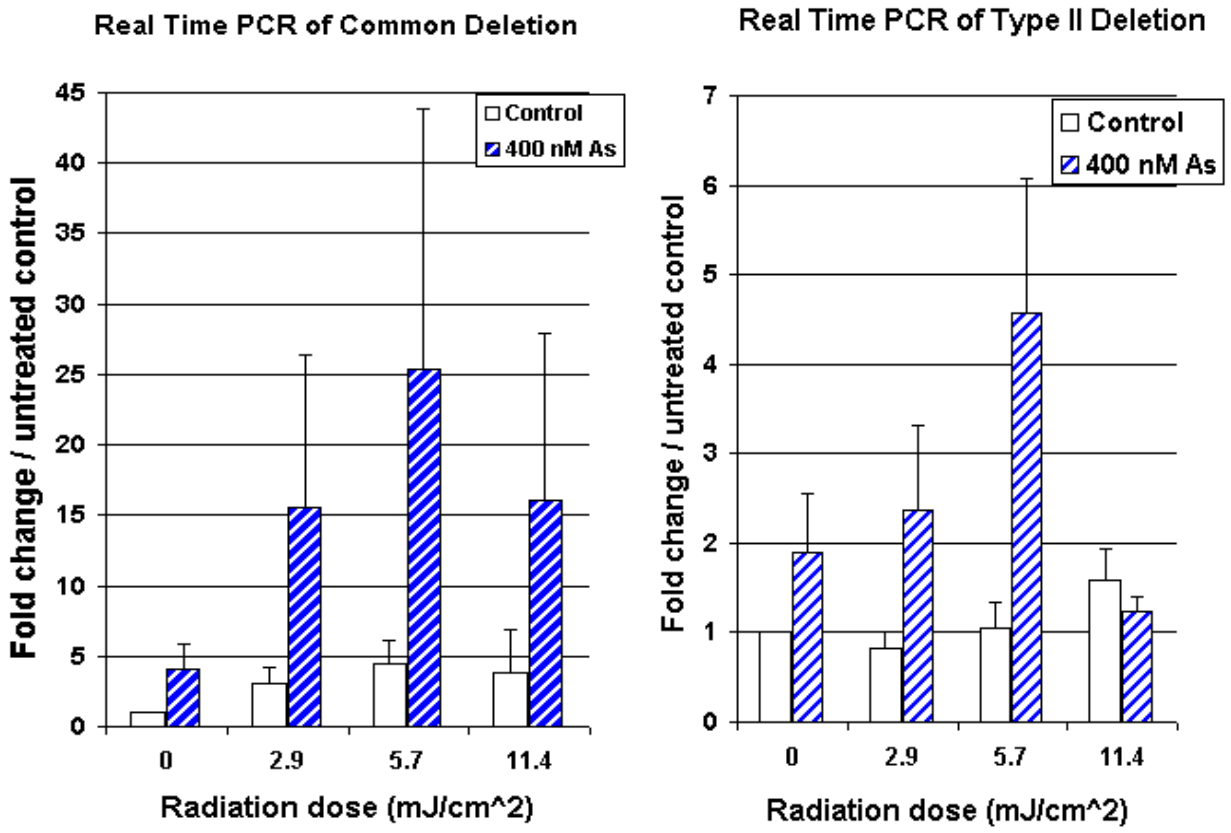

Figure 14. Two types of mtDNA deletions were induced by UVB and arsenite.

Real time PCR results of NHEKs treated with and without arsenites under different doses of UVB irradiation. Induction ratios were expressed in Log scales. Left: common Deletion using FAM-labeled probe. Right: type II deletion using Sybr Green dye.

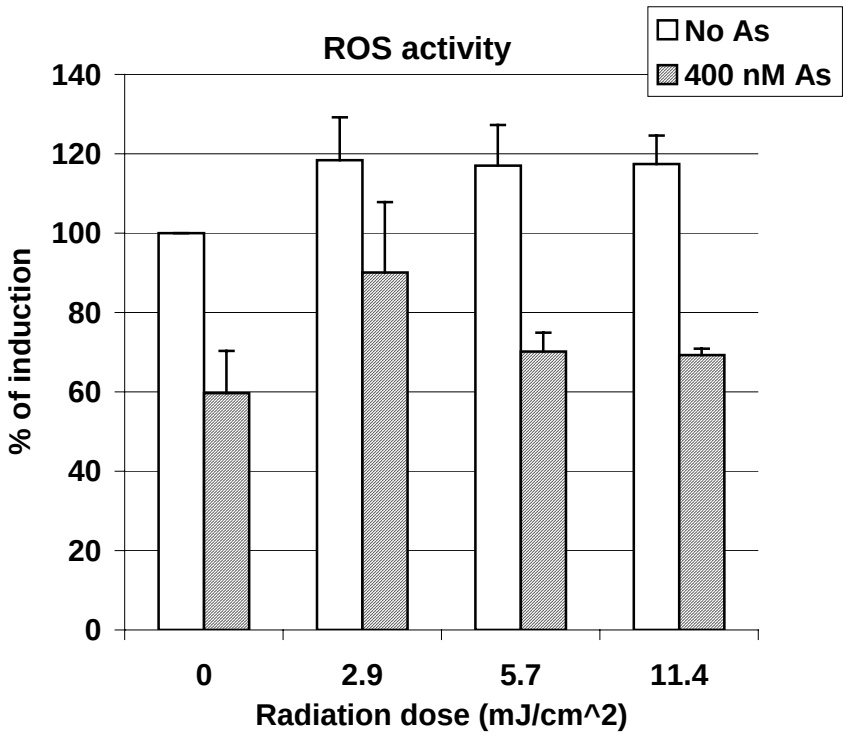

Figure 15. Reactive oxygen species (ROS) quantities measured from FACS.

NHEKs were treated with and without 400 nM sodium arsenite for 24 hours and irradiated with UVB for 2, 4, and 8 minutes. The next day, cells were then incubated with 2 μM 5′, 6′-carboxy-2′, 7′-dichlorodihydrofluorescein diacetate for 40 minutes. The signals were compared to the untreated, no UV irradiated control.

Appendix III: Primers for mitochondrial DNA deletions:

Primer Information:			
Name	**Primer sequence**	**GC %, Tm**	**Reference**
			NC_001807:
Julie 1	cctgactcctacccctcaca	63%,72.3 °C	10969 → 10988
Julie 2	caaggtggggataagtgtgg	58%,72.3 °C	11131 ← 11150
Delta UV	tttgaaatatccacaacctt	30%,60.0 °C	8241~8247-TATCC-13379~13387
UV1	atggttttgagtagtcctcc	47%,66.2 °C	13415 ← 13434
UV2	gaatatcttgttcattgttaagg	32%,64.6 °C	13384 → 13406
MT1A	gaattcccctaaaaatctttgaaat	28%,66.0 °C	8225 → 8247
MT1C	aggcgctatcaccactcttgttcg	59%,75.6 °C	13177 →13194
MT2	aacctgtgaggaaaggtattcctgc	48%,74.2 °C	13478 ← 13502
MT3	gcgatgagagtaatagatagggctcaggcg	57%,80.9 °C	13552 ← 13581
ML 1	catgcccatcgtcctagaat	50%,59.9 °C	8204 → 8223
ML 2	tacccccctctagagcccact	60%,60.1 °C	8280 → 8299
ML 3	cccctctagagcccactgta	60%,59.3 °C	8283 → 8302
ML 4	atggcccaccataattaccc	50%,60.6 °C	8390 → 8409
ML 5	ttgatccccacctccaaata	45%,60.1 °C	8615 → 8634
ML 6	ccctctattgatccccacct	55%,60.2 °C	8608 → 8627
MR 1	ttggttgatgccgattgtaa	40%,59.9 °C	13281 ← 13300
MR 2	ggtgagggaggttgaagtga	55%,60.1 °C	13440 ← 13459
MR 3	tcgatgatgtggtctttgga	45%,60.1 °C	13508 ← 13527
MR 4	gctcaggcgtttgtgtatga	50%,59.9 °C	13541 ← 13560
MR 5	cagggaggtagcgatgagag	60 %,60.0 °C	13572 ← 13591

Bibliography

Agarwal, S. and Sohal, R.S. **1994.** DNA oxidative damage and life expectancy in houseflies. *Proc. Natl. Acad. Sci.* 91: 12332-12335.

Aishima, J., Gitti, R.K., Noah, J.E., Gan, H.H., Schlick, T., and Wolberger, C. **2002.** A Hoogsteen base pair embedded in undistorted B-DNA. *Nucleic Acids Res.* 30 (23): 5244-5252

Arai, T., Nakahara, K., Matsuoka, H., Sawabe, M., Chida, K., Matsushita, S., Takubo, K., Honma, N., Nakamura, K., Izumiyama, N., and Esaki, Y. **2003.** Age-related mitochondrial DNA deletion in human heart: its relationship with cardiovascular diseases. *Aging Clin. Exp. Res.* 15 (1): 1–5.

Asmuss, M., Mullenders, L.H., Eker, A., and Hartwig, A. **2000.** Differential effects of toxic metal compounds on the activities of fpg and XPA, two zinc finger proteins involved in DNA repair. *Carcinogenesis.* 21 (11): 2097-2104.

Berneburg, M., Grether-Beck, S., Ruzicka, T., Vriviba, K., Sies, H., and Krutmann, J. **1999.** Singlet oxygen mediates the uva-induced generation of the photaging-associated mitochondrial common deletion. *J. Biol. Chem.* 274: 15345–15349.

Berneburg, M., Plettenberg, H., Medve-K¨onig, K., Pfahlberg, A., Gers-Barlag, H., Gefeller, O., and Krutmann, J. **2004.** Induction of the photoaging-associated mitochondrial common deletion in vivo in normal human skin. *J. Invest. Derm.* 122 (5): 1277–1283.

Corsini, E., Asti, L., Viviani, B., Marinovich, M., and Galli, C.L. **1999.** Sodium arsenate induces overproduction of interleukin-1 alpha in murine keratinocytes: role of mitochondria. *J. Invest. Dermatol.* 113 (5): 760-765.

Chouchane, S., and Snow, E.T. **2001.** In vitro effect of arsenical compounds on glutathione-related enzymes. *Chem Res Toxicol.* 14(5):517-22.

Eblin, K. E., Bowen, M.E., Cromey, D. W., Bredfeldt, T. G., Mash, E. A., Lau, S. S., and Gandolfi, A. J. **2006.** Arsenite and monomethylarsonous acid generate oxidative stress response in human bladder cell culture. *Toxicol Appl Pharmacol.* 217: 7-14

Fang, J., Pierre, Z., Liu, S., Hwang, B.-J., Hill, H.Z., Hubbard, K., and Steinberg, M. 2006. Novel mitochondrial deletions in human epithelial cells irradiated with an FS20 ultraviolet light source in vitro. *J. Photochem. Photobiol. A: Chemistry.* 184: 340-346.

Frank-Kamenetskii, M.D. and Mirkin, S.M. **1995.** Triplex DNA structures, *Ann. Rev. Biochem.* 64: 65–95.

Johns, D.R., Flier, J.S. and Underhill, L.H. **1995.** Mitochondrial DNA and disease. *The New England Journal of Medicine.* 333 (10): 638-644.

Gu, G., Reyes, P.E., Golden, G.T., Woltjer, R.L., Hulette, C., Montine, T.J., and Zhang, J. **2002.** Mitochondrial DNA deletions/rearrangements in parkinson disease and related neurodegenerative disorders. *J. Neuropathol. Exp. Neurol.* 61 (7): 634–639.

Hartwig, A., Gröblinghoff, U.D., Beyersmann, D., Natarajan1, A.T., Filon, R., and Mullenders, L.H.F. **1997.** Interaction of arsenic(III) with nucleotide excision repair in
UV-irradiated human fibroblasts. *Carcinogenesis.* 18(2): 399–405.

Hei, T.K., Liu, S.X., and Waldren, C. **1998.** Mutagenicity of arsenic in mammalian cells: Role of reactive oxygen species. *Proc. Natl. Acad. Sci.* 95: 8103-8107.

Hou, J.H. and Wei, Y.H. **1998.** AT-rich sequences flanking the 5’-end breakpoint of the 4977-bp deletion of human mitochondrial DNA are located between two bent-inducing DNA sequences that assume distorted structure in organello. *Mutat. Res.* 403 (1–2): 75–84.

Lane, H., Bermingham, N., Farrell, M.A., Redmond, J., Connolly, S., and Brett, F.M. **2003.** Mitochondrial disorder with a common 4977-bp deletion presenting as a novel multisystem neurodegenerative disorder. *Ir. Med. J.* 96 (8): 249–250.

Larsson, N.-G.and Holme, E. **1992**. Multiple short direct repeats associated with mtDNA deletions. *Biochem. Biophys. Acta* 1139: 311-314.

Lee, T.-C., Huang, R.Y., Jan, K.Y. **1985**. Sodium arsenite enhances the cytotoxicity, clastogenicity, and 6-thioguanine-resistant mutagenicity of ultraviolet light in Chinese hamster ovary cells. *Mutat Res.* 148(1-2): 83-89.

Li, J.H. and Rossman, T.G. **1989**. Mechanism of comutagenesis of sodium arsente with N-methyl-N-nitrosourea. *Biol. Trac. Elem. Res.* 21: 373-381.

Li, J.H. and Rossman, T.G. **1991**. Comutagenesis of sodium arsenite with ultraviolet radiation in Chinese hamster V79 cells. *Biol Met.* 4(4): 197-200.

Liu, S.X., Athar, M., Lippai, I., Waldren, C., and Hei, T.K. **2001**. Induction of oxyradicals by arsenic: Implication for mechanism of genotoxicity. *Proc. Natl. Acad. Sci.* 98 (4): 1643-1648.

Liu, S.X., Davidson, M.M., Tang, X., Walker, W.F., Athar, M., Ivanov, V., and Hei, T.K. **2005**. Mitochondrial Damage Mediates Genotoxicity of Arsenic in Mammalian Cells. *Cancer Res,* 65: 3236-3242.

Lin, P.H., Lee, S.H., Su, C.P., and Wei, Y.H. **2003**. Oxidative damage to mitochondrial DNA in atrial muscle of patients with atrial fibrillation, Free Radic. *Biol.Med.* 35 (10): 1310–1318.

Lynn, S., Lai, H.T., Gurr, J.R., and Jan, K.Y. **1997**. Arsenite retards DNA breat rejoining by inhibiting DNA ligation. *Mutagenesis.* 12 (5): 353-358.

Maximo, V., Soares, P., Lima, J., Cameselle-Teijeiro, J., Sobrinho-Simoes, M. **2002**. Mitochondrial DNA somatic mutations (point mutations and large deletions) and mitochondrial DNA variants in human thyroid pathology: a study with emphasis on Hurthle cell tumors. *Am. J. Pathol.* 160 (5): 1857–1865.

Moore, L.E., Smith, A.H., Hopenhayn-Rich, C., Biggs, M.L., Kalman, D.A., and Smith, M.T. **1997.** Micronuclei in exfoliated bladder cells among individuals chronically exposed to arsenic in drinking water. *Cancer Epidemiol. Biomarkers Prev.* 6:31-37.

Moraes, C. T., Atencio, D. P., Oca-Cossio, J., and Diaz, F. **2003.** Techniques and pitfalls in the detection of pathogenic mitochondrial DNA mutations. *J. Molecular. Diagnostics.* 5(4): 197-208.

Niaudet, P., Heidet, L., Munnich, A., Schmitz, J., Bouissou, F., Gubler, M.C., and Rotig, A. **1994.** Deletion of the mitochondrial DNA in a case of de Toni–Debre–Fanconi syndrome and Pearson syndrome. *Pediatr. Nephrol.* 8 (2): 164–168.

Pogozelski, W.K., Hamel, C.J., Woeller, C.F., Jackson, W.E., Zullo, S.J., Fischel-Ghodsian, N., and Blakely, W.F. **2003.** Quantification of total mitochondrial DNA and the 4977-bp common deletion in Pearson's syndrome lymphoblasts using a fluorogenic 5'-nuclease (TaqMan) real-time polymerase chain reaction assay and plasmid external calibration standards. *Mitochondrion* 2(6): 415–427.

Ray, A.J., Turner, R., Nikaido, O., Rees, J.L., Birch-Machin, and M.A. **2000.** The spectrum of mitochondrial DNA deletions is a ubiquitous marker of ultraviolet radiation exposure in human skin, *J. Invest. Derm.* 115 (4): 674–679.

Rocher, C., Letellier, T., Copeland, W.C., and Lestiennea, P. **2002.** Base composition at mtDNA boundaries suggests a DNA triple helix model for human mitochondrial DNA large-scale rearrangements. *Mol. Genet. Metabol.* 76: 123–132.

Rogounovitch, T.I., Saenko, V.A., Shimizu-Yoshida, Y., Abrosimov, A.Y., Lushnikov, E.F., Roumiantsev, P.O., Ohtsuru, A., Namba, H., Tsyb, A.F., and Yamashita, S. **2002.** Large deletions in mitochondrial DNA in radiation-associated human thyroid tumors. *Cancer Res.* 62 (23): 7031–7041.

Rossman, T.G., Uddin, A.N., Burns, F.J. and Bosland, M.C. **2001.** Arsenite is a cocarcinogen with solar ultraviolet radiation for mouse skin: an animal model for arsenic carcinogenesis1. *Toxicol Appl Pharmacol.* 176(1): 64-71

Rossman, T.G., Uddin, A.N., Burns, F.J. and Bosland, M.C. **2002.** Arsenite cocarcinogenesis: an animal model derived from genetic toxicology studies. *Health Perspect.* 110 Suppl 5:749-52.

Rossman , T. G. **2003.** Mechanism of arsenic carcinogenesis: an integrated approach. *Mutat. Res./Fundamental and Molecular Mechanisms of Mutagenesis*. 533(1-2): 37-65.

Rossman, T.G., Uddin, A.N., and Burns, F.J. **2004.** Evidence that arsenite acts as a cocarcinogen in skin cancer. *Toxicol Appl Pharmacol.* 198(3): 394-404.

Schaumloffel, N. and Gebel, T. **1998.** Heterogeneity of the DNA damage provoked by antimony and arsenic. *Mutagenesis.* 13 (3): 281-286.

Schuliga, M., Chouchane, S., and Snow, E.T. **2002.** Upregulation of glutathione-related genes and enzyme activities in cultured human cells by sublethal concentrations of inorganic arsenic. *Toxicol Sci.* 70(2):183-92.

Shi, H., Shi, X., and Liu, K.J. **2004a.** Oxidative mechanism of arsenic toxicity and carcinogenesis. *Mol Cell Biochem.* 255(1-2): 67-78.

Shi, H., Hudson, L. G., and Liu, K.J. **2004b.** Oxidative stress and apoptosis in metal ion-induced carcinogenesis. *Free Radic Biol Med.* 37(5): 582-593.

Snow, E.T., Sykora, P., Durham, T.R., and Klein, C.B. **2005.** Arsenic, mode of action at biologically plausible low doses: What are the implications for low dose cancer risk? *Toxicol Appl Pharmacol*. 207(2S):557-564.

Soong, N.-W., and Arnheim, N. **1996.** Detection and quantification of mitochondrial DNA deletions. *Methods Enzymol.* 264: 421–431.

Tabaku, M., Legius, E., Robberecht, W., Sciot, R., Fryns, J.P., Cassiman, J.J., and Matthijs, G.. **1999.** A novel 7.4 kb mitochondrial deletion in a patient with congenital progressive external phthalmoplegia, muscle weakness and mental retardation. *Genet. Couns.* 10 (3): 285–293.

Wang, T.S., Kuo, C. F., Jan, K.Y., and Huang, H. **1996.** Arsenite induces apoptosis in Chinese hamster ovary cells by generation of reactive oxygen species. *J. Cell. Physiol*. 169(2): 256-268.

Wei, Y.H. 1998. Oxidative stress and mitochondrial DNA mutations in human aging. *Proc. Soc. Exp. Biol. Med*. 217: 53-63.

Yamagata, K., Muro, K., Usui, J., Hagiwara, M., Kai, H., Arakawa, Y., Shimizu, Y., Tomida, C., Hirayama, K., and Kobayashi, M. **2002.** A. Koyama, Mitochondrial DNA mutations in focal segmental glomerulosclerosis lesions. *J. Am. Soc. Nephrol.* 13 (7):1816–1823.

Zhao, C.Q., Young, M.R., Diwan, B.A., Coogan, T.P., and Waalkes, M.P. **1997.** Association of arsenic-induced malignant transformation with DNA hypomethylation and aberrant gene expression. *Proc. Natl. Acad. Sci.* 94 (20): 10907-10912.